41789

A STUDY OF THE CHARGED PARTICLES EMITTED FROM CERTAIN FAST-NEUTRON INDUCED REACTIONS

by

Kenneth H. Purser

Submitted to the Australian National University in partial fulfillment of the requirements for the degree of Doctor of Philosophy.

PREFACE

This thesis presents the results of a programme of fast neutron research which was undertaken at the Australian National University. The main purpose of these investigations was to obtain more information about the relative importance of direct and evaporative processes in fast neutron interactions with medium weight nuclei. In this work a low background counting system was developed to study neutron interactions and was used in a study of the protons and deuterons from Ni^{58} bombarded by 14.9MeV neutrons. Complementary measurements were made on the partial cross-sections for Ni^{58} by induced activity experiments at 14.1MeV. Also reported is a detailed study of the cross-section of $Li^6(n,H^3)He^4$ within the energy range 2.0MeV to 2.65MeV.

Angular distribution measurements showed that the protons from Ni^{58} were emitted isotropically for energies below 6MeV with some forward peaking apparent at higher energies. The angular distributions suggest direct interaction contributions $\Delta l = 0$ and $\Delta l = 2$ transitions to unresolved levels near the ground state of the residual Co^{58}. A large fraction of the proton emission cross-section could be explained by an evaporative decay of a compound nucleus, the spectra giving nuclear temperatures of 1.35 ± 0.03MeV and 0.50 ± 0.03MeV for the reactions (n,p) + (n,pn) and (n,np), respectively. Total cross-section for proton emission was 830 ± 70mb. Partial cross-sections were: (n,p) + (n,pn), 490mb; (n,np), 340mb.

Direct observation of the emitted deuterons was used to establish $Ni^{58}(n,d)Co^{57}$, which was found to have an integrated cross-section of 25 ± 6mb. The deuteron spectrum showed a prominent group to a level (or levels) close to the ground state of Co^{57}. The angular distribution of this group suggested unresolved transitions to the $7/2^-$ ground state of Co^{57} and to a new level at approximately 0.5MeV. The intensity of the $\Delta l = 1$ transition implied approximately 13% p-wave admixture in the Ni^{58} ground state configuration.

The final chapters discuss the possibility of using inorganic scintillators as target and detector when studying neutron induced reactions. The technique was employed with a $Li^6I(Eu)$ in a study of Li^{7*} between 9.0MeV and 9.55MeV excitation; a region where photodisintegration experiments have indicated the presence of levels. No level structure was found and possible reasons for its absence are discussed.

The major effort of this research was devoted to the development of the low-background counting system which is described in Chapter II. This system employed a counter telescope of novel design which could measure angular distributions in the range 0° - 150°. Additional circuitry distinguished between particles of different mass. To eliminate reactions from scattered neutrons and to further reduce the background, millimicrosecond coincidence techniques were also employed.

The majority of the equipment described in Chapter II was designed jointly with Dr R.N. Glover, who also collaborated in the experiment on Ni^{58}. An important exception was the particle identification system which was constructed by a fellow Research Scholar, Mr. E. Weigold, for use in an independent experiment.

No part of the work reported here has been submitted for a degree to any other University.

Kenneth H. Purser.

Kenneth H. Purser.

ACKNOWLEDGMENTS

I should like to express my gratitude to Professor E.W. Titterton for his helpful criticisms during the course of this work and also for his patience during the many months required to develop and perfect the counter telescope and its associated circuitry. I am deeply indebted to Dr R.N. Glover who supervised this work for the final eighteen months and who has read and commented on the contents of this thesis.

I wish to thank Messrs E. Weigold and G. Hogg who assisted with data taking during the Ni^{58} experiment. Also, Dr R. Mills and Mr M.J. Vernon who carried out the chemical separations for the activation measurements. Acknowledgments are due to Professors K.J. Le Couteur and S.T. Butler, and to Drs D.C. Peaslee and F.C. Barker for help with aspects of the theory.

A collective vote of thanks is due to Mr F.C. James and his workshop staff for many difficult construction jobs; to Mr Norman Bowkett for help with the Cockroft-Walton accelerator; to the electronics group for building much of the circuitry; and to Mr W. Tys for the many glass-blowing operations which he performed.

K.H.P.

PUBLICATIONS

(1) Purser, K.H. and Titterton, E.W. "The $Ni^{58}(n,p)Co^{58}$, $Ni^{58}(n,2n)Ni^{57}$, and the $Ni^{58}(n,np)Co^{57}$ Cross-sections at 14.1MeV."
Aust. J. Phys. 12, 103, (1959)

(2) Purser, K.H. "A Search for Levels of Li^7 between 9.0 and 9.55MeV Excitation".
Aust. J. Phys. 12, 231, (1959).

(3) Purser, K.H. and Richards, J. "A Liquid Air Level Controlling Device".
J. Sci. Instruments 36, 142, (1959)

(4) Glover, R.N. and Purser, K.H. "Protons and Deuterons from Ni^{58} Bombarded by 14.9MeV Neutrons".
Submitted to Nuclear Physics.

(5) Glover, R.N., Purser, K.H. and Weigold, E. "Coincidence Telescope for Measuring Protons and Deuterons from 14.9MeV Neutron Interactions".
Submitted to Nuclear Instruments.

TABLE OF CONTENTS

CHAPTER I

INTRODUCTION

The models which have been used to explain the observed features of nuclear reactions have had a chequered history of waxing and waning popularity. Nearly three decades ago it was suggested that single particle direct interactions might prove a satisfactory basis for a model of nuclear reactions; however, the theory was discarded when the discovery of narrow resonance structure in reaction cross-sections forced the adoption of the compound nucleus model. Over the years, this compound nucleus model has played an important part in predicting the details of reactions going through discrete states and has been extended to include the cases where the compound nucleus has available a statistically large number of overlapping levels.

Notwithstanding the successes of the compound nucleus model, direct interaction theory had a revival early in the last decade when examinations of the details of many reactions showed features which were foreign to the decay of compound nuclei. These investigations, which gave widespread support to the theory of direct interactions, raised many doubts about the usefulness of the statistical model and caused extensive discrediting of this part of compound nucleus theory. Today, however, it appears likely that the two models are reconcilable and can exist side by side. It has been suggested that direct interactions and evaporation processes can be simultaneously present in many nuclear reactions and are extreme models for the fast and slow components of nuclear interactions.

In order that details may be obtained about these important limiting cases, it is necessary to study reactions where one of the mechanisms is of considerably greater importance than the other. In the past few years, direct reactions have been investigated more extensively than those reactions involving the evaporative decay of a compound nucleus; in the literature there are comparatively few experiments reporting the details of statistical evaporation. Because of this, the present experiments were designed to examine the evaporative processes induced by 14.9MeV neutron interactions with medium weight nuclei and to compare these results with theory.

The isotope studied for this thesis was proton rich Ni^{58} and the reactions investigated were $Ni^{58}(n,p)Co^{58}$, $Ni^{58}(n,np)Co^{57}$, $Ni^{58}(n,d)Co^{57}$; all at 14.9MeV. In the next section the stage is set for the presentation of these experimental results by a brief summary of the relevant predictions of reaction theory. The following sections of this chapter review previous (n,p) investigations at 14MeV, the experimental techniques which have been employed by other investigators and the reasons which led to the choice of the present experimental arrangement.

Section (1.1.): Some Results from the Theory of Nuclear Reactions.

Compound Nuclear Reactions. According to the compound nucleus theory of reactions, (see Bl52), a bombarding particle which penetrates the surface of a nucleus is absorbed immediately to form an excited compound nucleus. The theory further assumes that the kinetic and binding energies of the incident particle are rapidly distributed throughout the compound nucleus causing it quickly to lose its identity amongst the other nucleons. After a life-time which is long, compared to a particular configuration of nucleons, the compound nucleus de-excites by emitting heavy particles or by interactions with the radiation field.

When the incident energy is such that many over-lapping levels lie within the energy spread of the incident beam, the decay of the compound nucleus may be treated by the statistical model of Weisskopf (We37). In this model it is assumed that as so many states are formed, it is permissible to take statistical averages over all possible configurations of the same total energy. A condition for the correctness of the model is that the lifetime of the intermediate system should be of sufficient length that thermodynamic equilibrium can be established over all the available degrees of nuclear freedom. Under these circumstances the expected energy spectrum for each type of decay particle is close to a Maxwellian distribution; a consequence of the rapid increase with energy of the level density of the residual nucleus.

Weisskopf has formulated the spectrum of particles evaporated from a compound nucleus as:

$$N(E)dE = \text{const.}\, E.\, \sigma_c(E).\, W(E_x).\, dE \tag{1}$$

where $N(E)dE$ is the number of particles emitted with kinetic energy between E and (E + dE)

$\sigma_c(E)$ is the cross-section for the inverse reaction which forms the compound nucleus by a collision of the emitted particles, of energy E, with the excited residual nucleus.

$W(E_x)$ is related to the density of states of the residual nucleus at the excitation energy, E_x.

All of the $\sigma_c(E)$ which have been calculated, to date, refer to the residual nucleus in its ground state. This proceedure would be correct for a black-nucleus model but it is not necessarily so for a complex potential as the parameters might be expected to vary with nuclear excitation. Another point which must be considered is the diffuseness of the nuclear surface as this would allow of easier penetration than the conventional square well with sharp boundary.

$W(E_x)$, the effective level density, is not necessarily the total density at E_x. Rather, it is the density of states whose angular momentum is small enough to have been brought in by the incident particles. Bethe(Be37) has shown that for a Fermi gas of nucleons contained within a box, the level density will be given by:

$$\bullet \quad W(E_x) = const'.\, E_x^{-2}.\, e^{2\sqrt{aE_x}}$$

If the maximum excitation, E_{max}, is considerably greater than the average energy of the particles the exponential may be expanded as a series and equation (1) reduces to:

$$N(E)dE = const''.\, \sigma_c(E).\, E.\, e^{-E/\sqrt{\frac{E_{max}}{a}}} \qquad (2)$$

This is a Maxwellian distribution with a temperature

$$T = \sqrt{\frac{E_{max}}{a}}$$

Experimentally, the temperature can be found from

$$\frac{1}{T} = -\frac{d}{dE}\left(\ln \frac{N(E)}{E.\,\sigma_c}\right) \qquad (3)$$

A number of experiments have indicated that T only varies slowly with excitation energy, instead of

$$E_x = aT^2$$

Indeed, some experimental data reviewed by Peaslee (Pe55) suggested that in some reactions the nuclear temperature decreased, rather than increased, with greater excitation.

Using statistical theory, Le Couteur and Lang (Le59) have recently analyzed a number of experimental results for the evaporative decay of compound nuclei excited from a few MeV to 100MeV. These workers plotted "a" as a function of mass number and their conclusions were that, while shell effects are apparent, the overall level density suggested by the Fermi-gas model is a reasonable approximation to that of actual nuclei.

Angular Distribution of Products. A fundamental postulate of the statistical model is that a sufficiently large number of states are involved so that all interferences average to zero. Because the orbital angular momentum brought in by the incident particles lies in the plane normal to the incident beam and because the angular momentum vector precesses negligibly during the lifetime of the compound nucleus, the emitted particles are symmetrically distributed about $\theta = 90^{\circ}$ (see Wo51; Ch57). If, however, the statistical assumptions are not fulfilled and the number of states is not sufficiently great to cancel all interference, fore and aft assymetries can be present even in the compound nucleus model.

It has become fashionable to ascribe to non-compound nucleus modes the forward peaking which is aften found in angular distributions. While this is undoubtedly correct in most cases, forward anisotropy is still possible, within the framework of the statistical model, if there is an incomplete cancellation of phases. It would be expected, however, if this were the sole explanation for the observed anisotropies, that there would be a comparable number of instances where maxima in the backward hemisphere are observed. This does not appear to be the case, although practical problems make it difficult to observe many reactions near to $\theta = 180^{\circ}$.

It has sometimes been stated that the random phase assumption of the statistical model implied isotropy. Recently, Douglas and MacDonald (Do59) have examined this point using a level-density of the form:

$$W(E, I_B) = W(E)(2I_B + 1)\exp\left\{\frac{-(I_B + \frac{1}{2})^2}{2\sigma^2}\right\}$$

$2\sigma^2$ is a nuclear constant which has the effect of limiting the maximum angular momentum available to the compound nucleus.

Their calculated angular distributions were symmetric about $\theta = 90^{\circ}$ for $Cu^{63}(n,p)$ and $Fe^{54}(n,p)$ at 14MeV but showed anisotropies as great as 1.9 between $\theta = 0^{\circ}$ and $\theta = 90^{\circ}$.

In the years since the statistical theory was suggested, various experiments have been performed to check the applicability of the model (see Ki57a; Le59a). The available evidence indicates that when a compound nucleus is formed in the region of overlapping states the decay is indeed independent of the mode of formation. However, there is also considerable evidence that many reactions go by other routes than through a compound nucleus (see, for some examples: Bu51; Pa53; Ba54; Co54; El54; Gu54; Co57a; Co57b; Fu58; Au60).

Direct Interactions. Over the last decade, the alternative direct interaction model has been used, successfully, to explain many features of reactions which cannot be understood on the basis of a compound nucleus model. In contrast to the statistical theory, where the intermediate nucleus is assumed to be long-lived and to have available a large number of degrees of nuclear freedom, direct interactions are thought to be of short duration and to connect the initial and final states by comparatively simple transitions without the intervention of a compound nucleus. In its extreme form, the model views a reaction as a direct transference of the bombarding particle and the struck nucleon to their final states, with the remaining particles of the target nucleus playing the role of passive spectators. While direct interactions have provided explanations for several problems of the compound nucleus theory, (Pa53; Co54; Co57c; Gl59; Au60), the most widespread application of direct processes has been toward understanding the persistent forward peaking of many angular distributions.

A semi-classical arguement has been advanced by Butler (Bu58) to explain the lack of symmetry in angular distributions from direct interactions. When a reaction takes place the change in momentum, Δp, is given by:

$$\Delta p = h(\vec{k}_i - \vec{k}_f)$$

where $\vec{k}_i$ and $\vec{k}_f$ are the wave vectors of the initial and final particles.

If a definite impact parameter, r_o, can be assigned to the reaction the change in orbital angular momentum, ΔL , between the incoming and outgoing particles will be

$$\Delta L = h r_o . (\vec{k}_i - \vec{k}_f)$$

or $l = |\vec{Q}| . r_o$

where $\vec{Q} = \vec{k}_i - \vec{k}_f$

and $l = \Delta L / h$

where $h\vec{Q}$ is the momentum transferred to the final nucleus.

As l may only be an integer, the angular distribution is only expected to have maxima when $|\vec{Q}|. r_o$ has integral values. Furthermore, l is limited by the selection rules of angular momentum and parity so that there are available even fewer angles for which the angular distribution is a maximum.

The earliest evidence for the importance of direct interactions came from the deuteron stripping reactions,(d,p) and (d,n). In these reactions it is thought that a nucleon is torn from the incident deuteron and absorbed into the target nucleus leaving the remaining component of the deuteron relatively unaffected. Butler (Bu51) has shown that, if a definite radius can be assigned to such reactions, momentum conservation causes a correlation between the angular distribution pattern and the changes in parity and angular momentum between the initial and the final states. As a result of this, the deuteron reactions have proved valuable in the study of nuclear spectroscopy (Aj59).

Recently, J.B. French has pointed out that important information can be obtained about nuclear states by making comparisons between the measured deuteron stripping intensities and the reduced widths which have been calculated on the basis of particular nuclear models(Mc60). These comparisons depend upon the stripping reduced width being factored into a product of two probabilities: one, that the nuclear wave-function will be found in the same configuration as the final state; the other, that when this happens, the two components will actually separate. A knowledge of these probabilities will allow comparisons to be made between calculated wave-functions and actual nuclei. Unfortunately, simple stripping transforms usually predict excessive cross-sections and do not always determine correctly the angular momentum transfer. For this reason, comparisons cannot yet be made between reactions that do not involve closely related states; however, considerable successes have been achieved in comparisons between similar configurations calculated according to the shell model. Preliminary calculations of stripping cross-sections, using distorted waves rather than the plane-wave approximation of Butler, indicate that significant improvements in the theory are likely and that more general use of the reduced width formalism may be possible. Because of this it would appear to be important to measure absolute differential cross-sections for stripping and pickup, throughout the periodic table.

Glendenning (Gl59) has pointed out that direct nucleon-nucleon reactions might be expected to occur predominantly in the nuclear surface in the same manner as deuteron reactions. It is pointed out that, because of the Pauli principle, a nucleon entering a nucleus cannot interact with a bound nucleon unless both can be scattered into unoccupied states. This is most easily achieved for loosely bound nucleons which are thought to exist near the nuclear surface. A consequence of this surface effect (Au53; Bu57b; Ha57a; Au60) is that when transitions take place to definite states of the residual nucleus, the angular distributions should be of the form:

$$\sum_{\ell} a_{\ell} j_{\ell}^{2}(Q.R)$$

$$|\vec{J}_f + \vec{J}_i|_{MIN} \leq \ell \leq |J_f| + |J_i|$$

ℓ is $\begin{Bmatrix}\text{odd}\\ \text{even}\end{Bmatrix}$ if $\begin{Bmatrix}\text{a}\\ \text{no}\end{Bmatrix}$ parity change occurs

As the mean free path of a nucleon within nuclear matter is preater than that of deuterons of the same energy (Au60), the interaction radius for nucleon-nucleon reactions is less well defined than for deuteron reactions. While this increase in diffuseness of the interaction radius does not eliminate forward peaking, it does blurr the details of the angular distributions so that the patterns are less characteristic of the angular momentum transferred than are the stripping distributions for deuteron interactions.

Weisskopf and his co-workers (Fr55; We57) have suggested that all reactions have some direct features; even when a compound nucleus is formed, the incoming particle moves, initially, in the optical potential of the target nucleus and, upon entering the nuclear field, does not immediately establish a compound system. In the primary stage of such reactions it is thought that direct interactions take place, within the limitations of the Pauli Principle, and that these collisions become progressively more complex until a classical compound nucleus is established. According to this view, compound nuclear reactions should be thought of as a three-stage process, with the first stage a formation period, rather than according to the two-stage model of Bohr where a compound nucleus is established immediately. An important difference between the models is that, while the compound states of both can decay according to the rules of the classical compound nucleus theory, de-excitation can also take place during the formation period of a three-stage reaction giving rise to direct components in the cross-section.

To date, investigations aimed at predicting the details of direct nucleon-nucleon interactions have assumed that the levels of the residual nucleus are discrete and that they have a definite spin and parity. Little work has been done to predict the details of interactions where the final states are ill-defined or overlapping. One calculation by Brown and Muirhead (Br57a) for such interactions used a Monte-Carlo routine to follow particle collisions throughout a Fermi-model nucleus. It was assumed that the incoming nucleon made collisions with the nucleons of the target exciting these to unoccupied states. The excited nucleons, in turn, were assumed to give rise to interaction cascades which become progressively more complex until the total energy was distributed over many degrees of nuclear freedom to establish thermodynamic equilibrium. The results of the calculations were found to be in reasonable agreement with some experimental (n,p) data at 14MeV if the assumtion was made that particle de-excitation of the system could take place at any time throughout the reaction, both before and after formation of the compound nucleus. This work gives support to the three-stage model of reactions and also gives evidence that the compound nuclear and direct interaction mo models are merely limiting examples of the fast and slow components of any nuclear reaction.(1)

(1) See further remarks and experiments on this point which are reported in International Conference on Nuclear Structure (Kingston, 1960). Editors, Bromley, D.A. and Vogt, E.W.

Section (1.2.): Previous Charged Particle Investigations at 14MeV.

Because of experimental difficulties, extensive studies have not yet been made on the charged particles from 14MeV neutron interactions. However, the relatively high excitations available and the relative ease of generating intense fluxes of these monoenergetic neutrons make the investigations attractive.

The detection of charged particles from fast neutron reactions poses special problems for the experimenter. First, the intensity of the particles is low and the range of energies is broad. Secondly, because of the high penetrability of neutrons, an intense flux usually passes through the detector elements inducing background reactions which obscure the desired events. These technical difficulties have allowed only two techniques of charged particle spectroscopy to be widely employed for recording (n,p) spectra: (i) Nuclear Emulsions; (ii) Counter Telescopes.

I. Nuclear Emulsion Experiments. The methods used in emulsion experiments with fast neutrons have been well described in the literature (Al57; Al58; Ku60). A major disadvantage of the technique is the necessity for scanning the exposed plates with a high-power microscope to identify individual events and to separate them from the background of recoil proton tracks which originate throughout the volume of the emulsion. This tedium of analysis has often been apparent from the poor statistical accuracy which has been achieved. A further criticism of the technique is the infeasibility of using grain counting methods to distinguish between low energy proton tracks and low energy deuteron tracks (A157). Such particle identification is important as it was shown in this work, and also by Colli et al. (Co59a; Co59c), that a significant number of deuterons are emitted, with protons, from 14MeV neutron interactions.

The first work on the protons from neutron interactions was reported by Allan who has used emulsions in a series of experiments on Al^{27}; Fe^{54}; Fe^{56}; Ni^{58}; Ni^{60}; Cu^{63} (A155; A157; A158; A159). The experiments with Fe^{56} and Cu^{63} are particularly praise-worthy as approximately 20,000 events were measured for each isotope and good statistical accuracy was obtained. It was found that many of the proton energy distributions had the shape of evaporation spectra but a maximum in the distribution which was often well below the accepted height of the Coulomb Barrier. This apparent lowering of the barrier was most noticeable for neutron deficient isotopes, where the binding energy of the final neutron may be several MeV greater than that of the final proton, and Allan suggested that many of the low energy protons were contributed by (n,np) processes. Although the greater part of the proton emission cross-sections appeared to be a consequence of evaporative de-excitation of a compound nucleus, the results indicated some direct interactions: the spectra which were recorded in the forward direction from some nuclei showed evidence of discrete groups; and gross angular distributions, obtained for each 2MeV interval, showed forward peaking above 6MeV.

The Glascow group, (Br57; Ma58a; Ma58b; Ma58c) have measured the protons from 13.9MeV neutron interactions with Al^{27}; Fe^{54}; Fe^{56}; Rh^{103}. Good evidence for discrete energy groups was presented for $Al^{27}(n,p)Mg^{27}$, the peaks in the proton spectra corresponding to known levels of the residual nucleus, Mg^{27}. Although the results from the medium weight nuclei bore a strong resemblance to those reported by Allan, the presence or absence of structure could not be confirmed as only 1,500 tracks were analyzed for each of the isotopes.

Overseth and Peck (Ov59) used emulsions within heavy shielding to record protons from $Al^{27}(n,p)Mg^{27}$ and to measure the angular distribution of the resolvable groups. While their results suggested transitions to several levels of Mg^{27}, their data and its interpretation is questionable for two reasons: first, the collimated neutron spectrum at the target foil appears to have been contaminated by elastic and inelastic neutrons from the massive shielding so that the flux was no longer monoenergetic (see Pe57); secondly, the recorded intensity of protons from the target foil increased with proton energy in the energy region forbidden to proton emission by the Q-value for the reaction; a possible explanation for this curious behaviour could be contamination of the recorded spectra by recoiling protons from the hydrogen content of the emulsion.

Since the completion of the present work Kumabe and Fink (Ku60) have published the spectrum of protons from $Ni^{58}(n,p)Co^{58}$ at 14MeV. Some forward peaking was observed but this was almost entirely at proton energies below 7MeV making identification with a direct process doubtful. The angular distributions below 4MeV were found to show a minimum at $\theta = 90^{\circ}$. However, as only 1,500 events were analyzed at all angles of observation, the statistical accuracy of the experiment was poor and the results must be treated with reserve.

II. Coincidence Telescope Experiments. The counter technique which has met with the widest success in (n,p) studies utilizes the coincidence telescope. Telescopes eliminate the neutron induced background by recording events only when a specified combination of coincidence/anticoincidence conditions are fulfilled by several independent detectors arranged along the trajectory of the emitted particles. A common construction consists of two proportional counters for dE/dx measurements and an inorganic scintillation detector for kinetic energy measurements (see Ri54). Energy pulses are not recorded unless all the detector channels provide coincidence signals within $2T \sim 1\mu S$. Design considerations and the detailed operation of these instruments have been well described by Johnson and Trail (Jo56) and Bame et al. (Ba57).

The Milan group, Colli, Facchini and others, have reported the details of three coincidence telescopes, each being an improvement on its predecessor. The most recent instrument(Ma58c) included an ingeneous anti-coincidence counter for eliminating events originating in the target backing and the walls of the telescope. However, the instrument had poor angular resolution and also had a high background counting rate for protons of energy below 4MeV. Equally important was that when $\theta = 90^{\circ}$ the neutron flux to the target had to enfilade a massive vacuum flange. It is possible that absorption and scattering of the incident flux by this flange could explain the minima in the angular distributions which were reported for Cu, Ni, Mo, Ag, (Co59). Much of the work of this group has been measurements of energy spectra at forward angles, using targets of natural isotopic abundance. The elements studied include Mg, Al, Si, S, Sn, Fe, Ni, Cu, Zn, Mo, Ti, Rh, Ag, Ta and Au (Ba56; Co56 - Co59; Fa60). Within the limitations of the experiments the distributions were found to be similar to those reported from emulsion work. However, background difficulties prevented measurements below 4MeV and some evaporation maxima from medium weight nuclei could not be seen. An important contribution from this group has been the recent observation of prominent peaks in the energy spectra from Mg, Al, Si and S which they attributed to deuteron emission (Co59a; Co59b; Co59c).

Eubank and Peck have published angular distribution measurements for $S^{32}(n,p)P^{32}$ and Sb(n,p)Sn; (Eu58; Pe59). Unfortunately, insufficient details have been presented to allow of a critical evaluation of the experimental techniques. However, a thick target of sulphur gave a source to background ratio of unity or less (Pe58) which suggested that the counter telescope and its associated electronics had poor sensitivity.

Deuteron Emission from 14MeV Neutron Interactions with Medium Weight Nuclei. As stated earlier in this chapter, pickup reactions are of interest as they provide information about residual nuclear states. However, technical difficulties have prevented the detection of deuterons from 14MeV interactions until recently and it was only after the inception of the present experiments that deuteron emission was reported from medium weight nuclei; Colli et al. (Co59a; Co59c) and Velyukov (Ve60).

Section (1.3.): Experimental Arrangement of the Present (n,p) Experiments.

From the survey of (n,p) studies it can be seen that the present knowledge of these interactions is scanty. In the past, the major effort has been devoted to the measurement of energy spectra at forward angles and to obtaining crude angular distributions, often with targets of natural isotopic abundance, and few detailed investigations have been made. However, previous work has shown that it is possible to obtain information about

(i) The evaporative decay of excited compound nuclei

(ii) Direct interactions to overlapping as well as discrete levels of the residual nucleus

(iii) Partial cross-sections for the contributing reactions.

Clearly, to obtain the maximum amount of information it is essential that the experimental equipment be capable of measuring energy spectra and angular distributions with good resolution. Separation of deuteron producing reactions from proton reactions is desirable, not only to obtain information about the (n,d) interaction, but also to avoid confusion between discrete deuteron groups and (n,p) direct interaction effects.

An aim of the present work was to develop a counting technique which would allow the detailed study of (n,p) interactions for many isotopes.

Scintillating Crystals as Target and Detectors. One possibility which was considered was that of using inorganic scintillators as target and detector for neutron induced reactions. A similar technique had met with some success at Canberra where investigations on the photodisintegration of lithium, sodium and caesium by $Li^7(p,\gamma)$ gamma rays had been made using inorganic scintillators as target and detectors (Ma57; Op58a). Such a system has several advantages over the more conventional arrangement of a target foil and external detector:

(i) As the particles do not escape from the target, thick crystals may be used giving high counting rates for low cross-section reactions.

(ii) The detector has 4π geometry.

(iii) The electronic circuitry is trivial.

Chapter V discusses this technique in more detail and explains why, for the 14MeV neutron measurements, it was discarded in favour of a more complicated coincidence telescope.

<u>Coincidence Telescope</u>. Figure 1 shows the first satisfactory telescope constructed for this work. Charged particles, passing through both proportional counters and stopping within the CsI(Tl) scintillator, resulted in coincident signals from each of the channel amplifiers. Energy pulses from the scintillator were not recorded unless this coincidence condition was fulfilled.

The characteristics of this telescope were such that typical channel counting rates were many thousands per second, making chance coincidences a serious problem. It was found that a major portion of the random events arose from the background of charged particles which passed through two of the detectors, diagonally. Under these circumstances, two of the counters were automatically in coincidence and the random rejection was, essentially, only that of a two-fold system.

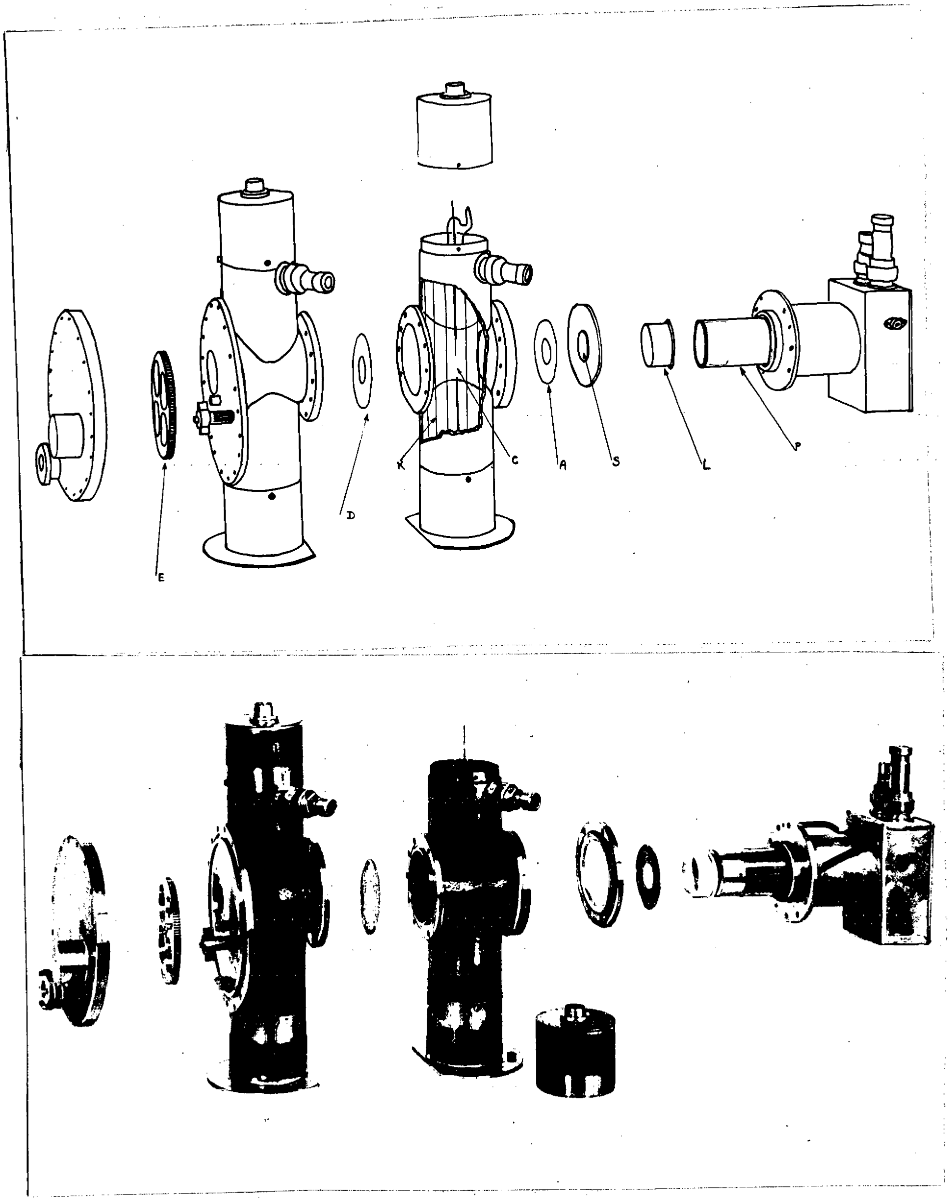

FIGURE 1: COUNTER TELESCOPE, MkI.

E	Target Foil Holder (four positions)
D	Non-defining Aperture
K	Cathode Wires
C	Anode Collection Wires
A	Defining Aperture
S	CsI(Tl) Scintillator
L	Perspex Light Pipe
P	Photomultiplier

For protons having an energy below 5MeV, the background rate was found to be significantly higher than that estimated by assuming reasonable interaction cross-sections for the telescope liners and for the target backing. Tantalum, platinum, carbon and lead were all tested for this duty but, after chance coincidences were eliminated, only slight changes were effected in the telescope background from one material to another. The conclusions reached were that the unexplained residual counts arose from both the charged particle reactions within the gas of the first proportional counter and also from reactions in the volume of the inorganic scintillator. Particles from both sources could travel through all detectors of the telescope giving rise to spurious coincidences.

Initially, it was thought that the backward-going protons from the scintillation detector set a fundamental limit on the smallest reaction yields which could be satisfactorily investigated. Later, however, it was realised that additional coincidence requirements could distinguish between the situation where a particle travelled towards the scintillation detector and that where a particle moved in the reverse direction. The experiments reported here satisfied these requirements by demanding that simultaneously with the detection of the reaction products, a neutron arrived at the target foil; this condition ensured that the reaction products which were recorded arose from interactions within the target foil.

Each neutron from a $t(d,n)He^4$ source is in time coincidence with an energetic alpha particle which is emitted within the conjugate solid angle. In this work, these alpha particles were employed to yield the instants of time during which neutrons could interact with the target foil and so permit discrimination against backward travelling protons. The manner in which the standard circuitry of a coincidence telescope was ammended to include this extra condition is shown in Figure 2. As the neutron flux into 4π was commonly of the order of 5.10^8 neutrons/second, millimicrosecond requirements were essential for the double coincidence arm; furthermore, it was necessary that the fast circuitry be capable of accepting alpha particle pulses at rates in excess of 5.10^6 counts/second.

An important supplementary function of the fast coincidence conditions was the automatic elimination of background reactions induced by scattered neutrons and by neutrons from sources such as $d(d,n)He^3$ and $C^{13}(d,n)N^{14}$. This rejection resulted as recoil particles from the neutron source, with the momentum necessary to satisfy the coincidence requirements, were not produced simultaneously with the background reactions.

<u>Particle</u> <u>Identification</u>. The previous sections of this chapter have stressed the desirability of recording, separately, the proton and deuteron spectra from 14MeV interactions.

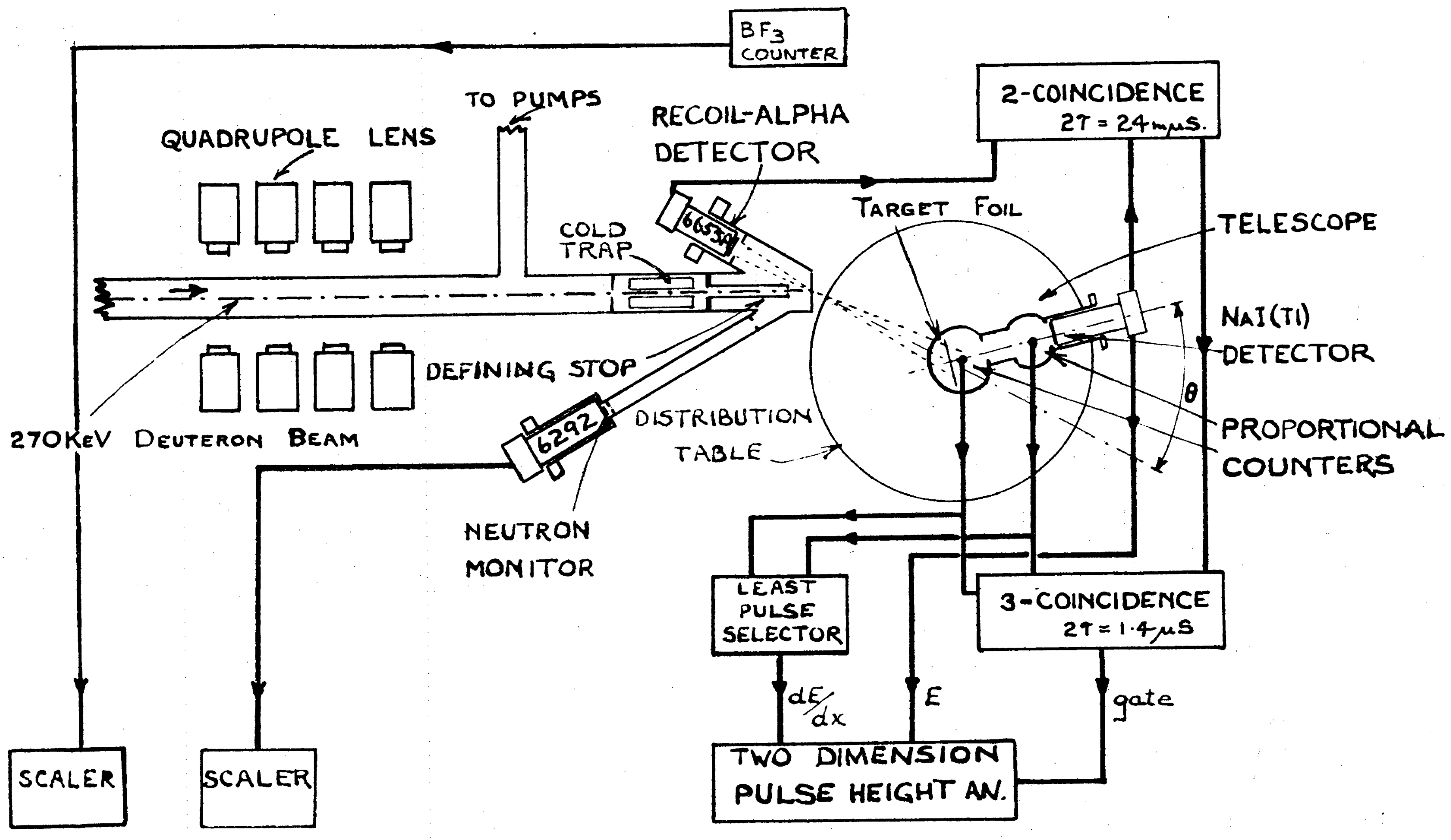

FIG. 2: OVERALL EXPERIMENTAL ARRANGEMENT.

To calculate the mass of a particle it is necessary to measure, together with the energy, some other related parameter of the motion such as the velocity or the momentum. With a counter telescope the auxillary quantity most readily available is the specific ionization, dE/dx. This measurement is useful as it is well known that the mass of a particle of given charge is approximately proportional to the product E.dE/dx. In the present work a photographic technique was used to record the energy and the specific ionization for each event; these records were later analyzed to supply proton and deuteron spectra.

As only small losses can be tolerated in a counter telescope for the dE/dx measurements, mass discrimination becomes unreliable with the E.dE/dx technique. This is due to Landau-Symon scattering of individual electrons within the gas of the proportional counters giving a high energy tail to the dE/dx spectrum (Ro52; Ig54). These high energy contributions may be largely removed if the outputs from the individual gas counters are passed through a least-pulse selecting circuit which transmits only the smallest pulse of those arriving simultaneously, at its input terminals (Ig54). The signal obtained by this technique is a better representation of the specific ionization than that from a single counter and such a system was used here to improve the separation between proton and deuteron events.

By its very nature, the mass identification system permitted strong discrimination against the random coincidences occuring between the various channels. This resulted, because the ungated spectrum of pulses from each of the three telescope detectors had a maximum intensity at zero energy making the most probable random event a small dE/dx pulse with a small E pulse. This combination is contrary to that expected from real charged particles where low energy is associated with large specific ionization and vice versa. This effect permitted a confident identification of random coincidences to be achieved and allowed the intensity of the neutron fluxes to be several times greater than would have been possible without random event identification. Furthermore, the virtual elimination of random coincidence at low energies allowed data to be collected in the energy range 1MeV to 4MeV; a region which has been inaccessible to previous counting experiments.

Chapter II is devoted to a detailed description of the design parameters of the equipment used and of the testing proceedures which checked its operation. Chapters III and IV describe the experimental data obtained and the analysis which was used to handle these results.

CHAPTER II

A DETECTION SYSTEM FOR CHARGED PARTICLES FROM REACTIONS INDUCED BY 14.9MeV NEUTRONS

Section (2.1.): A Survey of the Techniques used in the Present Experiments.

The arrangement of the experimental equipment used in these experiments is shown in the block diagram of Figure 2. A target foil of the isotope under study, having a thickness ~10mg/cm^2, was placed with one diameter along the vertical axis of an angular distribution table and within a cone of neutrons defined in space by detecting, in the conjugate solid angle, the associated alpha particles from the t(d,n)He^4 neutron source (see O"N54 and Ok58). Coincidences between the three channels of the counter telescope were not recorded unless, simultaneously, a recoiling alpha particle was detected.

To avoid unnecessary scattering of the tagged neutrons, the walls of the telescope through which the beam passed were of minimum thickness (0.015") consistent with resisting implosion by atmospheric pressure. The geometry of the walls of the telescope was such that the amount of neutron scattering varied only slightly with the angular position of the axis of the telescope and at all angles was less than 2%. In order that angular distributions could be measured in the backward hemisphere at large positive and negative angles, transverse extensions to the counter were minimized by the use of a vertical holder for the target foil and test radiators. While this design presented greater mechanical difficulties than the conventional target wheel, its use here allowed angular distributions to be obtained to 150° in one direction and to 125° in the other.

The shortest time resolution which could be employed in the fast circuitry was set by the variations in the times of flight of particles along the telescope axis. It was desirable to be able to record proton events having energies ranging from 1MeV to 16MeV corresponding to times of flight along the telescope of 16mμS and 4mμS; thus, the resolving time could not be shorter than 12mμS. Fluctuations in the electron collection times within the gas of the proportional counters introduced time jitter to the slow circuits so that the minimum time resolution of the slow circuitry was 1.2μS.

Electronic circuits which will provide an output proportional to the product E.dE/dx have been discussed by several authors(Ch49; Br58; St58). However, either these circuits provide inadequate accuracy or they appear to be of such complexity that they were not suitable. Furthermore, once an event has been analyzed on the basis of the output from such a device, it is usually not possible to reanalyze the data with different values of the product E.dE/dx. For long experiments involving low counting rates this loss of information is undesirable and it would seem more useful to record the actual coincidence spectrum of E and dE/dx pulses. Two channel magnetic tape might be used for this purpose or alternatively, a two dimensional photographic technique (As55). The analysis of data recorded on photographic film tends to be slow, making it unsuitable for many experiments. However, in the present experiments this objection was not relevant as data taking extended over several hundreds of hours and allowed many opportunities for film analysis. An attractive feature of photography is its simplicity and reliability, compared with the alternative electronic circuitry.

Considerable care was taken when determining the neutron fluxes through the target foil to be sure that no systematic errors were affecting these measurements. Three completely independent monitoring systems were used. Two of these were absolute counters and the third, a BF_3 long counter, was used for consistency checks. One of the absolute counters detected, in known geometry, the recoil alpha particles from the $t(d,n)He^4$ source. The other employed the coincidence telescope itself, to count the number of recoil protons from a hydrogenous radiator of known mass at the target position. The parameters of both absolute monitors could be measured to an accuracy better than $\pm 3\%$ and when comparisons were made between flux determinations achieved by these two independent techniques, it was found that they agreed to better than 1%.

Section (2.2): Coincidence Telescope.

The important features of the telescope which was evolved for the present measurements are shown in Figure 3. Much of the counter was fabricated from 0.030" stainless steel tubing which has sufficient strength to withstand the forces from atmospheric pressure when it is evacuated but does not scatter neutrons significantly. To further reduce neutron scattering, the thickness of the walls, where the defined beam passed, was reduced to 0.015" and no vacuum flange was allowed to intercept the tagged neutron flux. Also, the foil holder and its vertical guides were pressed from tantalum sheeting having a thickness of 0.008".

It was necessary to have available a number of test radiators as well as the target foil for use in the preliminary setting up proceedures and in the tests which were made on the operation of the counting system during data taking. A typical complement of radiators which were sealed into the telescope included:

(i) Target foil plated onto 0.005" platinum.

(ii) Platinum blank for background measurements.

(iii) Polythene radiator for flux measurements and for energy calibrations.

(iv) Thick deuterated polythene radiator for checking the discrimination between proton events and deuteron events.

(v) Weak Po^{210} alpha particle source for measuring the gains of the proportional counters.

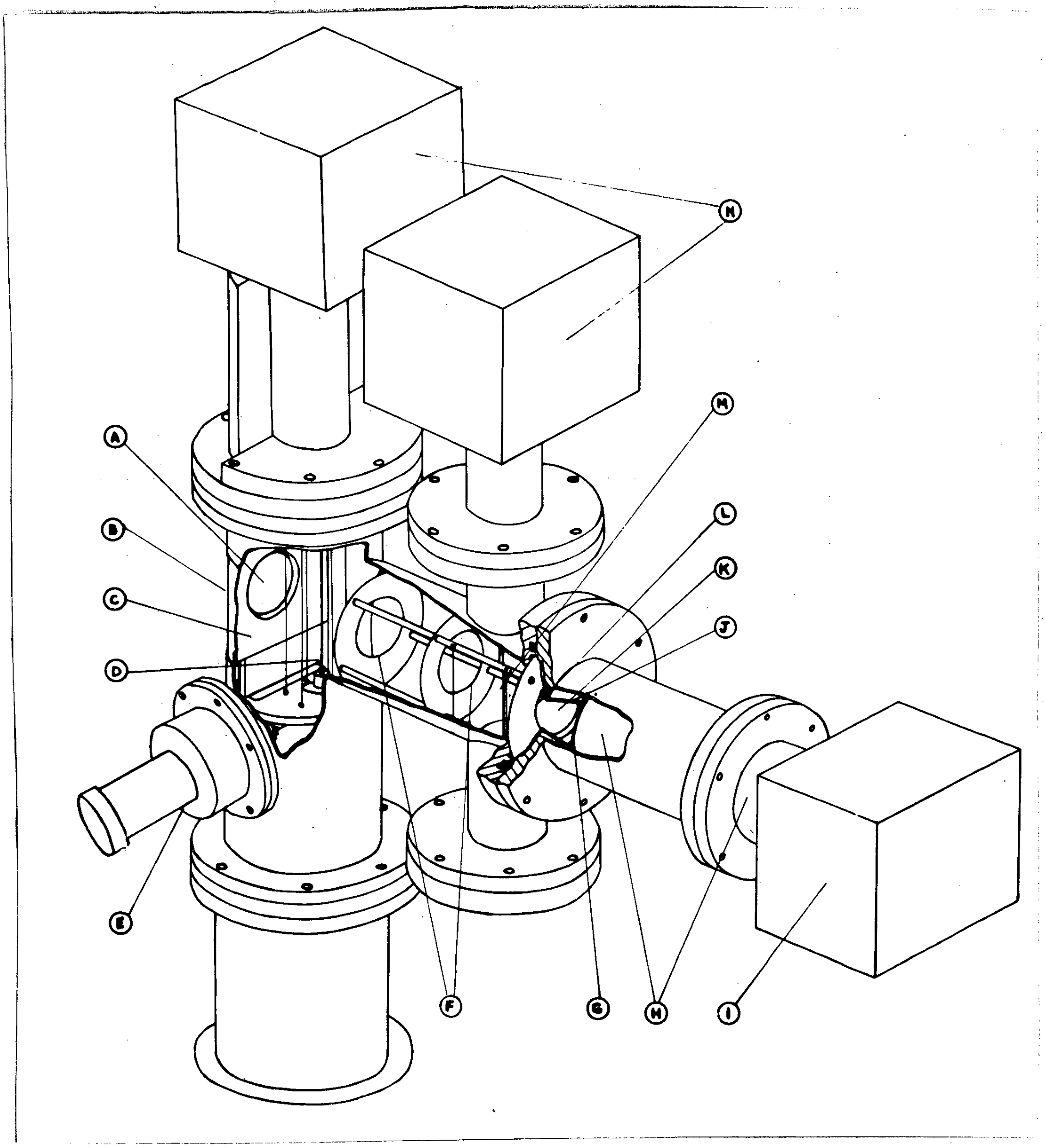

FIGURE 3: TRIPLE COINCIDENCE TELESCOPE, MkII.

A	Target Foil (10mg/cm^2)	H	Photomultiplier
B	0.015" Wall Section	I	White Cathode Follower
C	Platinum Liner	J	Reflecting Cone
D	Proportional Counter I	K	150µg/cm^2 Gold Foil
E	Target Strip Drive	L	Defining Aperture
F	Intermediate Aperture	M	Proportional Counter II
G	NaI(Tl) Scintillator	N	Head Amplifier

A sprocket which engaged with the target strip allowed the radiators to be changed. The drive for this sprocket was transmitted through the walls by a double O-ring seal (see Figure 4) which was used to avoid small gas leaks of the sealed-off proportional counters. In the original design a magnetic coupling was used making O-rings unnecessary. However, this design was discarded when gain shifts in the photomultiplier channel were traced to varying residual magnetic fields from the iron armature.

The number of chance coincidences where charged particles travelled diagonally through both proportional counters but not through the scintillator was reduced by the dead space between the two intermediate apertures. This space reduced the solid angle subtended by each proportional counter at the other.

Geometry. The essential defining apertures of the present experiment are shown in Figure 5. A neutron from the source at (x_o,y_o,z_o) may strike the target foil at any point (x_1,y_1,z_1) and, if the reaction is to be detected, the reaction products must pass through the defining aperture at (x_2,y_2,z_2). Because the incoming neutron may interact at any point within the target foil and the emitted particle may pass anywhere through the final aperture, the angle θ', between the incoming neutron and the emitted proton is, in

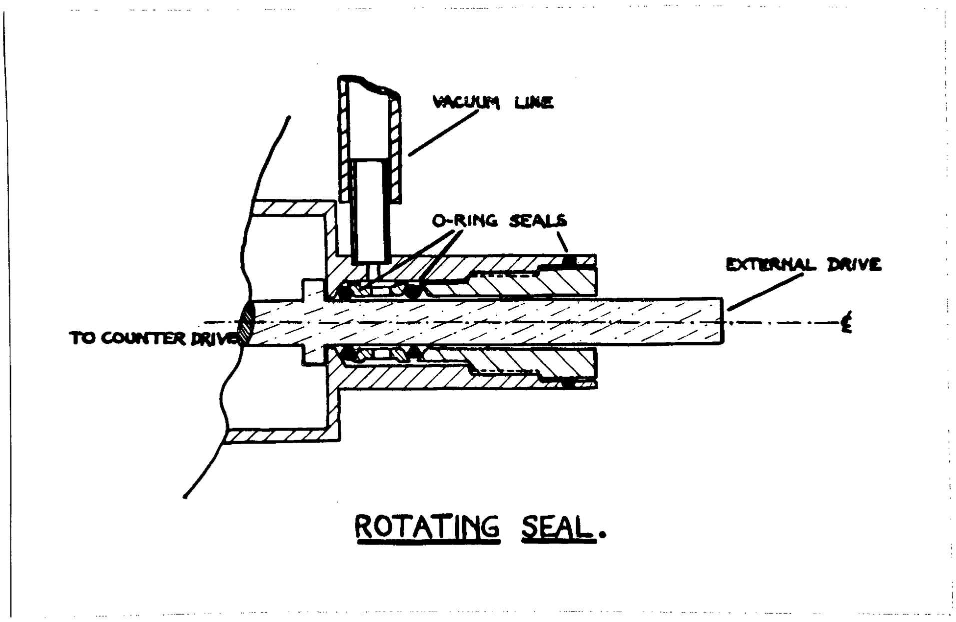

FIGURE 4: DOUBLE-SEAL FOR TARGET-STRIP DRIVE.

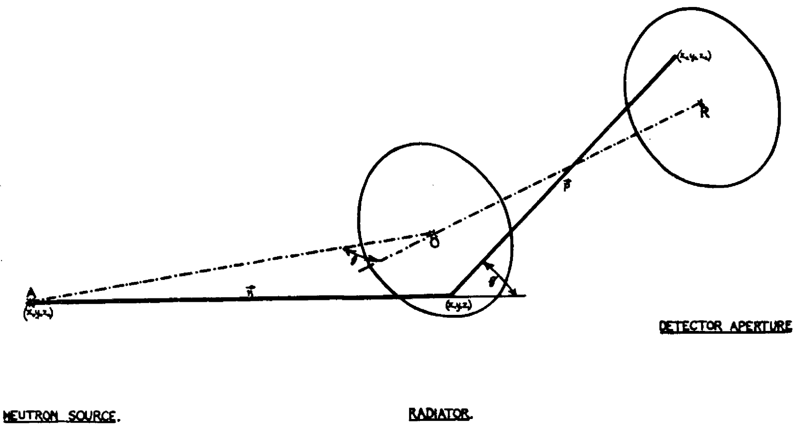

FIGURE 5: ESSENTIAL DEFINING APERTURES OF A COUNTER TELESCOPE.

general, not equal to the angle θ between the line joining the centre of the radiator to the neutron source and the axis of the counter. The spread in θ' fixes the angular resolution of the telescope and while this may be improved by reducing the diameter of the defining apertures, the ever-present demands of a workable counting-rate establish a practical lower limit below which the aperture cannot be reduced.

In the present telescope the following dimensions were used:

(i) Target diameter . . . . 1.12"

(ii) Neutron Source to Target Foil . . 5.25 ± .05"

(iii) Final Defining Aperture . . . . . 1.000 ± .003"

(iv) Target Foil to Final Aperture . . 5.95 ± .1"

An analytical calculation of the angular resolution as a function of θ involves considerable mathematical difficulty due to the necessity to evaluate a complicated integral. This difficulty was avoided here by programming the high-speed digital computer SILLIAC to make a Monte Carlo calculation for the system. In this calculation a large number of randomly selected events were traced through the counting system from neutron source to final detector to give the angle of scattering.

At every stage of the calculation, the model used exactly resembled the physical arrangement of the counting system. For example, experimentally, the coordinates of a detected particle were undetermined within the limits of the final aperture; in the calculation the corresponding situation was represented by randomly selecting the coordinates (x_2, y_2, z_2) for each of the events.

Three sets of position coordinates (x_0, y_0, z_0), (x_1, y_1, z_1) and (x_2, y_2, z_2) defined the trajectory of each event through the counter. (x_0, y_0, z_0), the coordinates of the neutron source with respect to the origin, O, was determined from the distance OA and the angle θ. The coordinates of the position of the reacting nucleus, $(x_1 y_1)$, within the target foil, were chosen randomly and in such a manner that any elementary area of the target foil had a constant probability of being used. (x_2, y_2), the point where the particle passed through the detector aperture, was chosen in the same way. The random numbers used in the calculation were generated by a sub-routine based on the mid-square method of Von Neumann (Me54). Because the neutron flux was not constant over the whole radiator, ($1/D^2$ attenuation), a correction term was introduced. A further small correction was necessary as the distance a neutron travels within a target varies with its angle of incidence.

The angle between the neutron and proton momentum vectors ($\vec{n}$ and $\vec{p}$) was calculated from the well-known identity:

$$\cos\theta' = \ell\ell' + mm' + nn'$$

where $\ell, \ell', m, m', n, n'$ were the direction cosines of the vectors $\vec{n}$ and $\vec{p}$. After 1,000 events had been followed through the system, the number falling within each half degree of was printed out. Figure 6 shows the smoothed results of this calculation after it has been multiplied by the appropriate constants to give a solid angle of acceptance.

Gas Counters. Basically, standard techniques were used when designing the proportional counters which were operated with a gas gain of approximately 10. The cathodes were cylinders of diameter, $2^1/_8$", defined by a ring of earthed wires. The central collection wire in each counter had a diameter of 0.008" and was maintained at a potential of approximately 1,000 volts. The sensitive length of the wires was limited to $1^3/_8$" by 0.030" sleeves which were threaded over the wire. These sleeves prevented gas multiplication where it was not required and minimized the singles counting rate from argon recoils and the stopping of slow electrons. The large diameter of the collector wires, compared to the diameter conventionally employed, allowed a more intense electric field within the gas and an improvement in electron collection time.

The gas used in the proportional counters consisted of a mixture of 90% argon and 10% carbon dioxide at a pressure of 11.0cm.Hg. This composition was chosen after a

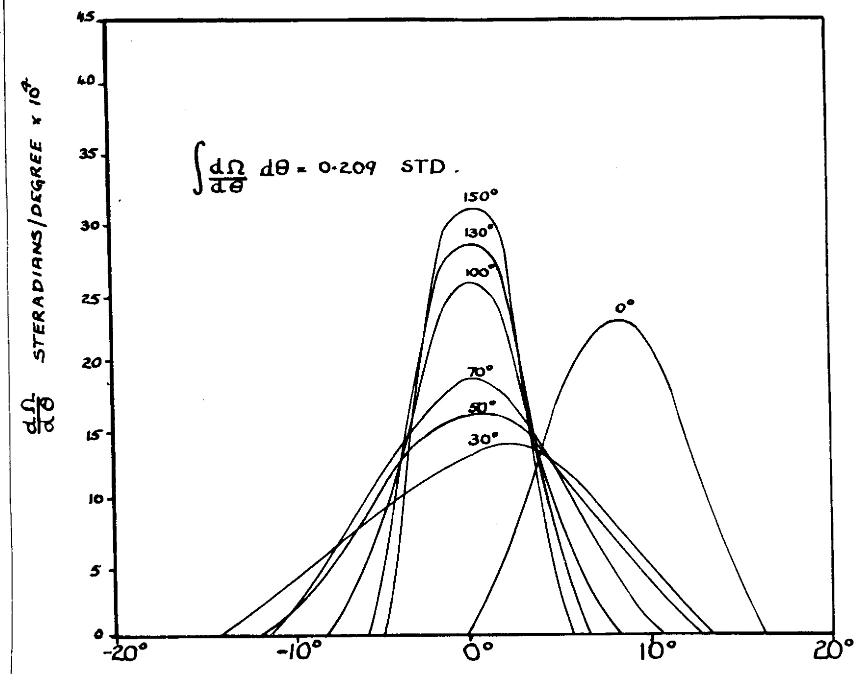

FIGURE 6: TELESCOPE ACCEPTANCE ANGLE.

series of measurements had been made on the collection speed and resolution of various argon/CO_2 combinations. For the mixture used here, an energy resolution was obtained of 9% full width at half height for the specific ionization pulses from Po^{210} alpha particles. The measured collection time was $\approx 1.3 \mu S$, in agreement with the results of English and Hannah(En53). Water vapour and oxygen impurities were removed from the argon by bubbling the gas through NaK, an alloy of sodium and potassium which is liquid at room temperatures. The carbon dioxide was purified by careful sublimation from solid CO_2 from which gaseous impurities had been removed by vacuum pumping.

As a precaution, lead gaskets were used wherever possible to reduce counter poisoning, rather than rubber O-rings. However, even with this precaution, persistent gain drifts were traced to outgassing from the counter walls. Unfortunately, baking the counter under vacuum was not possible and calcium purifiers (Ro49) had to be dismissed because of reactions with the CO_2 in the gas mixture. The solution which was adopted was the installation of a 20litre gas reservoir through which the counter gas was circulated continuously by a thermal pump. After the installation of this reservoir gain variations in dE/dx were observed to be less than $\frac{1}{2}$% per day.

Scintillation Detector. The energy detector in which the particles stopped was a NaI(Tl) disc, having a diameter of $1\frac{1}{2}$" and a thickness of 0.065". The crystal blank was roughly sawn in air and then lapped and polished to size in a drybox maintained at less than 5%R.H. Before mounting, the surface layers were removed by submerging the crystal for a few seconds in dry ethyl alcohol and finally in dry chloroform. The NaI(Tl) was mounted directly on the photocathode surface of a DuMont 6292 photomultiplier with no oil or cement as an optical coupling. In an effort to improve light collection both oil and epoxy resin were tested; however, at the vertical interface, even the most viscous oil failed to provide a stable coupling under vacuum and cement proved to be unsatisfactory because of slight opacity.

The light flashes from the scintillator were spread uniformly over the surface of the photocathode by a light-collection system similar, in principle, to that of Souch and Sweetman (So58). The system incorporated a truncated cone, coated with MgO on its inner surface, which sat over the crystal and the photomultiplier face. This technique consistently gave resolutions better than 5.5% for recoil protons from a thin hydrogenous radiator.

Section (2.3.) Electronic Circuitry.

The electronic equipment provided gating signals for the analyzers and allowed events to be recorded when specified coincidence conditions were fulfilled. Figure 7 is a block diagram of the interconnections between the individual circuits. Figure 8 shows the waveforms within the slow circuitry.

Amplifiers. Each of the telescope channels was pre-amplified at the target area and fed to a Fairstein DD2 amplifier (Fa56) in the counting room. The characteristics of the DD2 amplifiers included a high gain variable over a wide range, low noise, good stability and excellent overload characteristics. Their non-blocking feature was essential in the proportional counter channels as argon recoils provided pulses up to fifty times as great as the specific ionization pulses from a 15MeV proton.

The linearity of the electronic circuitry was checked by feeding the output from a precision pulse generator to the inputs of the channel amplifiers. The results of these measurements showed that any non-linearity in the scintillation channel amplifier was less than 1%. A more comprehensive check on the energy measurements was made by mounting a 2" x $1\frac{1}{2}$"NaI(Tl) detector on the photomultiplier and measuring the position of the photpeaks from several gamma rays.

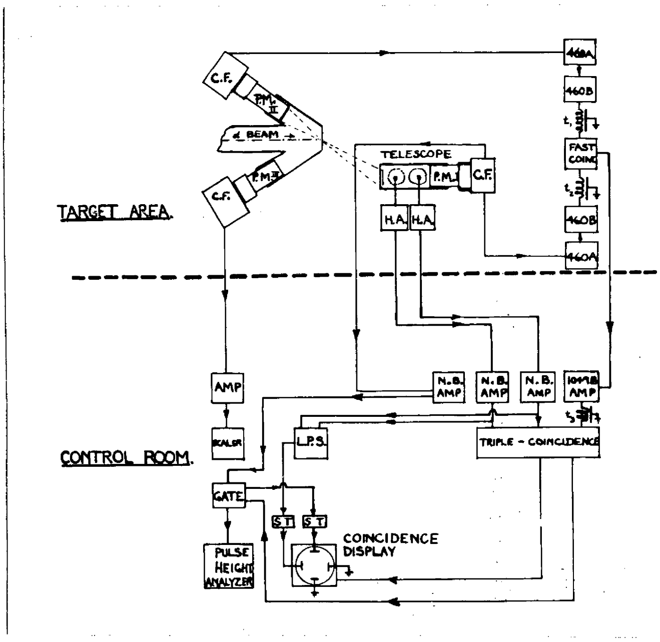

FIGURE 7: BLOCK DIAGRAM SHOWING THE ARRANGEMENT OF THE ELECTRONIC CIRCUITS.

P.M.	Photomultiplier
C.F.	White Cathode Follower
H.A.	Proportional Counter Head Amplifier
N.B.	Non-Blocking Amplifier
L.P.S.	Least Pulse Selector
S.T.	Stretcher Circuits
t_1 - t_3	Time Delays

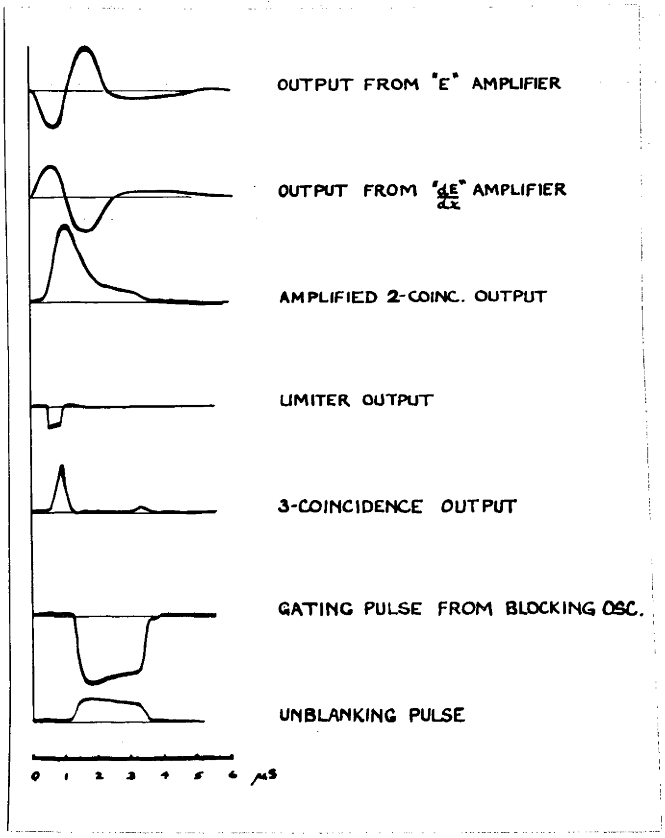

FIGURE 8: WAVEFORMS WITHIN SLOW CIRCUITS.

Mains noise proved to be an exasperating problem because of its very triviality. Unwanted coincidences from this source were finally eliminated by introducing line filters at each amplifier, D.C. heating on all circuitry and extensive shielding of the amplifiers and their first clipping line. Pickup, between the target room and counting area, was reduced by double shielding of the connecting cables. When these precautions were complete spurious counts were reduced to less than one count every two hours.

<u>Fast Coincidence</u>. The timing signals which were used to tag the neutrons in the defined beam originated as current pulses from the final dynode of P.M.II. These signals were amplified* and fed to one input of a gated beam type coincidence circuit having a resolving time of $2T \approx 24$muS. The other input was the amplified signals from the final dynode of P.M.I.

The fast circuit used here was an adaption of that reported by Fisher and Marshall (Fi52). Conventional limiters (Le54) were used to shape the signals from the distributed amplifiers and apply narrow (≈ 12mµS) positive pulses to the grids of a 6BN6 gated beam tube. 6BN6 operates as a series coincidence element (Bo29) and circuits employing this

---

*Hewlett Packard Co.'s Distributed Amplifiers 460A and 460B in tandem.

tube are superior to many other arrangements as they are very reliable, have a high coincidence/singles output and can be made capable of handling extremely large counting rates in one channel. In the present circuit the coincidence/singles ratio was $\sim$5 and ~~it~~ the circuit operated satisfactorily with alpha particle counting rates in excess of 5×10^6 c/sec.

Slow Coincidence. The function of the triple coincidence was to supply intensifying pulses to the coincidence analyzer and gating pulses to the kicksorter which would allow selected events to be recorded. The circuit of the arrangement used is shown in Figure 9. Three fast pentodes (E180F) were arranged as limiters with their grids 5volts or more negative. A positive signal arriving at a grid resulted in a negative signal from the anode with a width determined by the anode clipping line. The triple coincidence section is a modification of a coincidence arrangement suggested by Garwin(Ga50; Ga53). The circuit has a very high rejection ratio of singles to coincidence events and is similar to the familiar Rossi parallel circuit except that the non-coincident signals are eliminated by the clamping action of the diode in the plate circuit.

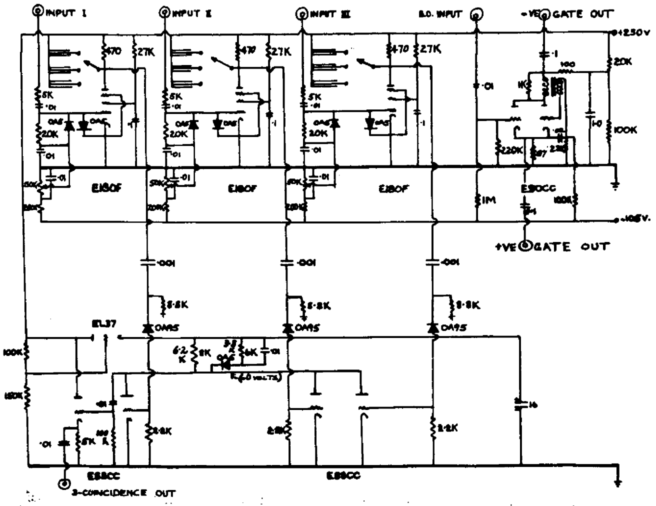

CIRCUIT OF TRIPLE—COINCIDENCE UNIT

<u>FIGURE 9</u>: <u>TRIPLE COINCIDENCE UNIT</u>; <u>2T = 1.4μS</u>.

Section (2.4.): Coincidence Display.

The amplified E and dE/dx pulses were stretched in time for a few microseconds and fed to the vertical and horizontal deflector plates of a cathode-ray tube. When the coincidence conditions were fulfilled, an intensifier pulse caused a bright spot to appear on the screen. The horizontal deflection was proportional to the specific ionization and the vertical deflection was proportional to the energy. These spots were photographed with a Cosser Oscillograph Camera on Kodak R55 film, the number of coincidence pulses per frame being regulated so that no significant overlapping occured. Figure 10 is an example of a record obtained when a thick piece of deuterated polythene with a deuterium/hydrogen ratio of about 1:1 was irradiated. In the fast neutron flux, the radiator produced both protons and deuterons each having a continuous energy distribution extending from zero to the maximum recoil energy. As $(E+1)dE/dx$ is approximately constant for each species of nuclear particle, the coincidence photograph shows a pair of hyperbolae corresponding to protons and deuterons.

Section (2.5.): The Neutron Source.

A magnetic quadrupole lens was used to focus a few microamperes of deuterons, accelerated to 250keV, onto a

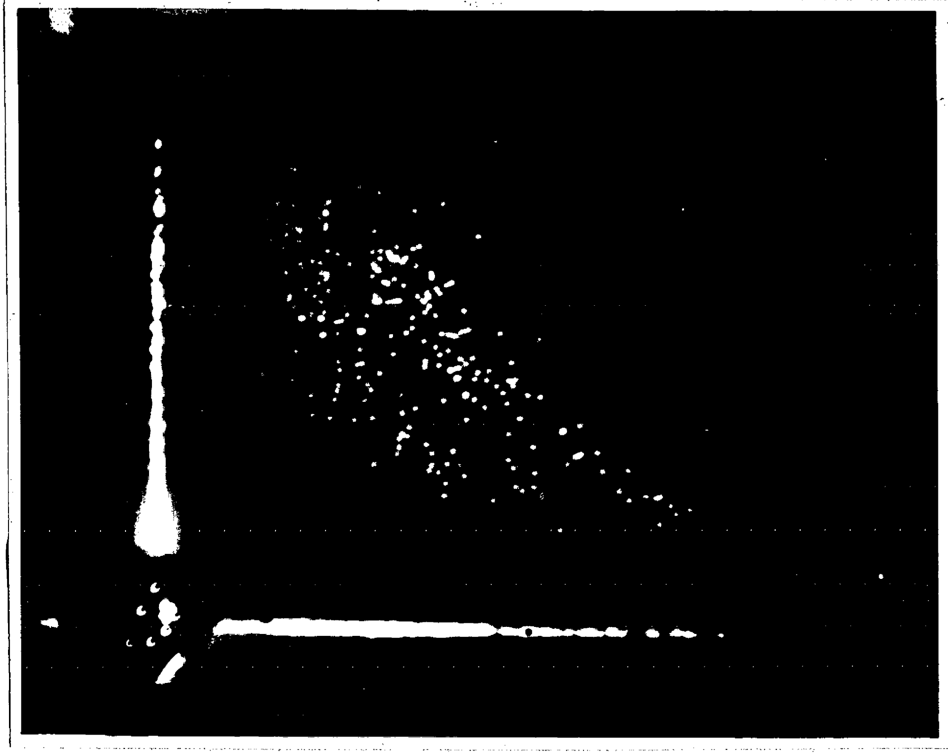

FIGURE 10: COINCIDENCE OSCILLOGRAM.

A thick radiator of deuterated polythene was used as a source of recoil deuterons and protons. The ratio of deuterium to hydrogen was approximately 1/1 and gave equal numbers of protons and deuterons. It should be noted that many more coincidences were recorded here than was normal practice; this was done to emphasize the shape of the hyperbolae.

tritium target adsorbed in titanium. A defining aperture, of diameter 0.080", was placed sufficiently close to the target that small shifts in beam direction gave negligible movements of the neutron source. Initially, the necessity for this precaution was not realized and large fluctuations in the reaction yields were traced to small movements of the defined neutron beam across the target foil.

The neutrons used in these experiments left the tritium target in a cone of included angle 12° with its axis 30° away from the deuteron beam. The energy of this group was calculated by the proceedure of Benveniste and Zenger (see Be 59) and was 14.9MeV with a width at half intensity of ~ 250keV.

The recoiling alpha particles, which established the time of emission of each neutron in the tagged beam, were defined by a circular stop in front of a plastic scintillator. This detector was 0.002" thick and was formed by dissolving NE860 phosphor in toluene and painting this solution onto the photocathode surface of an RCA-6655A photomultiplier. Although poor, the energy resolution from this detector was adequate(see Figure 11), as it was only necessary to establish the time of emission of each neutron.

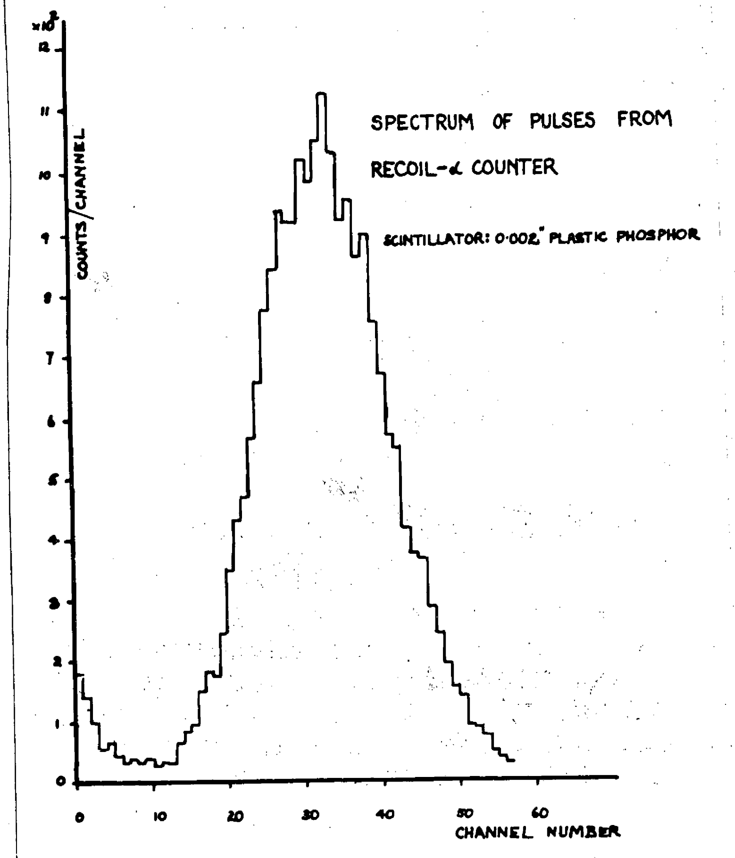
SPECTRUM OF PULSES FROM
RECOIL-α COUNTER
SCINTILLATOR: 0·002" PLASTIC PHOSPHOR
COUNTS/CHANNEL
CHANNEL NUMBER
0
10
20
30
40
50
60

FIGURE 11

Section (2.6.): Setting Up and Testing Proceedures.

Location of Telescope in Defined Neutron Beam. Before experimental data could be obtained it was necessary to locate the target foil completely within the cone of the defined neutron beam. This was achieved, approximately, by geometrical measurements and, finally, with precision, by moving the counter across and along the neutron beam to find a maximum in coincidence counting rate. The accuracy and speed with which these measurements could be made was improved considerably by placing the mask, shown in Figure 12, over a thick polythene radiator. This device provided a ring of recoil protons whose coincidence counting rate, was a maximum when the defined beam just exceeded the maximum diameter. Because of the geometry, a transverse movement of the telescope of about $^1/_8$" from the optimum position reduced the coincidence counting rate by a factor of two. A maximum was also observed when the counter was moved longtitudinally along the neutron beam through the point where the defined neutron cone had the diameter "D".

Adjustment of the Electronic Circuits. To ensure absolute counting it was necessary to adjust the proportional counter gains and the time delays t_1, t_2, t_3, shown in Figure 7, to optimum values. It was also necessary to have the minimum

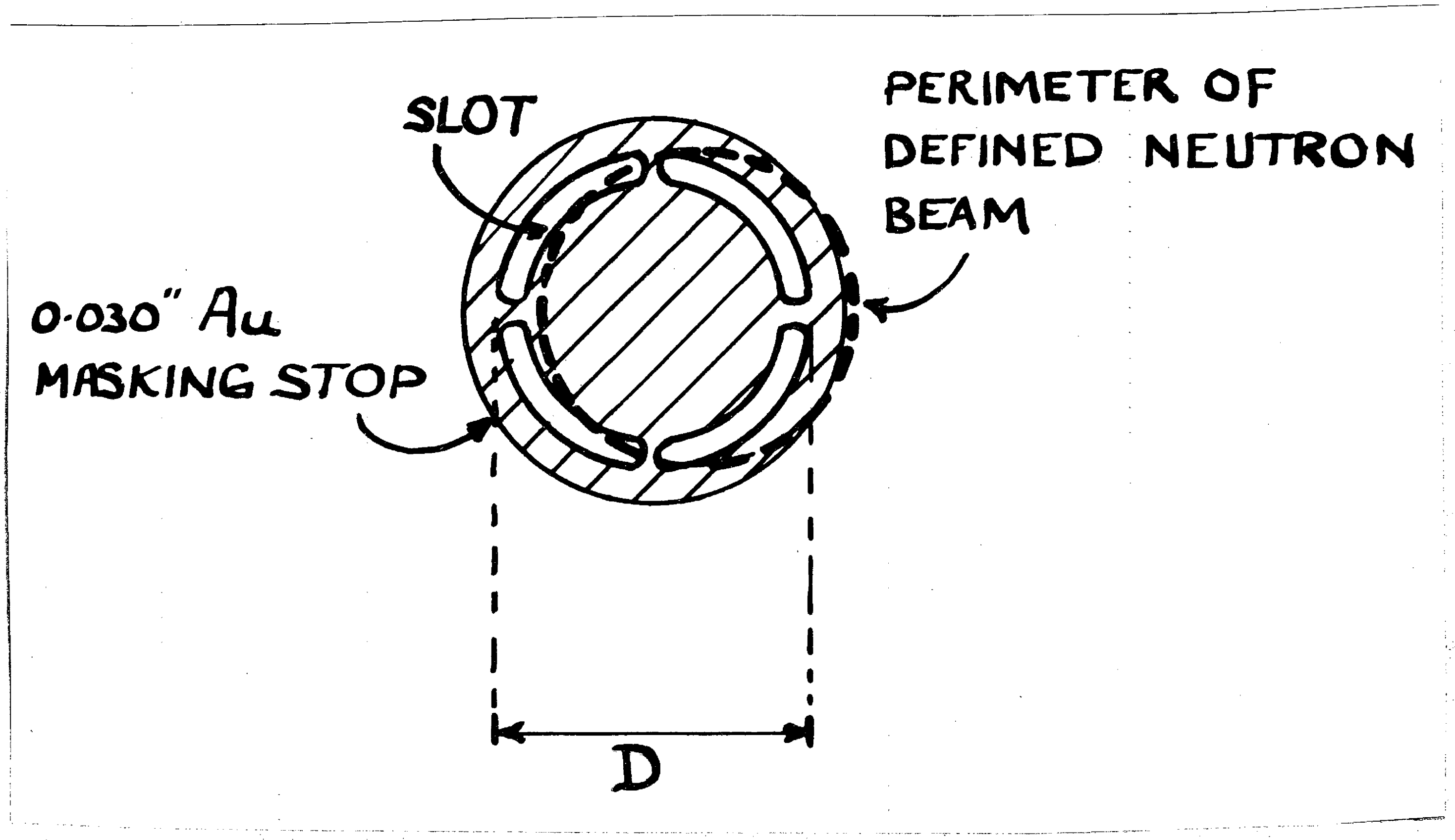

FIGURE 12: MASKING STOP.

voltage on the photomultiplier P.M.I, consistent with recording events of all energies, so that noise would not operate the limiters of the fast coincidence circuit unnecessarily. Johnson and Trail (Jo56) have published details for optimizing the parameters of a coincidence telescope. Where applicable, their proceedure was used.

Initially, Tektronix 517 and 555 oscilloscopes were used to adjust the gains and time delays to give some triple coincidences. A gated dE/dx spectrum, for a monoenergetic group of protons, was then displayed on the kicksorter and accurate adjustment was made to the gains of both gas counters to set them to the correct level, and to equality. Equality of gains was necessary if the least pulse selector circuit was to operate correctly. Figure 13 shows the improvement in dE/dx measurements which was achieved when these circuits were correctly adjusted.

The output from the fast coincidence circuit was proportional to the time overlap between the pulses arriving at the grids of the 6BN6 coincidence tube. Because of this, the time delays in the recoil alpha particle detector and the proton counter, t_1 and t_2, were most readily adjusted by displaying the gated output from the fast coincidence circuit on a pulse height analyzer. With complete overlap the amplified signal was approximately 50volts high; with zero

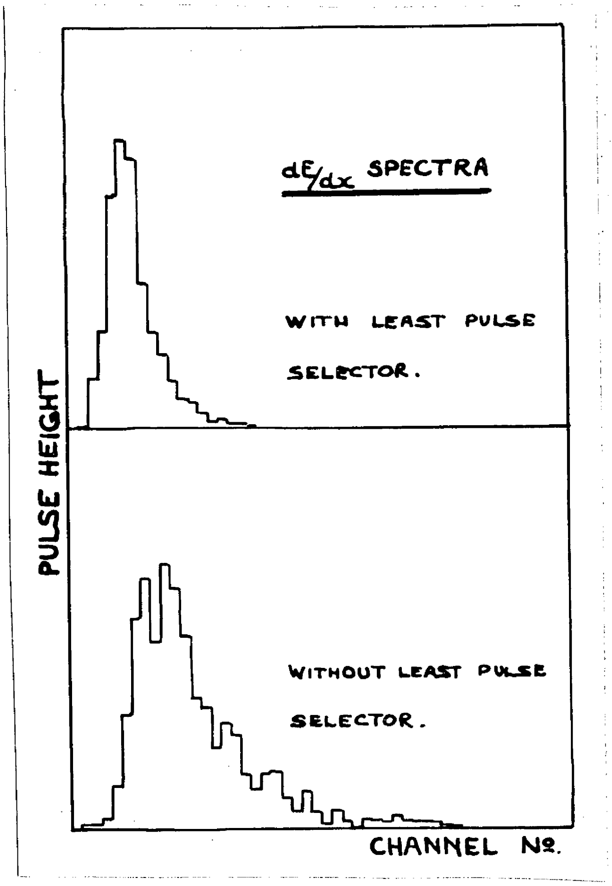

FIGURE 13: dE/dx SPECTRA OF 15MeV PROTONS LOSING A MEAN ENERGY OF 25keV.

overlap less than 10volts. Displaying the fast coincidence output in this fashion made it possible to detect a fraction of a millimicrosecond change in the fast timing and to optimize the delays. The final adjustment to the circuits was of the slow delay, t_3. This was chosen by the time-honoured method of plotting, for a variety of proton energies, the count-rate versus the inserted delay.

Choice of Photomultiplier. The lowest energy of proton which could be recorded was limited by photomultiplier noise. Using a DuMont 6292, noise became the limiting factor when the circuit parameters were adjusted to record protons having an energy rather less than 1MeV. R.C.A.6655A allowed this lower limit to be reduced somewhat but the resolution obtained using these detectors was almost a factor of two worse than that available from DuMont photomultipliers. With 6292, the lowest energy which could be recorded at the scintillator, was below 0.95MeV. This is almost 3MeV lower than other workers have achieved with coincidence telescopes.

Separation of Protons and Deuterons and Random Events. Coincidence oscillograms, such as that shown in Figure 10, allowed the separation between proton and deuteron events to be convincingly demonstrated. This was done by taking the product $(E+1).dE/dx$ over energy intervals of a few MeV and plotting the results as shown in Figure 14. Using such

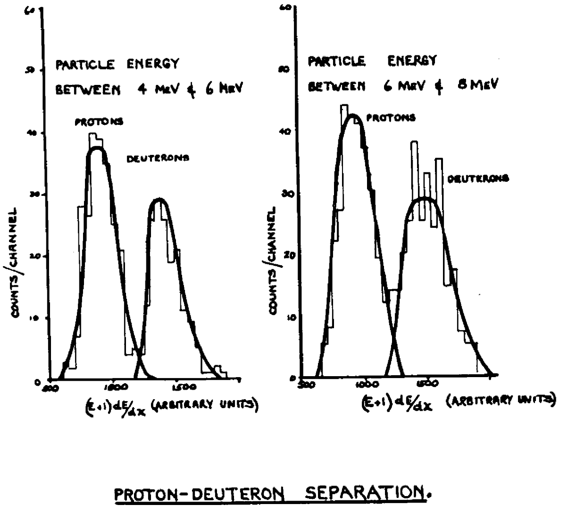

FIGURE 14: PRODUCT, E.dE/dx, FOR PROTONS AND DEUTERONS.

curves, each oscillogram could be divided into regions corresponding to proton events, deuteron events and random coincidences. Figure 15 is a copy of a chart which was developed to analyze quickly the mass of particles associated with each event.

A typical oscillogram, taken during one run of the Ni^{58} experiment is shown in Figure 16. The points enclosed by circles are certain deuterons. Those lying on the hyperbola, below, protons. Because the counting rates in each detector channel were greatest at low energies the random coincidences in the system tended to congregate in the lower left hand corner.

Angular Distribution Measurements. An important series of experiments was made with the telescope and its circuitry to ensure that instrumental effects were not distorting the angular distributions. The basis of these tests were measurements on the differential (n,p) scattering cross-section at 14.9MeV; this cross-section is known to be close to isotropic in the centre-of-mass frame of reference. When this cross-section is transferred to laboratory coordinates

$$\Omega(\theta) = 4.\sigma.\cos\theta \qquad (1)$$

where $\Omega(\theta)$ is the differential cross-section in laboratory coordinates for detection of recoil protons.

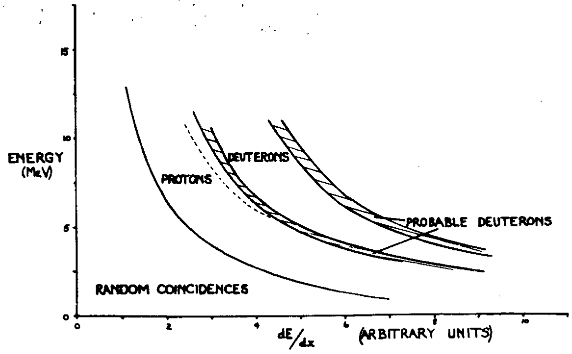

<u>FIGURE 15</u>: <u>SAMPLE OF CHART USED TO ANALYZE EVENTS</u>.

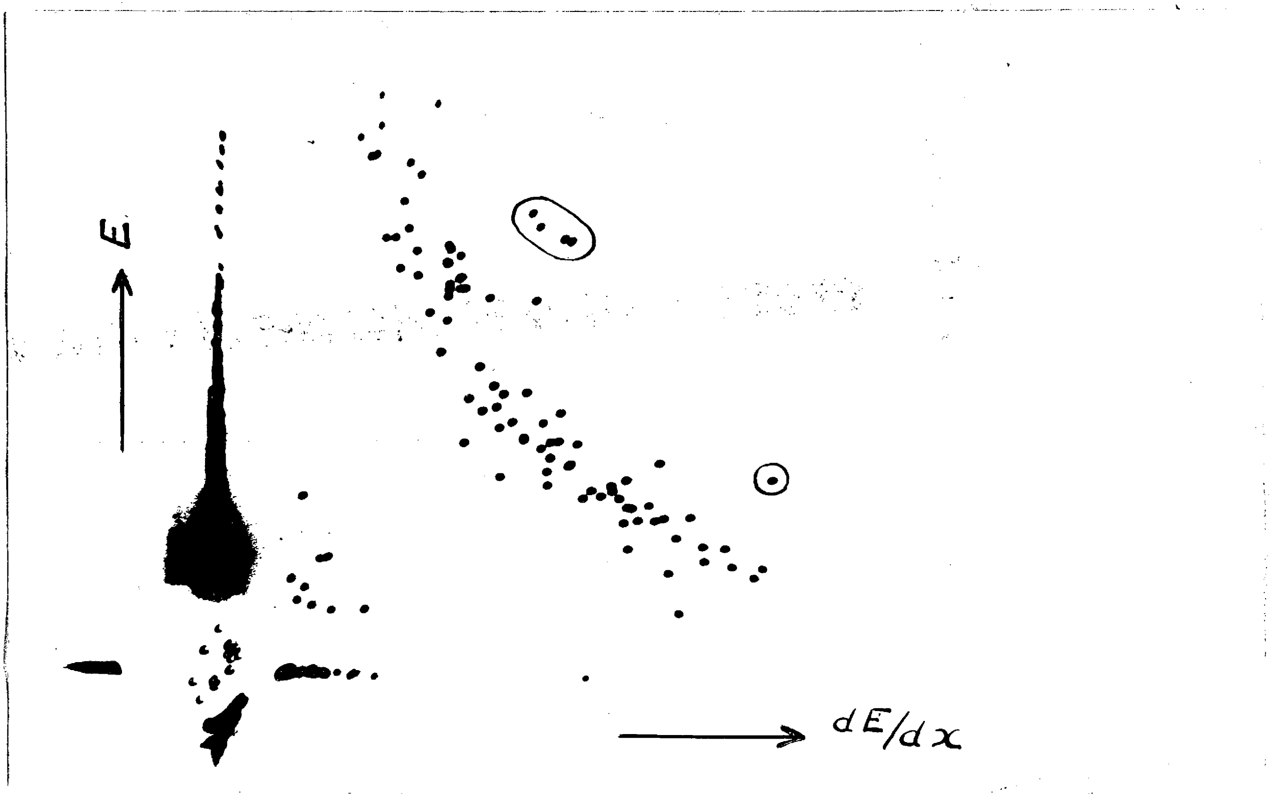

FIGURE 16: A TYPICAL OSCILLOGRAM OF DATA OBTAINED DURING ONE RUN ON Ni^{58}.

Certain deuterons are circled. The random coincidences can be seen clustered in the left-hand corner.

σ is the differential cross-section in centre-of-mass coordinates for (n,p) scattering.

θ is the angle of emission of the recoil protons in laboratory coordinates.

As the collimation was far from perfect in the present telescope, (see Figure 6), protons having a range of scattering angles with the incident neutrons, could pass into the detector. For this reason, it was not possible by a simple substitution into expression (1) to calculate the number of protons expected for a given setting of the telescope axis.

To calculate the number of recoil protons expected at each angle the Monte Carlo routine described in Section (2.2.), was extended. As each neutron-proton trajectory was followed through the counter by SILLIAC, the proton energy was calculated from

$$E_P = E_N \cos^2\theta.$$

and the relative probability of the event was found from the laboratory differential scattering cross-section. Corrections were then made for the ionization losses in the radiator and in the gas of the proportional counters. The results of this calculation are shown in Figure 17 where the

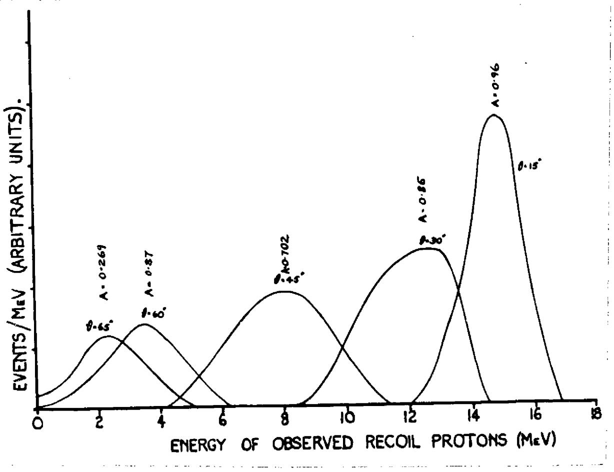

<u>FIGURE 17</u>: <u>CALCULATED DISTRIBUTION OF RECOIL PROTONS RECORDED BY THE SCINTILLATION DETECTOR OF THE COUNTER TELESCOPE</u>.

('A' is the integrated area, above 1MeV, under each of the curves which are normalized to unit area at $\theta \approx 0^{\circ}$).

area under the curves has been normalized to unity at $\theta = 0^\circ$. Comparisons between the shapes of these curves and the distributions obtained experimentally were excellent and gave confidence that the detection system was operating satisfactorily.

Backgrounds. The smallest reaction cross-sections which can be studied with a counter telescope are set by the background counting rates. For the present system, the backgrounds were found to be strongly dependent upon the angular position of the telescope axis, being most intense in the forward direction. Figure 18 shows the proton backgrounds plotted as a function of the angle of observation and of the particle energy. The cross-sections have been established by relating the observed backgrounds to a hypothetical nucleus, with $A \sim 60$, assuming that this "background target material" has a thickness of $\approx 10 mg/cm^2$ and a diameter of $1^1/_8$". Use of these curves allows source/background ratios to be established for foils of any composition. The maximum at $\theta = 0^\circ$ was thought to be a consequence of anisotropy in the Pt(np) cross-section and also backward-going protons. However, the relative importance of these possibilities was not determined.

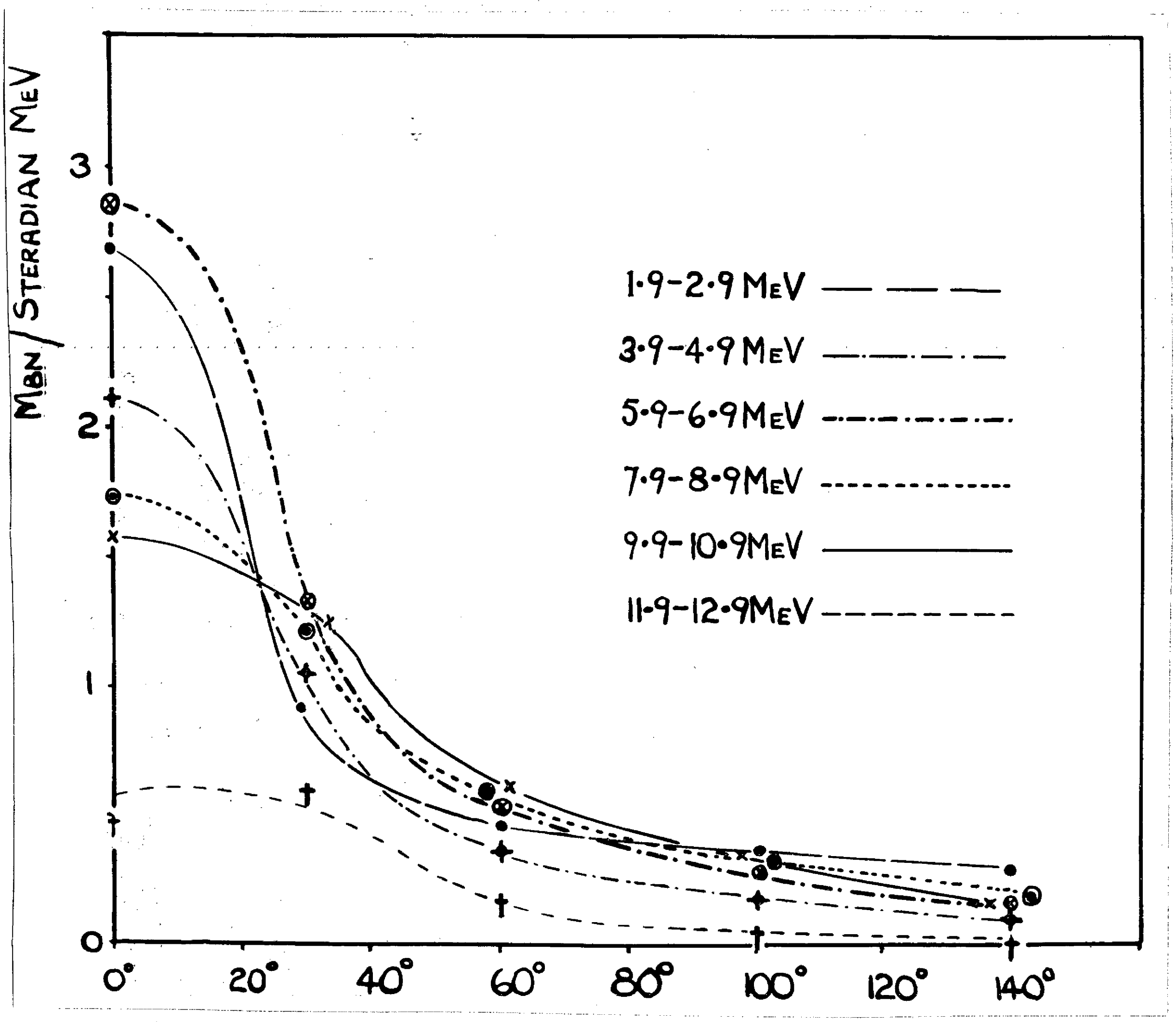

FIGURE 18: PROTON BACKGROUND OF TELESCOPE AS A FUNCTION OF THE ANGLE OF OBSERVATION AND OF THE PROTON ENERGY.

Section (2.7.): Flux Measurements.

The Associated Alpha Monitor. The associated alpha detector subtended a solid angle of $8.26 \pm .08 \times 10^{-6}$ steradians at the neutron source and was placed at the laboratory angle of 150° with respect to the incoming deuteron beam. Small angle scattering of alpha particles from the walls of the target chamber into the detection element was prevented by suitably placed non-limiting stops. The alpha particles passed through thin aluminium foil, to remove scattered deuterons, and were then stopped by a thin CsI(Tl) scintillator ($\frac{1}{4}$" x $\frac{1}{4}$" x 0.0015"). The dimensions were small enough so that a negligible number of large background pulses were produced within the scintillator. The protons from $d(d,p)H^3$ passed right through, producing a smaller light pulse than that from the stopping of a 2.6MeV alpha particle (see Figure 19).

Because of the effects of centre-of-mass motion, it was necessary to apply a correction factor to convert the number of alpha particles per unit solid angle, at the recoil alpha particle detector, to the number of neutrons per unit solid angle in the direction of the target foil. Methods of calculating this correction factor, for targets of finite thickness, have been developed by Benveniste et al (Be59). For the geometry used here, this correction factor, from alpha particles/unit solid angle to neutrons/unit solid angle, was calculated to be 1.21.

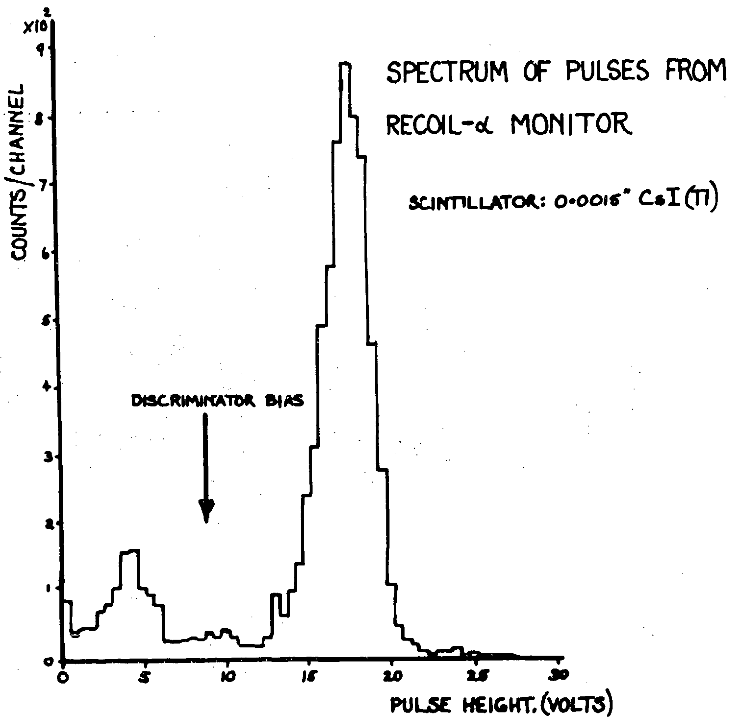

FIGURE 19: SPECTRUM OF PULSES FROM RECOIL ALPHA COUNTER.

The crystal was sufficiently thin that protons from $d(d,p)H^3$ passed right through giving the low energy peak at the bottom of the spectrum.

<u>Recoil Proton Monitor</u>. The number of recoil protons detected by a coincidence telescope is dependent upon:

(i) The solid angle of acceptance of the telescope.

(ii) (n-p) differential scattering cross-section.

(iii) Number of hydrogen nuclei in the radiator.

(iv) Neutron flux at the radiator.

As the first three of these parameters were known with some accuracy, integrated neutron fluxes could be established from the number of protons under the peak of the recoil spectrum (see Figure 20).

The hydrogen content of the polythene was calculated from its mass, assuming the composition to be $(CH_2)^n$; chemical measurements reported by Bame et al. (Ba57) have shown that several grades of commercial polythene were $(CH_2)^n$ to an accuracy of better than 1%.

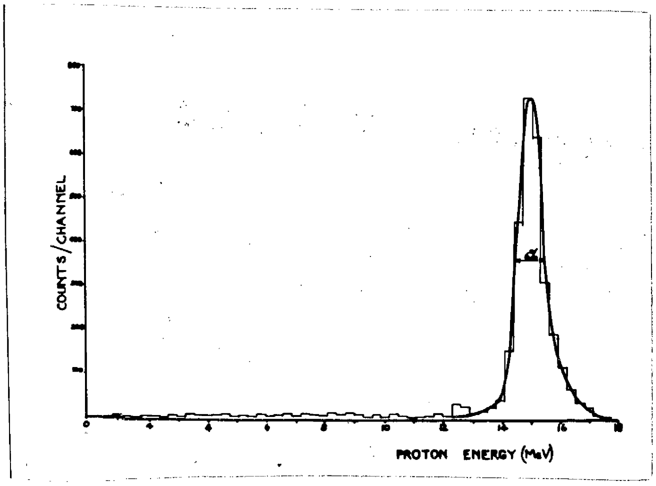

FIGURE 20: RECOIL PROTONS AT 0°.

CHAPTER III

THE PROTONS FROM 14.9MeV NEUTRON INTERACTIONS WITH Ni^{58}

Section (3.1.): Introduction.

Although the general features of the distribution of protons from 14MeV neutron interactions with Ni^{58} were known before this investigation, the spectra and angular distributions available had poor statistical accuracy. Also, as nuclear emulsion techniques had been used for most experiments, the importance of deuteron contamination in the spectra had not been established. Other reasons which made Ni^{58} an attractive target for initial experiments with the coincidence telescope include:

(i) The cross-section for the emission of protons was known to be large, allowing good statistical accuracy to be achieved in a short counting period.

(ii) The results from previous experiments by other workers allowed broad comparisons with the present data from the coincidence telescope.

(iii) A suitable target of isotopically enriched Ni^{58} was readily available.

The first measurements to be reported on the protons from $Ni^{58}(n,p)Co^{58}$ were made by Allan(Al57). In this work, nuclear emulsions were employed to measure the kinetic energy distribution of the protons from an enriched Ni^{58} foil, in the angular range $34^{o} \pm 20^{o}$ to the direction of the incident neutrons. The proton spectrum showed features expected from the statistical evaporation from a compound nucleus. However, the position of the intensity maximum was well below the height of the accepted Coulomb barrier for Ni and Allan suggested that protons from (n,np) reactions accounted for the low energy events. By invoking statistical model considerations the total cross-section for proton emission was separated into [(n,p) + (n,pn)] , 310mb; (n,np) , 220mb. Approximately 1,600 tracks were analyzed for this work, but this number was insufficient to allow the details of any high energy structure to be resolved.

Verbinsky et al.(Ve57) used a coincidence technique and heavy shielding to collimate the incident neutrons, when examining the proton spectrum from foils of Mg, Ni, Cu, Rh, Pd, of natural isotopic composition. Notwithstanding the use of thick targets (2.5MeV loss for 6MeV protons), the low fluxes at the target foils allowed only poor statistical accuracy. Cross-sections and gross angular distributions were measured for $E_p \geqslant 6$MeV giving a proton emission cross-section of 170mb. and a forward peaked angular distribution.

Several counter telescopes have been used by Colli et al. to investigate the charged particles from unenriched nickel foils (Co57d; Co58a; Co59). Experimental difficulties did not allow proton events to be recorded when their energy was below 3.5MeV and the maxima in the evaporation spectra reported by Allan could not be reproduced. Cross-sections were measured relative to that of copper and gave the total cross-section for proton emission as 590mb.

Recently, Kumabe and Fink(Ku60), using emulsion techniques, have measured energy and angular distributions for Ni^{58}. As only 1,500 events were analyzed, the statistical accuracy was poor and resulted in wide energy intervals for the summations necessary for the angular distribution measurements. Although some small direct interaction contribution was suggested by these workers, examination of the angular distributions shows that forward peaking occurs almost entirely below 7MeV, making the direct interaction interpretation doubtful.

In short, proton angular distributions have not been measured adequately and neither the presence of direct interaction effects nor deuteron emission have been established.

Section (3.2.): Experimental Details.

A metallic foil of nickel, enriched in Ni^{58} to 95.6%, was electroplated by A.E.R.E., Harwell, onto a 0.005"Pt backing and used as a radiator in the telescope. This foil had a thickness of $\sim$10mg/cm^2, a diameter of $1^1/_{16}$" and a total mass of 61.9mg. After deposition, water contamination was removed from the foil by vacuum dessication and care was taken during shipment and on receipt in Canberra that no hydrogenous contamination was added.

Kinetic energy spectra for protons and deuterons were measured at ten angles to the neutron beam. These angles, between the axis of the telescope and the line joining the centre of the target foil to the neutron source, were 0°, 20°, 40°, 50°, 60°, 80°, 100° and 140°. With the exception of the measurements at 140°, all the data was obtained equally from angles on both sides of zero in random order. Within the statistics, the angular distributions obtained on both sides of zero were identical, suggesting that no geometrical factor was affecting their quality.

A run of data taking at each angle lasted approximately one hour and consisted of an energy spectrum together with a background from a platinum blank identical to the target backing. After each run a series of checks was made on the operation of the equipment. The most important of these was a measurement of the spectrum of recoiling protons from the thin polythene radiator. This served three purposes:

(i) to calibrate the recoil-alpha neutron monitor.

(ii) to establish whether gain shifts had occured in the scintillation channel.

(iii) to allow gain checks to be made on the proportional counters.

Three times in each twenty-four hour period, the entire system was tested: the resolution of the gas counters was established from the specific ionization pulses of Po^{210} alpha particles; the amplifiers were checked for drift; the coincidence circuitry was tested using a pulse generator.

Protons covering the whole range of energies displayed in the spectra were not recorded simultaneously in the Ni^{58} experiments. Rather, the circuitry dictated that the measurements for each spectrum be divided into sections which could later be normalized to a constant integrated flux and compounded to form a complete spectrum. One advantage of this proceedure was that the range of proton energies accepted could be adjusted to omit the low energy end of the spectrum, and allow higher neutron fluxes to be used, without introducing an excessive number of random events.

Initially, four sets of data were taken at each angle for the proton energies 5MeV to 16MeV. The statistical accuracy of the high energy end of the spectrum was then improved by adjusting the system to count only within the region 9MeV - 16MeV, where a further set of four runs was made at each angle. The spectra were completed by making measurements in the range 1MeV to 9MeV. A final check was made on the long term stability by adjusting the system to record a further set of data under the original conditions. No significant differences were found between the spectra obtained at the beginning of the experiment and those recorded several weeks later. Furthermore, after normalization the various energy regions of the spectra were found to fit together well.

Flux Measurements. As the polythene radiator, used for neutron flux measurements, had the same diameter as the Ni^{58} foil, the cross-sections could be related directly to the known (n,p) scattering cross-section. This proceedure eliminated counter geometry and other uncertainties such as gas scattering and the absorption of the counter wires. The cross-sections were related by:

$$\Omega(\theta) = \sigma(n,p;0^{\circ}) . \frac{N_H}{N_R} . \frac{C_R}{C_H}$$

where $\Omega(\theta)$ . . . is the required differential cross-section in laboratory co-ordinates at the angle θ .

$\sigma(n,p;0^{\circ})$ is the differential cross-section, in laboratory co-ordinates for (n,p) scattering at the mean angle of the counter when the axis is pointing at the neutron source.

N_H . . . . total number of hydrogen nuclei in radiator.

N_R. . . . total number of target nuclei.

C_H . . . . counts from polythene radiator per unit flux.

C_R . . . . counts from target foil per unit flux.

<u>Data Reduction</u>. After composite spectra had been formed for the whole energy range 1MeV to 16MeV, changes were made in the energy associated with each channel to allow for the ionization losses within the proportional counters and give the energy spectrum at the surface of the target foil. Because the protons originated anywhere throughout the volume of the foil, a simple change in scale was not capable of correcting for these ionization losses. In the present work, considerable effort was expended to develop a computer programme which would reduce the experimental data, obtained using a target foil of finite thickness, to that spectra which would be observed if the foil caused no ionization losses. A programme for this data reduction was designed for the computer SILLIAC. Also included was a routine to convert the results to centre-of-mass coordinates and to linearize the energy scales of the observed spectra. A flow diagram for this programme is presented in the Appendix.

A first approximation to the thin target spectrum was found by assuming that each elementary layer of the target foil contributed an equal number of events to any particular channel of the observed spectrum. Thus, if the target was divided into ten layers, $^{1}/_{10}$th of the counts observed in each channel were assumed to originate in each layer of the target foil. By making this assumption it was possible to estimate the energy which had been lost by each group of

$^{1}/_{10}$th of the particles of a given channel of the observed spectrum, replace this energy and form a new spectrum. The computer did this calculation, channel by channel for each layer of the target foil, until a complete spectrum was built up; a first approximation to that expected from a target of zero ionizing power.

The derived spectrum, itself, was then used as primary data in a similar calculation, in the reverse direction, to find the spectrum which would be observed at the surface of a real foil if, throughout its volume, reactions gave rise to protons having an energy distribution similar to that of the calculated zero approximation. The channel by channel differences between this spectrum and that which was observed experimentally, was a measure of the errors in the zero approximation and could be used to improve this spectrum. The process was iterated until truncation errors were negligible; in practice, this required about three complete cycles.

Section (3.3.): Proton Spectra.

A histogram of the energy spectrum of protons at 8° in the centre-of-mass system is reproduced in Figure 22. The background, which has been subtracted already, was found to be dependent upon the angle of observation as well as the energy of the proton group. The background:source ratio has been plotted in Figure 23. At all energies the background was greatest at $\theta = 0^{\circ}$ and fell considerable when the scintillation counter was moved from the tagged beam.

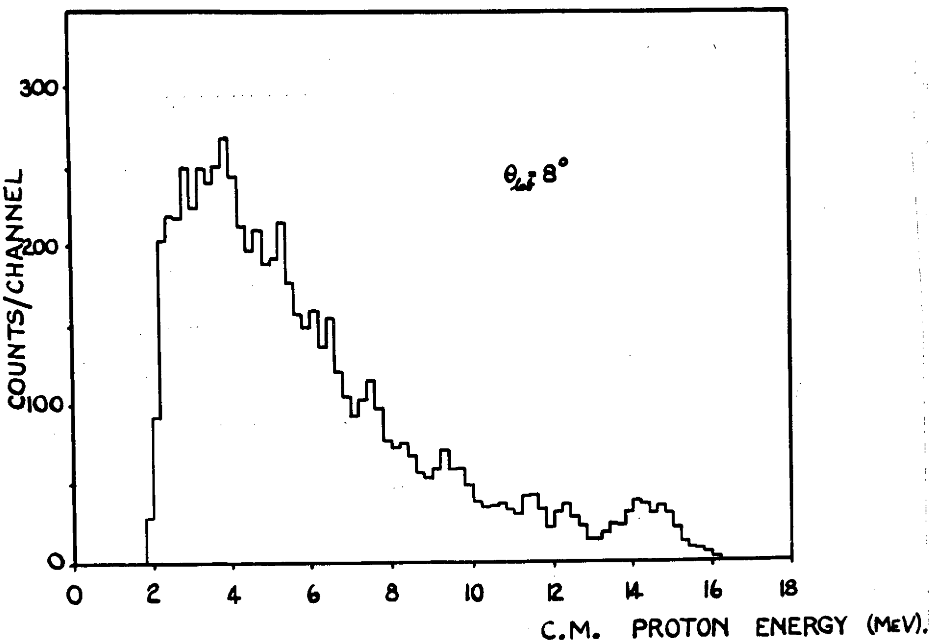

FIGURE 22: HISTOGRAM OF THE PROTON SPECTRUM AT 8°.

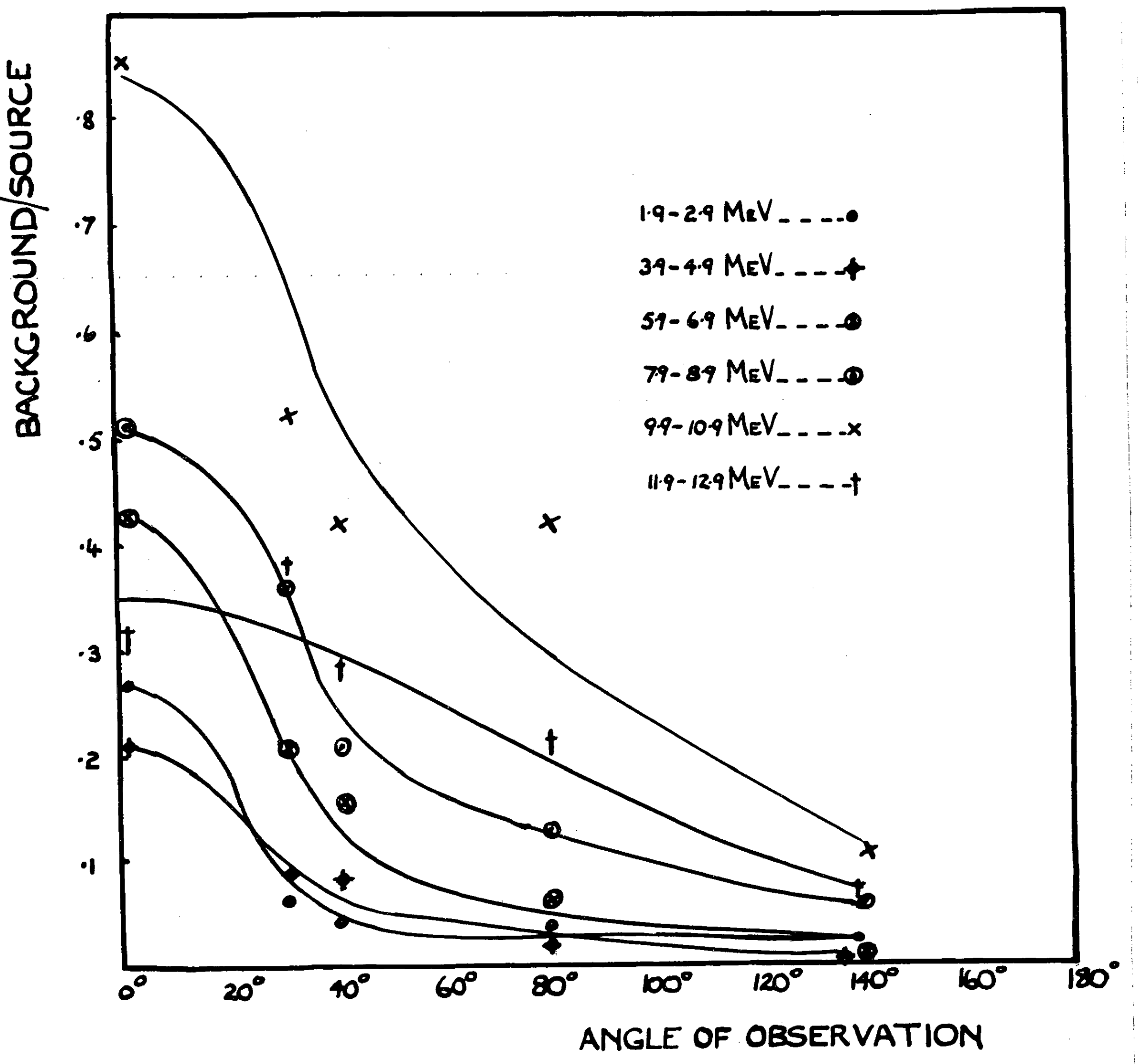

FIGURE 23: BACKGROUND TO SOURCE RATIO AS A FUNCTION OF ENERGY AND ANGLE OF OBSERVATION.

Figure 22 shows indications of structure; possibly from direct (n,p) transitions between the Ni^{58} nucleus and low levels of Co^{58}. It was not overlooked, however, that some of the high energy events at forward angles might be a consequence of hydrogenous contamination within the target. To check this, comparisons were made between the angular variation of the high energy protons and that expected from recoil protons from (n,p) scattering. Figure 24 is the spectrum of the anistropic events at $\theta = 0^{\circ}$; recoiling protons, from a water layer distributed through the nickel layer, could contribute events only to the dotted section of the plot. Furthermore, the intensity of the group would be expected to vary as cosine θ, θ being the angle of observation. No evidence of this nature was established and an upper limit of $20\mu g$ was placed on the total water contamination of the target foil. The presence of this amount of water would cause an error of $\approx$2mb in the total proton cross-section (i.e. $\approx$0.3%).

Photomultiplier noise and large counting rates at low energies prevented the recording of events when the protons arrived at the scintillator with less than 0.95MeV; after ionization corrections had been made, this lower limit corresponded to protons of energy $\approx$1.8MeV at the site of their parent reactions. This experimental cut-off was sufficiently low that evaporation maxima could be seen clearly in the spectra recorded at all angles and permitted confirmation of the low energy features reported by emulsion workers.

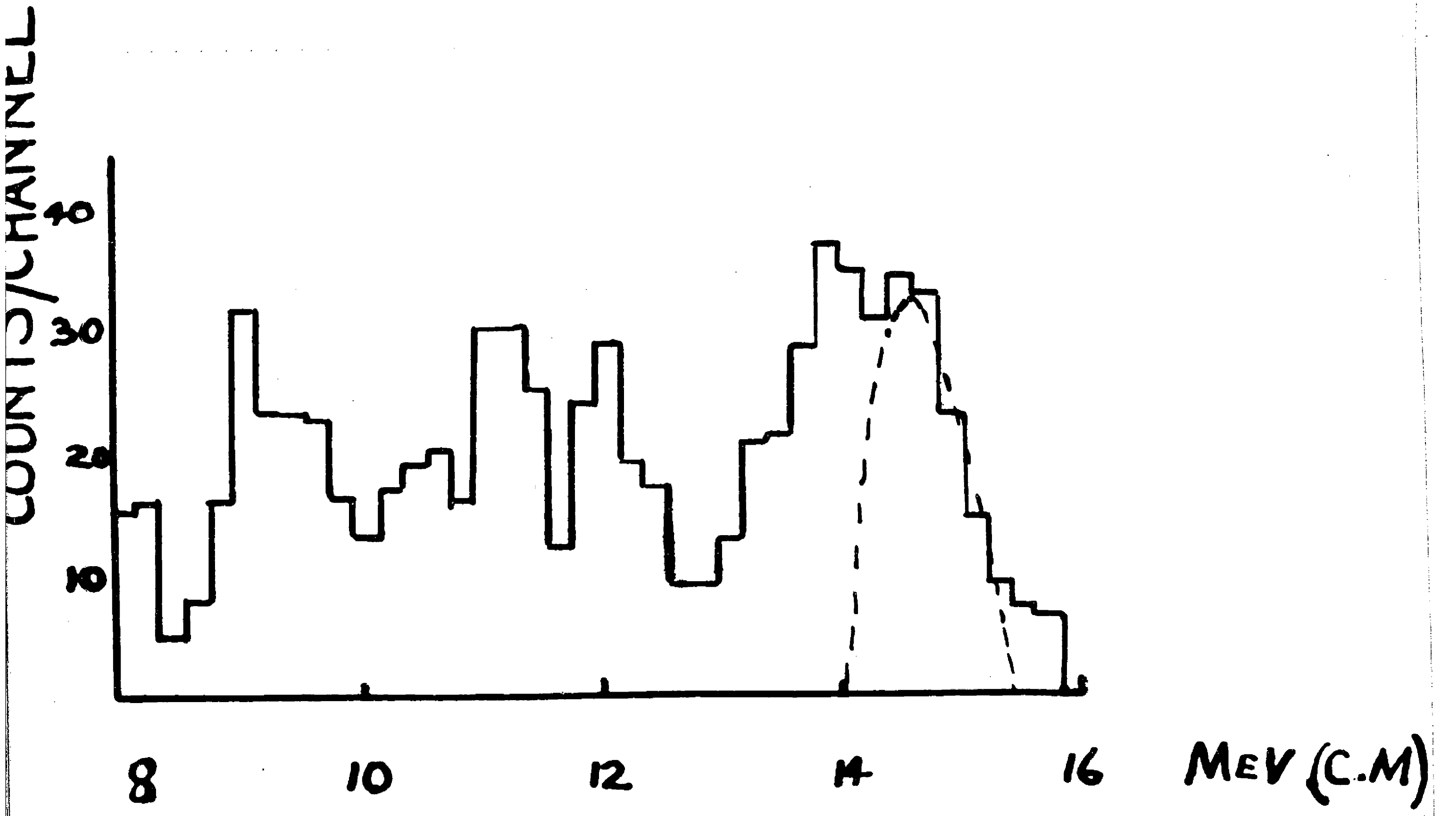

FIGURE 24: SPECTRUM OF ANISOTROPIC EVENTS AT $\theta = 0^{\circ}$.

Recoiling protons could give a contribution only under the dotted section of the curve.

In addition, because mass selection was used here, the short range events were definitely established as protons eliminating, completely, the possibility suggested by Allan (Al57) that they might be deuteron tracks which had been incorrectly identified.

<u>Identification of Discrete Structure</u>. Several independent sets of data were recorded at $\theta = 0^{\circ}$ to ensure that the particle groups in the spectra reproduced in Figure 22 were not the result of statistical fluctuations. Although the group around $E_p = 14.5$MeV showed some indication of doublet structure, the widths of its components were still much greater than the known resolution of the system. This fact, together with Co^{58} being an odd-odd nucleus with high level density, was interpreted as the result of the groups being compounded from a large number of single particle transitions to states of Co^{58} closely related according to the shell model picture of nuclear structure.

Shell model calculations (Ma55) indicate that the configuration of Ni^{58} consistes of a closed shell of $1f_{7/2}$ protons togther with two $2p_{3/2}$ neutrons which surround a core configuration. From the simple model, it is anticipated that captured meutrons would be absorbed most readily into $2p_{3/2}$, $1f_{5/2}$, $2p_{1/2}$ or $1g_{9/2}$ states. Emitted protons would be expected to come from the $1f_{7/2}$ shell. The energy expected for particular single particle transitions can sometimes be estimated from nuclear binding energies after allowance has been made for the pairing energies (see Eu58). Such estimates were made for $Ni^{58}(n,p)Co^{57}$ and it was found that, when neutrons are captured to $2p_{3/2}$ and $1f_{7/2}$ states, the $1f_{7/2}$ valency protons can be emitted in two groups separated by $\simeq 0.5$MeV with a mean energy of $\simeq 15$MeV. These transitions were tentatively identified with the observed doublet structure at 14.5MeV. Further support for this interpretation came from the angular distribution data which is discussed in the next section.

<u>Statistical Effects</u>. The energy spectra for the angles 100°, 120° and 140° were used to derive the statistical plots shown in Figures 25 and 26. As the Q-value of $Ni^{58}(n,np)Co^{57}$ is -7.7MeV(As59), protons of energy greater than 7MeV could only have come from $(n,p\gamma)$ processes; below this energy, (n,pn) and (n,np) were also energetically possible. The straight line through the experimental points around 8MeV was derived from a least-squares fit to the experimental data recorded in the backward hemisphere between 7MeV and 9MeV. This energy range was established, at the lower end, from the energetics of the (n,np) reaction and, at the upper, where the relative yield of protons deviated significantly from the level-density formula of Lang and LeCouteur(La54). The logarithmic slope of this plot provided a temperature of 1.36 ± 0.06MeV, the error being found from the regression coefficients of the least squares fit(To55). A temperature of $0.50 \pm .03$MeV was found for (n,np), in agreement with the results of Kumabe and Fink (Ku60).

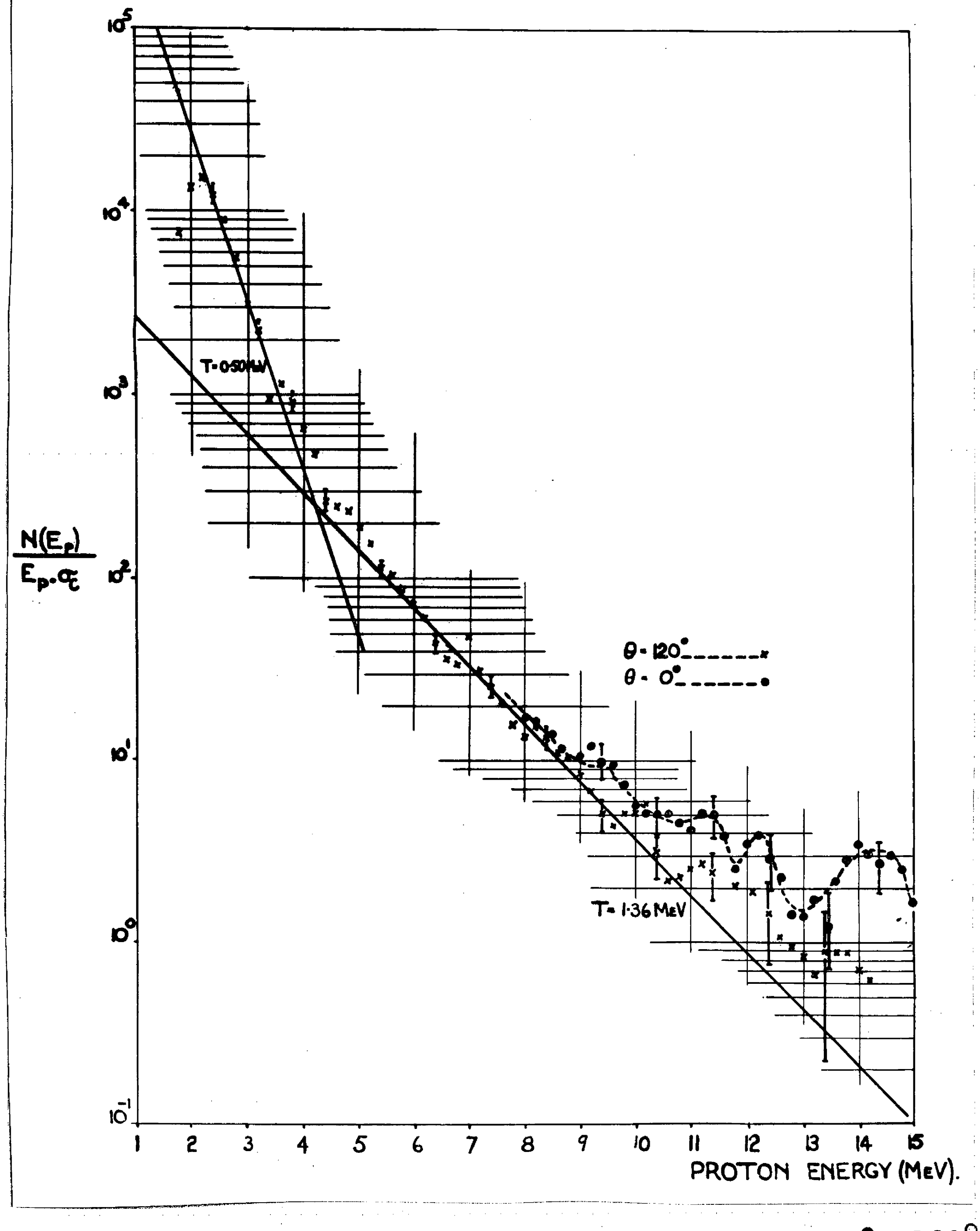

FIGURE 25: STATISTICAL PLOT OF PROTON DATA FROM $\theta = 120^\circ$ AND THE HIGH ENERGY DATA FROM $\theta = 0^\circ$.

σ_c was calculated from the tables of Shapiro (Sh53) using $r_o = 1.3$f.

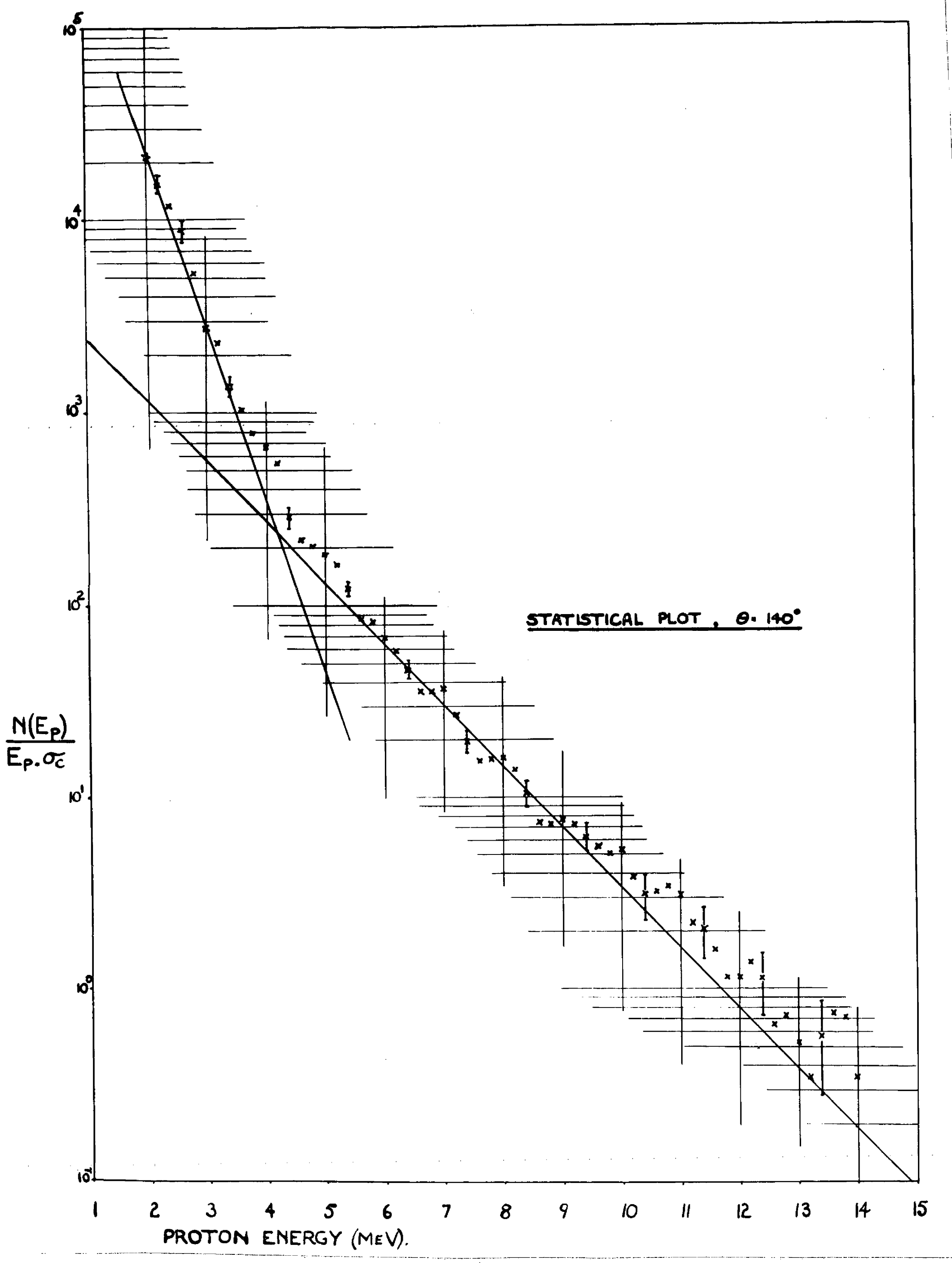
STATISTICAL PLOT, θ = 140°
$\frac{N(E_P)}{E_P.\sigma_C}$
10^5
10^4
10^3
10^2
10^1
10^0
10^{-1}
1 2 3 4 5 6 7 8 9 10 11 12 13 14 15
PROTON ENERGY (MeV).

FIGURE 26

Kumabe and Fink (Ku60) have found a temperature of 1MeV for the reaction $Ni^{58}(n,p)Co^{58}$. Their temperature measurements appear to have been influenced by (n,np) events and if their data is re-analyzed using only proton energies greater than 7MeV, the temperature increases to about 1.25MeV. Storey, et al.(St60) have reported 1.58MeV as the temperature for the reaction. Once again, a wide range of energies was used to establish the temperature but agreement could be reached if the range of energies was made smaller.

The convexity of the statistical plots to the energy axis, noticeable at all angles of observation, was particularly pronounced in the data taken in the forward hemisphere (see Figure 25). This shape, rather than a concave curve predicted from the level density, was considered to be the result of protons from direct-interaction processes. Brown and Muirhead (Br57) have pointed out that, because of internal reflection at the front surface of a nucleus, particles from direct interactions can be emitted at backward angles. Inserting reasonable values into their expression gave a ratio of about 1 : 5 for the direct protons expected in the backward hemisphere to those expected in the forward. This prediction appeared to be confirmed by the present experiment.

Le Couteur and Lang(Le59) have derived a relationship between the constant 'a' used in the level density formula, the temperature τ, and the excitation of the residual nucleus U following the emission of a proton of mean energy:

$$a = \frac{U}{\tau^2} + \frac{2.5}{\tau}$$

Using the value of τ obtained in these experiments gave

$$a = 7.8\text{MeV}^{-1}$$

which is in agreement with the values gathered for this mass region by Le Couteur and Lang.

<u>(n,np)</u> <u>Contributions</u>. An argument for the importance of (n,np) processes as the source of many of the low energy particles is based on the fact that in Ni^{58} the binding energies of the final neutron and the final proton make the threshold for $Ni^{58}(n,np)Co^{58}$ 4MeV lower than that for $Ni^{58}(n,2n)Ni^{57}$. Thus, there are a number of states of Ni^{58*} from which proton emission is energetically possible but where neutron emission is forbidden. Under these conditions quantum mechanical leakage of low energy protons through the Coulomb barrier can compete favourably with gamma emission and allow the escape of low energy particles.

Armstrong and Rosen (Ar60) have calculated the spectrum of protons expected from Zn^{64}, when it is bombarded by 14MeV neutrons and have included the contributions expected from (n,np) processes. When the results of this calculation were modified for Ni^{58} the agreement with the present work was excellent and gave support to the contention that the low energy protons were from (n,np) interactions.

Cross-Sections. The cross-sections for compound nuclear processes were estimated from the ordinates of the lines defining the nuclear temperature. In these calculations it was assumed that the straight lines of Figures 25 and 26 represented, correctly, the compound nucleus effects and that the cross-sections were isotropic. Direct interaction effects were estimated from the anistropy in the angular distributions.

The ratio of the (n,p) to (n,np) cross-sections is dependent upon the Coulomb barrier transparency used; in this work Shapiro's tabulations (Sh53) were employed with $r_o = 1.3$. Table 1 lists the cross-sections obtained by the use of these transparencies.

TABLE 1

PROTON CROSS-SECTIONS FROM CHARGED PARTICLE MEASUREMENTS

Reaction	Mechanism	Cross-section(mb.)
(n,p) + (n,pn)	Compound Nucleus	430
(n,p) + (n,pn)	Direct Interaction	60
(n,np)	Compound Nucleus	340
Total		830 ± 70

Section (3.4.): Proton Angular Distributions.

Because the energy resolution of the counting system and the close level spacing of the residual nucleus precluded observation of individual transitions, the spectra in the centre-of-mass frame were summed over 1MeV intervals to display the gross features of the angular distributions. These distributions are reproduced in Figure 27 and it may be seen that the character of the distributions changes abruptly from energy to energy. However, these changes were not solely the result of the arbitrary choice of boundaries for these summations, as the limits could be shifted by as much as 0.5MeV without changing the general pattern of the angular distributions.

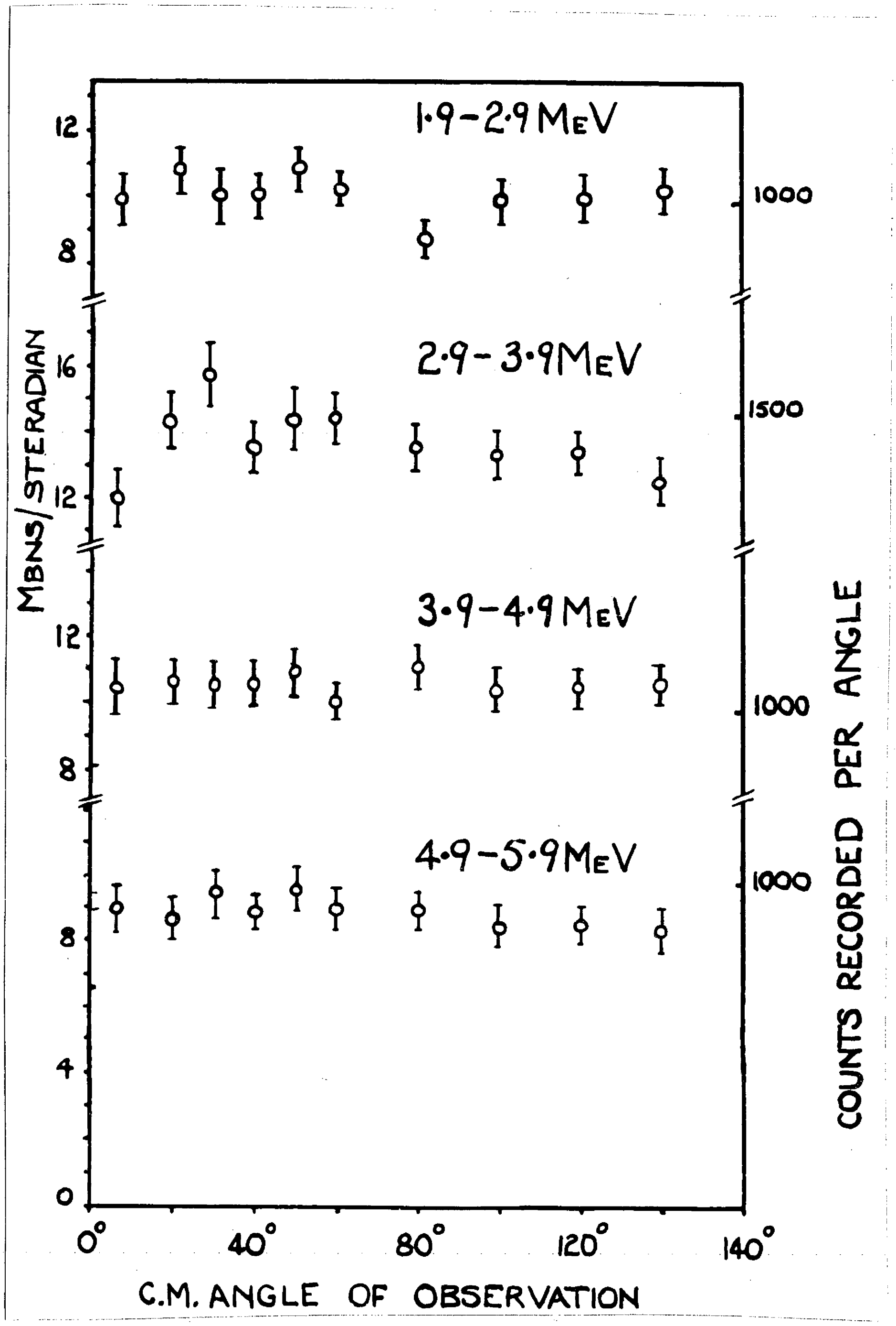

FIGURE 27: PROTON ANGULAR DISTRIBUTIONS.

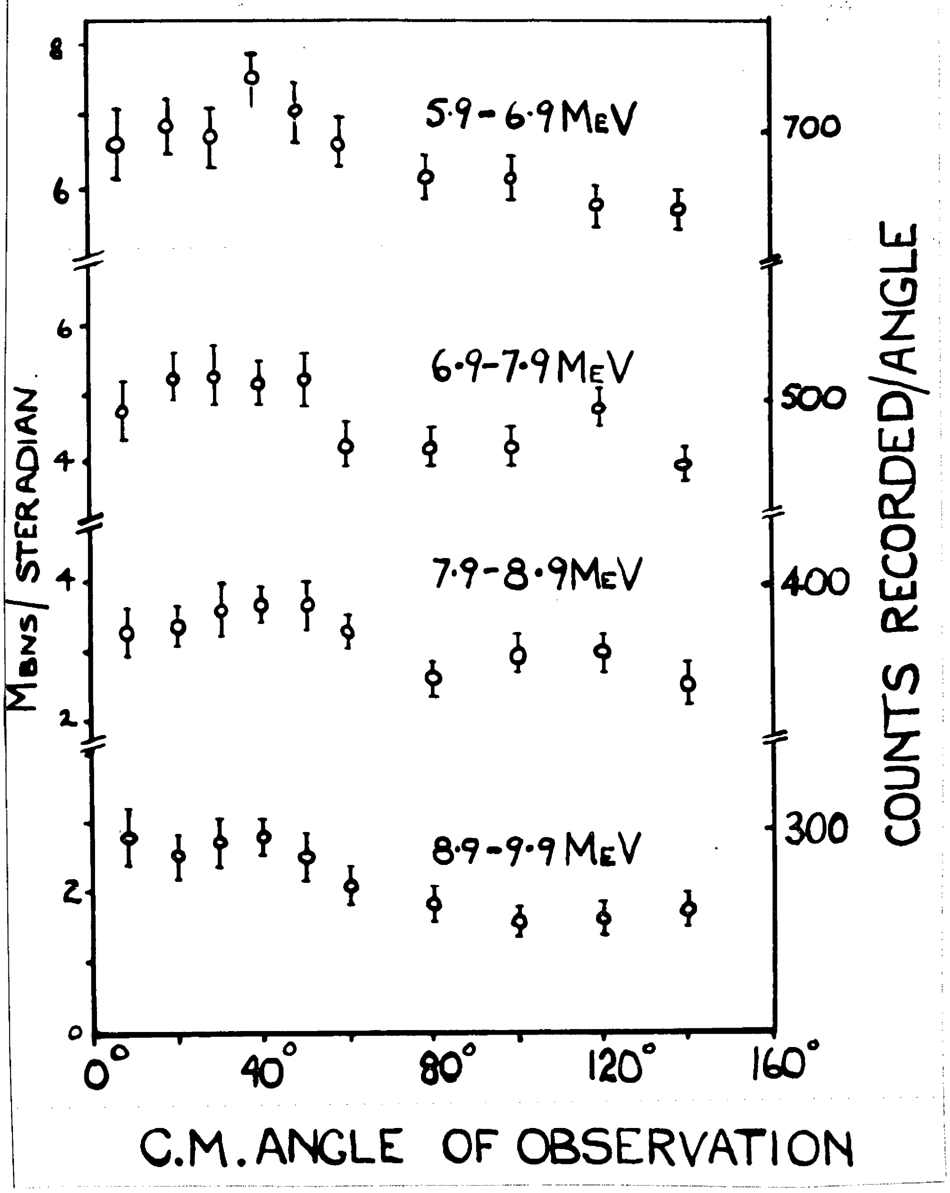

FIGURE 27(continued).

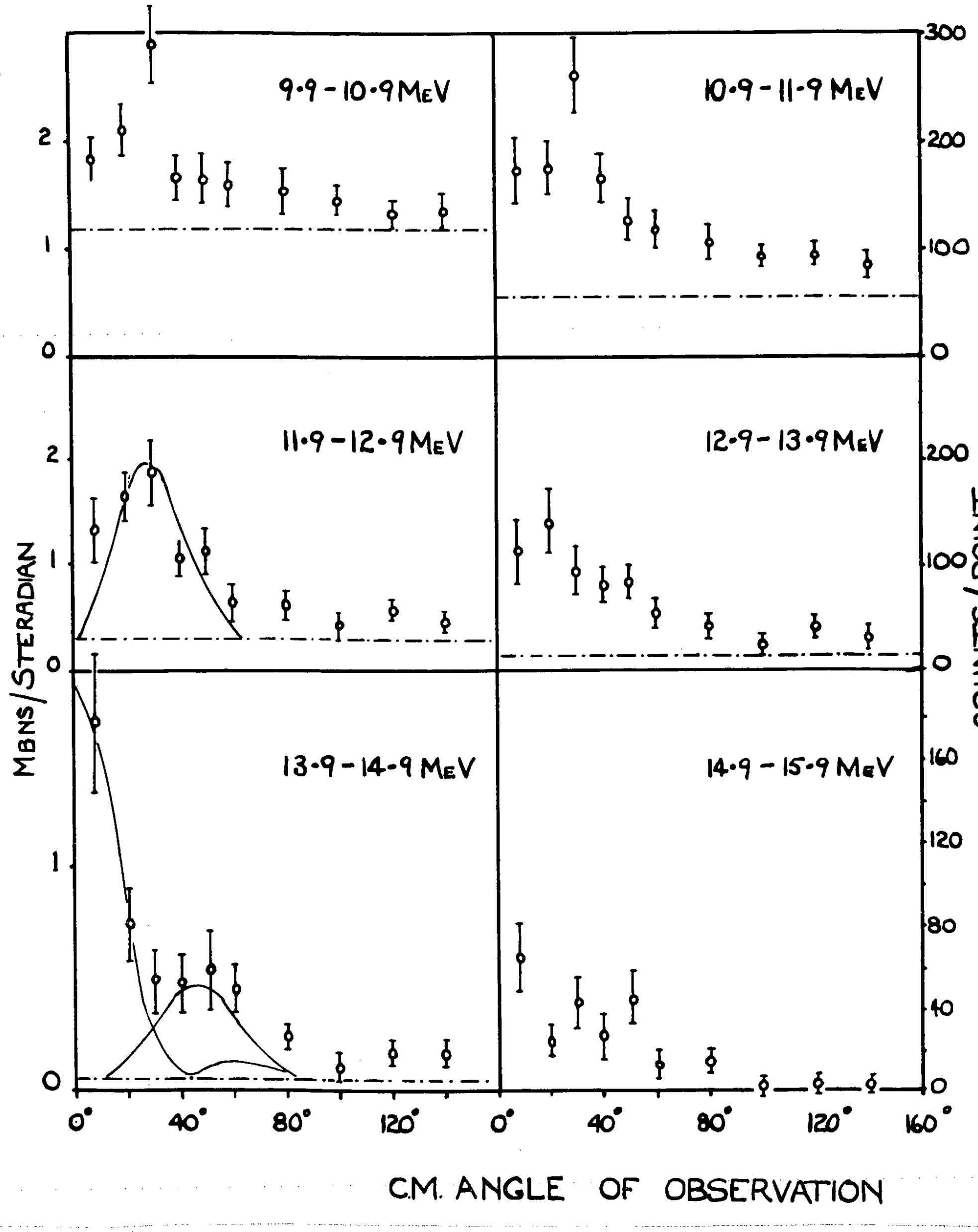

FIGURE 27(continued).

The dotted lines below the distributions show the amount of cross-section which was assumed to come from compound nuclear processes.

The data in the interval 1.9MeV to 2.9MeV was corrected for the forward peaking introduced to such angular distributions in the centre-of-mass system when the detection system has a low-energy cut-off. The manner in which this cut-off influences the angular distribution can best be illustrated by considering an isotropic, monoenergetic group of protons from Ni^{58} having a centre-of-mass energy of 2.0MeV. This group would give rise to protons in the laboratory system whose energy would vary between 2.2MeV at $\theta = 0^{\circ}$ and 1.86MeV at 140°. Even after allowance for the ionization losses within the target and counter gas has been made, all the 0° events would be above the 0.95MeV limit of detection. This is not true for the events at backward angles; not only do the particles start with a lower energy but they also lose more on their passage to the scintillator. Thus, the greatest number of events would be recorded at 0° and the smallest at 140°. In the present experiments the low energy cut-off introduced a 5% forward peaking to the 1.9MeV to 2.9MeV distribution.

Using a nuclear radius of 5.6f the angular distributions were fitted by a linear sum of squared Bessel functions, $[j_{\ell}(QR_0)]^2$, as suggested by the simple theory (Au53; Bu57a). For the range 13.9MeV to 14.9MeV a combination of $\Delta l = 0$ and $\Delta l = 2$ distributions provided a reasonable fit. This is just the combination which would be expected if the doublet group around 14.5MeV was from the transition discussed in the last section.

At lower proton energies the angular distributions showed $\Delta l = 1$ contributions so that odd-parity levels of Co^{58} appear above $E_x \sim 3$MeV. Such levels are expected and may be explained by the addition of a $1g_{9/2}$ neutron with the subtractions of a $1f_{7/2}$ proton.

Below 6MeV the angular distributions were isotropic within the limits of statistical accuracy. Thus it was not possible to make comparisons with the theory of Douglas and MacDonald in their calculations for (n,p) reactions (Do59).

<u>Section</u> (3.5.): <u>Induced Activity Measurements on Ni^{58} at 14.1MeV.</u>

Ni^{58} is one of the few nuclei in the periodic table for which induced activity measurements may be made to obtain both the (n,p) and the (n,np) cross-sections. If the (n,pn) contribution to the total cross-section is small, a direct comparison may be made between the partial cross-sect-sections obtained from the charged particle measurements and those obtained from induced activity experiments.

$Ni^{58}(n,p)Co^{58}$. Nickel foils were irradiated by 14.1MeV neutrons from the $T(d,n)He^{4}$ reaction at 90° to the deuteron beam. Because the position of the deuteron beam at the surface of the tritium target was known to only a few millimeters, the solid angle subtended by the target foil at the neutron source was uncertain. However, the effective solid angle was found by placing copper discs on both sides of the nickel foils, which in turn were placed 3.5cms from the neutron source. Copper foils were also placed 15cms from the source where the integrated flux was accurately known by counting associated alpha particles. By comparing the induced $Cu^{65}(n,2n)Cu^{64}$ activities, between the two sets of discs it was possible to estimate the integrated flux at the foil to better than ± 7%.

Co^{58} is formed by $Ni^{58}(n,p)Co^{58}$ in its ground state and also in a 9 hour isomeric state at 0.025MeV. Co^{58} decays with a half life of 72 days to a level of Fe^{58} at 805keV, by emitting a positron or by the electron capture process.

The number of Co^{58} atoms produced during the neutron irradiation was estimated by counting the positron annihilation quanta with a NaI(Tl) scintillation spectrometer, allowance being made for the self absorption which took place within the nickel foil. The efficiency of the spectrometer was found by calibrating the system with a Na^{22} source whose strength was known to ± 6%. When calibrating the system, the standard was placed in the same geometry to the NaI(Tl) detector as the irradiated foil. The K/β^+ ratio for the decay has been measured accurately by Good et al. (Go46) and a value of 5.89 was used in this work. A consideration of the uncertainties of the measurements included: spectrometer 12%; neutron flux 10%; counting errors 1%; and the K/β^+ ratio 5%. Total error $\pm$ 20%.

Three independent measurements of the cross-section were made and the weighted mean of these gave

$$\underline{Ni^{58}(n,p)Co^{58}(14.1\text{MeV}) = 560 \pm 110\text{mbn.}}$$

An endeavour was made to detect the fraction of Co^{58} nuclei which was left in the 9 hour isomeric state after neutron irradiation. This was done by following the 805keV gamma ray from Fe^{58} for some hours after the irradiation to see if the intensity of this line increased with the half life of the isomeric transition. Although some small rises in intensity appeared to take place no certain effect was observed. A consideration of the sensitivity of the system suggested that the cross-section for populating the 9 hour metastable state of Co^{58} was less than 10% of the total cross-section for the reaction.

$\underline{Ni^{58}(n,2n)Ni^{57}}$. Because Ni^{57} emits a positron when it decays to Co^{57}, the cross-section for $Ni^{58}(n,2n)Ni^{57}$ can be determined by using the same technique as was employed for $Ni^{58}(n,p)Co^{58}$. The value found was 38 $\pm$ 8mb., in good agreement with the measurements of Paul and Clarke (Pa53).

$\underline{Ni^{58}(n,np)Co^{57} + Ni^{58}(n,pn)Co^{57}}$. The ratio of the cross-sections for $Ni^{58}(n,2n)Ni^{57}$ and $Ni^{58}(n,np)Co^{57} + Ni^{58}(n,pn)Co^{57}$ was estimated by a technique which depended upon the fact that the 36 hour Ni^{57}, from (n,2n), decayed to 270 day Co^{57}, the same nucleus as was produced directly by $Ni^{58}(n,np)Co^{57}$. Because the half life of Co^{57} is 270 days, the number of these nuclei present after a short neutron irradiation was equal to the number formed by (n,np) reactions. After the Ni^{57} nuclei have decayed, however, the number is greater and is related to the sum of the cross-sections (n,np) and (n,2n). In practice, the contributions from these two cross-sections were separated chemically by "milking off" the cobalt nuclei present immediately after an irradiation and repeating the separation on the sample after most of the Ni^{57} nuclei had decayed to Co^{57}. This produced two cobalt samples: one with a Co^{57} activity proportional to $Ni^{58}(n,np)Co^{57}$; the other with an activity proportional to $Ni^{58}(n,2n)Ni^{57}$.

After bombardment the nickel foils, which had previously been analyzed and found to have a negligible cobalt contamination, were dissolved in a little HCl to which 5mg of $Co(NO_3)_2$ carrier had been added. A cobalt nitrite method was used to separate the cobalt atoms from the nickel sample. After a week the same separation technique was again applied to remove the cobalt which had formed in the intervening period from the decay of Ni^{57}. The chemical separation took about 45 minutes and better than 99% of the carrier could be recovered.

Co^{57} has a half life of 270 days and decays by electron capture to the 136keV excited state of Fe^{57}. The γ-rays from this state were detected to provide directly the ratio of the cross-sections $Ni^{58}(n,np)Co^{57}$: $Ni^{58}(n,2n)Ni^{57}$. The experimental ratio was 4.2 and was found to be reproducable to the order $\pm$ 10%. Combined with the known cross-section of $Ni^{58}(n,2n)Ni^{57}$ this gave

$Ni^{58}(n,np)Co^{57}$....160 $\pm$ 40mb.

Comparison between Charged Particle and Activation Measurements. Although the total cross-sections for proton emission by the charged particle and activation measurements were in reasonable agreement, the partial cross-sections were outside of assigned errors. Table 2 is a comparison between the two sets of measurements.

TABLE 2

COMPARISON BETWEEN PROTON CROSS-SECTIONS OBTAINED BY CHARGED PARTICLE AND ACTIVATION MEASUREMENTS.*

Reaction	Activation Cross-Sections(mb.)	Charged Particle Cross-Sections(mb.)
Total Protons Emitted	720 ± 120	830 ± 70
(n,p)	560 ± 110	490 ± 50
(n,np)	160 ± 40	340 ± 40

*It should be remembered that slightly different neutron energy was used for the two sets of measurements.

The comparisons in Table 2 show that the charged particle cross-section for (n,p) is low relative to the activation measurements and that the opposite is true for σ(n,np). If these differences are not caused by inaccuracy in the activation measurements they can be explained by the use of a diffuse potential, in the calculation of the Coulomb barrier penetrabilities, rather than a square well with sharp edges. Kikuchi (Ki57) has investigated such a possibility and has calculated the transmission coefficients for protons through a potential of the form:

$$V(r) = Ze^2/r - V_0\left[1 + \exp\left\{\frac{r-R}{d}\right\}\right]^{-1}$$

where d is the diffuseness of the nuclear surface($\sim$0.5f).

R is the classical radius.

V_0 is of the order of 40MeV.

The consequences of such a potential is that low energy events have a higher probability of emission. This allows the cross-section for (n,p) interactions to be increased at the expense of the (n,np) cross-section.

Decay of Compound Nucleus Ni^{58*}. One of the assumptions of the compound nucleus model is that, because the lifetime is long, the mode of decay of the intermediate nucleus is independent of the way in which it was formed. Some evidence for the correctness of this assumption for the compound nucleus Ni^{58*} is presented in Table 3. Here, a comparison is made of the various ways in which Ni^{58*} de-excites for a variety of modes of formation. The ratio of reaction cross-sections to Co^{57} and Ni^{57} are so similar for several bombarding particles that it provides some evidence that the decay is indeed independent of the method of formation.

TABLE 3

RATIO OF CROSS-SECTIONS TO Co^{57} AND Ni^{57} GOING THROUGH THE COMPOUND NUCLEUS Ni^{58*}.

Reactions	Ratio of Cross-Sections	Reference
$Ni^{58}(p,2p)Co^{57}/Ni^{58}(p,pn)Ni^{57}$	2.8	Co55
$Ni^{58}(\alpha,\alpha p)Co^{57}/Ni^{58}(\alpha,\alpha n)Ni^{57}$	5.0	Mi57
$Fe^{54}(\alpha,p)Co^{57}/Fe^{54}(\alpha,n)Ni^{57}$	4.0	Mi57
$Ni^{58}(\gamma,p)Co^{57}/Ni^{58}(\gamma,n)Ni^{57}$	2.35	Ca59
$Ni^{58}(n,np)Co^{57}/Ni^{58}(n,2n)Ni^{57}$	4.5	Present Work

Section (3.6.): Conclusions.

The results of this study of $Ni^{58}(n,p)Co^{58}$ at 14.9MeV have indicated the following conclusions:

(1) The angular distributions suggest that compound nucleus formation is probably the dominant process for at least 90% of the interactions.

(2) Many of the high energy protons, emitted in both the forward and backward hemispheres are from direct (n,p) interactions.

(3) The variation of level density with excitation energy indicates that the entropy varies as E^* rather than $\sqrt{E^*}$ as predicted by the Fermi gas model.

(4) The differences between the activation cross-sections and those obtained from the charged particle measurements indicate that the accepted penetrabilities for Coulomb barriers may be in error.

CHAPTER IV

THE DEUTERONS FROM $Ni^{58}(n,d)Co^{57}$

Section (4.1.): Experimental.

When analyzing the filmed record of the Ni^{58} experiment, stringent precautions were adopted to ensure that a negligible number of proton events were included in the deuteron spectra. This positive identification was achieved, at some cost to statistical accuracy, by only identifying an event with deuteron emission when its product, $(E+1).dE/dx$, was greater than the mean $\overline{(E+1).dE}/dx$ for the energy interval. While this proceedure eliminated proton contamination, the analysis suffered as only 50% of the recorded deuteron events were included in the final spectra.

The energy scale for the deuteron spectra was established by assuming that the scintillation response of NaI(Tl) was linear with energy and that its scintillation efficiency for protons and deuterons was as 1.04:1.00 (see Se55). Further justification for the correctness of this ratio was provided from companion work in this laboratory on $Al^{27}(n,d)Mg^{26}$, where the position of known levels of Mg^{26} were found correctly (Personal communication; Glover, R.N. and Weigold, E.).

A computer programme, similar to that described in the previous chapter, was devised to correct the raw deuteron data for ionization losses and to transfer the results to the centre-of-mass frame. The corrected spectra, from various angles in the forward hemisphere, are shown in Figure 28. While there was some evidence for a number of discrete transitions, only the group centred around 8.4MeV could be positively identified at all angles. The high energy group is even more apparent in the sum spectrum shown in Figure 29. It may be seen that a small number of events were recorded with an energy greater than 8.6MeV, a region forbidden to deuteron emission by the energetics of the reaction (As59). Investigations showed that these events were really protons which had been incorrectly identified in the mass selection proceedure. The number of these spurious events was small and at lower energies, where the dE/dx separation between protons and deuterons became greater, it was expected that the number was negligible.

The total cross-section for deuteron production was found by integrating the total yield of deuterons over 4 steradians. This measurement gave

$$\underline{Ni^{58}(n,d)Co^{57} = 25 \pm 5\text{mb. at } 14.9\text{MeV}.}$$

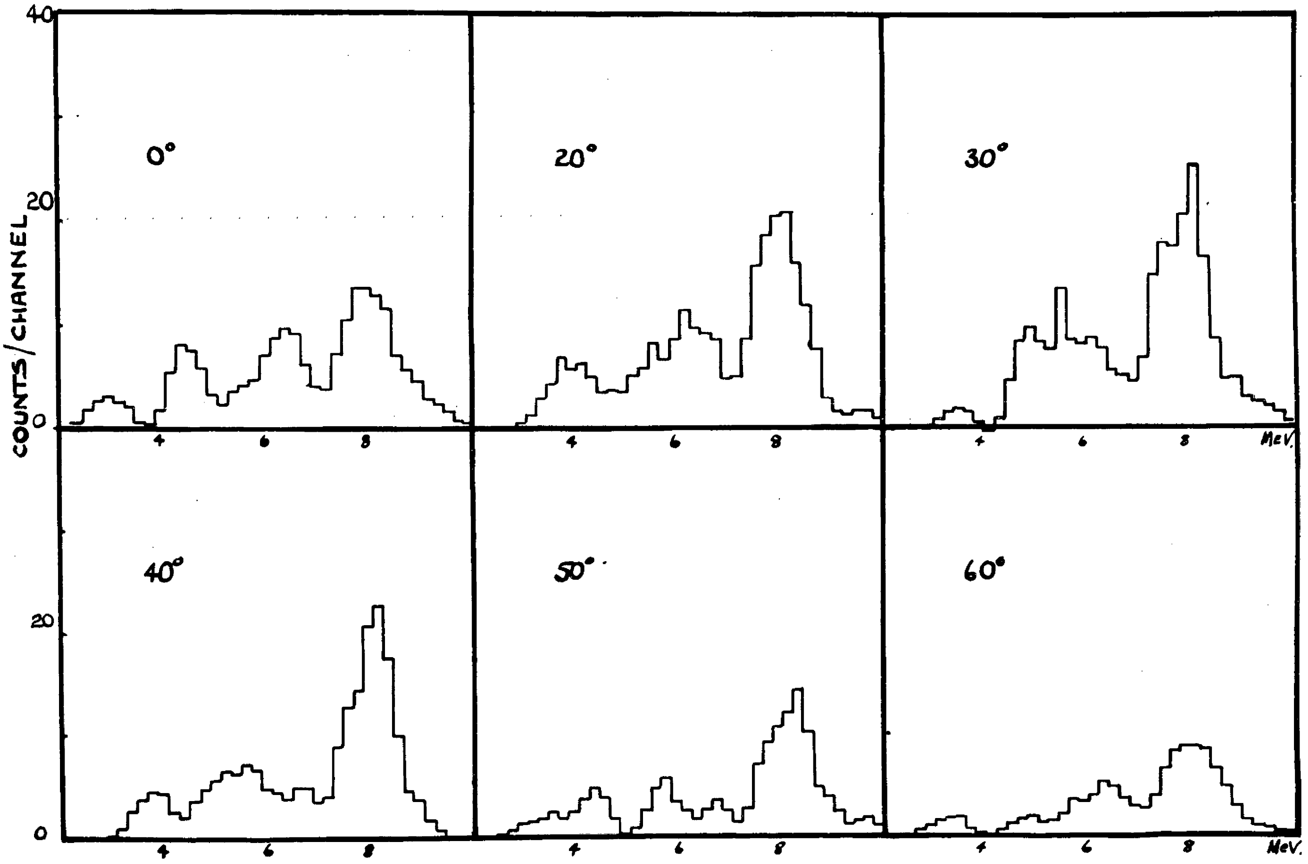

FIGURE 28: DEUTERON SPECTRA RECORDED IN THE FORWARD HEMISPHERE.

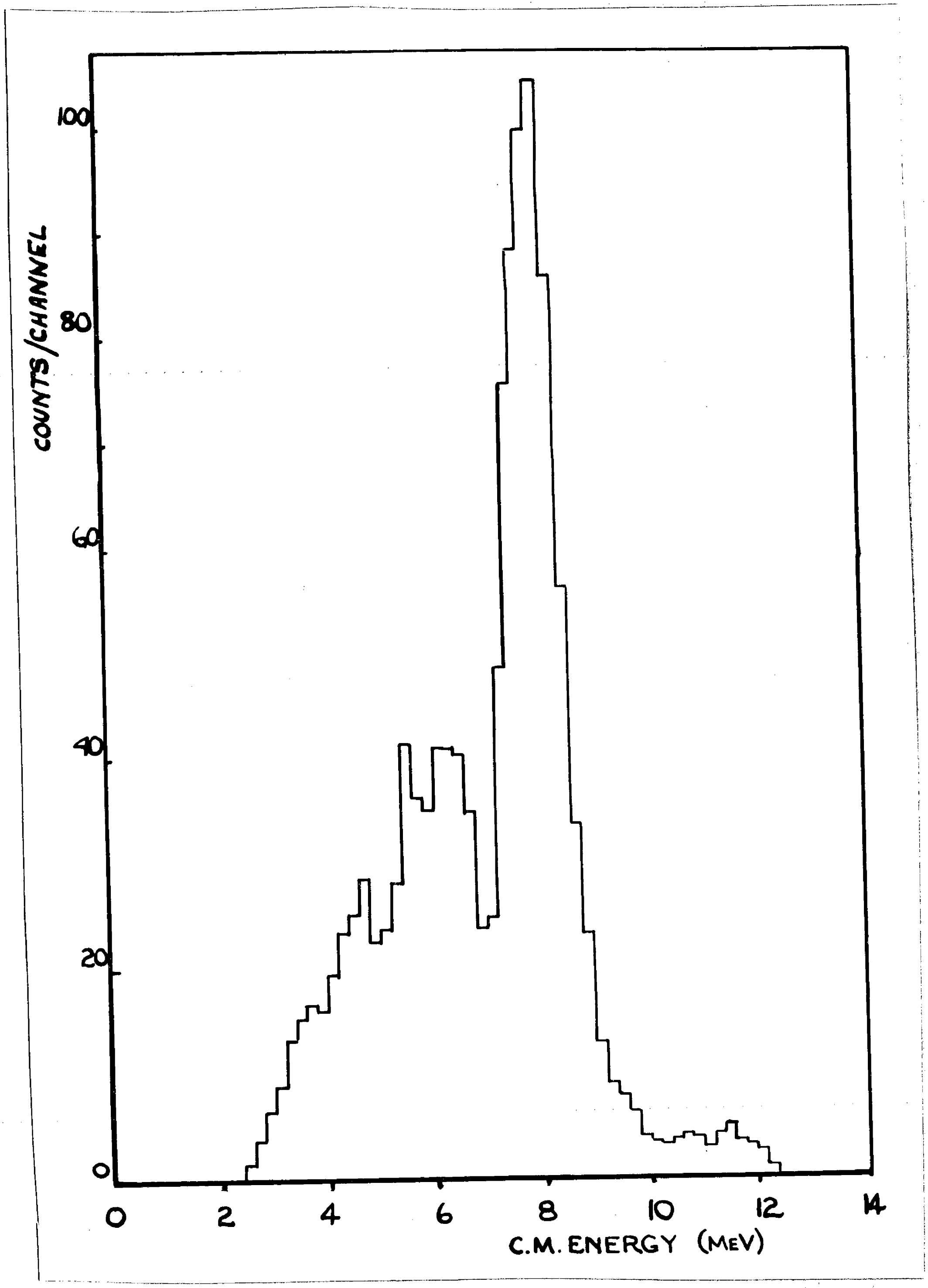

FIGURE 29: SUM SPECTRUM OF DEUTERON EVENTS RECORDED IN THE FORWARD HEMISPHERE.

Section (4.2.): High Energy Deuteron Group.

The angular distribution of the 8.4MeV deuteron group is shown in Figures 30 and 31. This data was fitted by Butler inverse stripping patterns using the numerical tables of Lubitz (Lu57). These tables contain the entire angular dependence of the stripping differential cross-sections for a variety of angular momentum transfers and interaction radii. Before making comparisons with the experimental data the theoretical curves of Lubitz were corrected for the smearing effect of the finite aperture of the telescope (see Section 2.2.). It was found that no reasonable combination of r_o and Δl for a single angular momentum transfer gave a satisfactory fit to the experimental points. It was necessary to use a mixture of $\Delta l = 1 + 3$, in the ratio 1 : 6.5, or alternatively a mixture of $\Delta l = 2 + 4$, in the ratio 1 : 3.1 (see Figures 30 and 31). While the $\Delta l = 2 + 4$ fit agrees better with the large angle data than the $\Delta l = 1 + 3$ fit, it is a factor of two low at the 8^o point.

If this interpretation of the distribution pattern is correct, and it is indeed a mixture of two stripping transitions, two separate Co^{57} states must be involved, as Ni^{58} has spin zero. Further evidence on this point comes from the resolution obtained for the 8.4MeV deuteron group. This width, compared to that obtained for an 8.15MeV deuteron

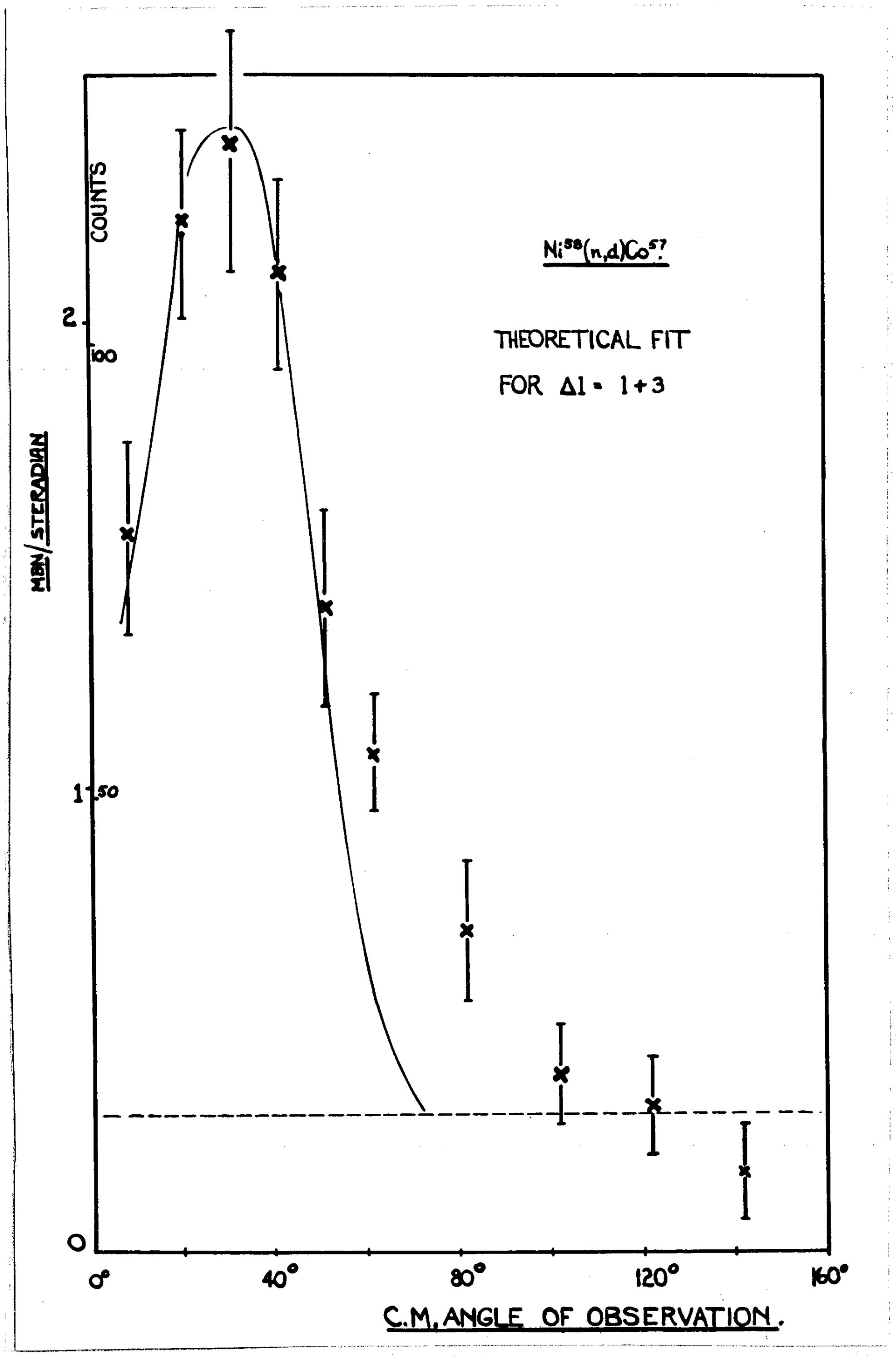

FIGURE 30: ANGULAR DISTRIBUTION OF HIGH-ENERGY PEAK.

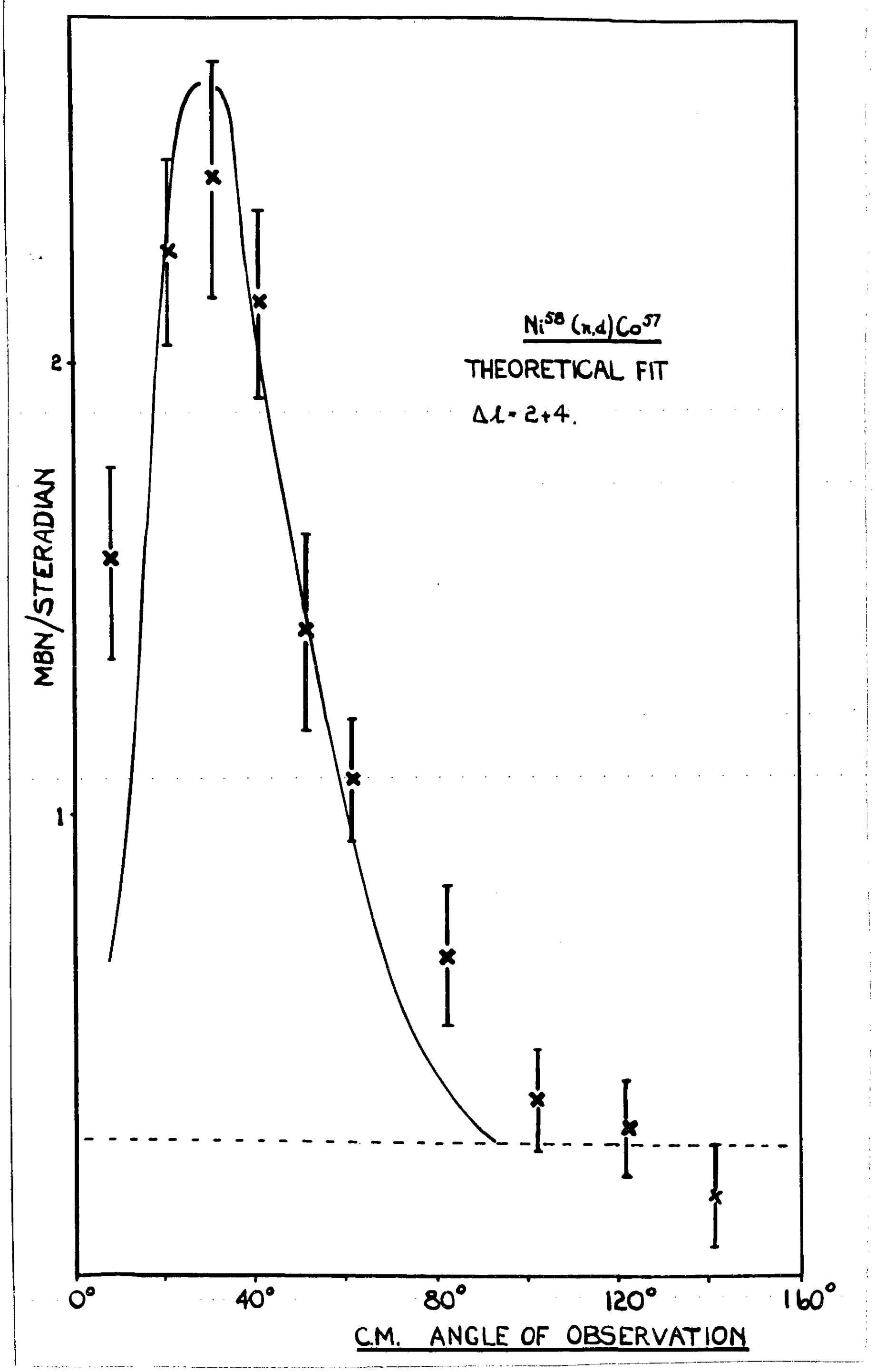

FIGURE 31: ANGULAR DISTRIBUTION OF HIGH-ENERGY PEAK.

group from $Al^{27}(n,d)Mg^{26}$ (Glover and Weigold; personal communication), was consistent with two transitions $\sim$0.5MeV apart.

Decay studies of Ni^{57} (Ko56; Ko58) have shown that the levels of Co^{57} are at 0MeV($^7/_2{}^-$); 1.36MeV($^3/2^-$); 1.49MeV($^1/_2{}^-$) and 1.89MeV($^5/_2{}^-$). Because of the negative parity, pick up transitions to these levels from Ni^{58} could not involve even angular momentum transfer making $\Delta l = 2 + 4$ unlikely. Also, on the simple shell model (El57), the final proton of Ni^{58} closes the f-shell and, if this is removed by simple extraction, could give an angular momentum change of three units to a Co^{57} core state.

The Q-value of $Ni^{58}(n,d)Co^{57}$ is quoted as -5.69MeV (As59) so that the 8.4MeV deuteron group goes to an excited level of Co^{57} at approximately 0.5MeV. It seemed reasonable to identify the $\Delta l = 3$ component with the ground-state transition to Co^{57} and postulate an error of approximately 0.3MeV in the experimental energy scale or in the Q-value. The former is a possibility as it has been reported (Pe59a) that the proton/deuteron response for scintillators depends somewhat on the geometrical arrangements. The pulse height ratio at the analyzer may also depend on the time-constants of the photomultiplier circuitry as there is no evidence that deuteron and proton pulses are identical.

To explain the possible presence of $\Delta l = 1$ transitions, it is necessary to invoke a new level of Co^{57} at approximately 0.5MeV with a spin and parity of $^1/_2{}^-$ or $^3/_2{}^-$. Such a level may be in conflict with the data of Koniju et al. (Ko58), who carried out a search for gamma rays of energy around 0.5MeV by β-γ coincidence techniques and placed an upper limit of 1% of the total gamma emission on the intensity of such transitions. However, allowed β transitions are most intense and the apparent absence from Koniju's work of states around 500keV may only indicate the presence of unfavoured β groups.

The implication of $\Delta l = 1$ transitions is that the Ni^{58} ground state contains p-wave admixture. The reduced widths, extracted according to the recipe of MacFarlane and French (Mc60), for the $\Delta l = 1$ and $\Delta l = 3$ transitions were 0.005 and 0.038, respectively, indicating 13% admixture. Assuming JJ-coupling the spectroscopic factor, S, would have a value of 8, suggesting 0.005 for the single particle reduced width $\theta_0^2(1f)$. This seems to be not inconsistent with $\theta_0^2(1f) \approx .012$, in the range A 17 - 45 (Mc60), if θ^2 decreases by a factor of the order 2-3 at the end of this shell as has been observed for the 1d shell.

CHAPTER V

THE USE OF SCINTILLATING CRYSTALS AS TARGET AND DETECTOR FOR NEUTRON INDUCED REACTIONS AT 14MeV

Section (5.1.): Experimental Details.

Before the decision was made to construct the coincidence counting system described in Chapter II, the possibilities were investigated of using a single organic scintillator as target and detector for neutron induced reactions. In practice, a crystal scintillator would be placed within a fast neutron flux and the energy of the charged particles produced from neutron interactions within the crystal volume measured from the intensity of the scintillations. Because the charged particles do not have to escape before detection, thick crystals could be used allowing reactions of small cross-section to be investigated. As an extensive variety of scintillating materials are available, measurements may be contemplated for a number of nuclei scattered throughout the periodic table.

Preliminary measurements were made to determine the feasibility of the technique and the quality of the results which might be expected. Neutrons having an energy of 14MeV were used to bombard several pieces of NaI(Tl) which had dimensions between 0.025" and 0.300". The scintillations from these crystals were viewed by a Dumont 6292 photomultiplier whose output was amplified and displayed on a Hutchison-Scarrot 100-channel analyzer. The energy scale was calibrated by Bi^{212} alpha particles, after independent measurements had established that the 8.05MeV group had the same scintillation response as 5.4MeV protons(personal communication, I.F. Wright).

Unfortunately, no pulse height spectra can be reproduced here as a serious laboratory fire destroyed the experimental data. However, the spectra showed no structure which would be evidence for direct transitions to low levels of the final nucleus. The counting rates were found to vary smoothly over the whole energy range, being greatest for low energy protons and least for those of high energy. The conclusion which was reached was that intense background counting rates must be anticipated when scintillators are submerged in a 14MeV flux. It is also possible that centre-of-mass effects broaden, significantly, the widths of discrete particle groups, causing these transitions to merge into the general background.

Section (5.2.): Background Pulses from a Scintillator Within a Fast Neutron Flux.

Neutron Scattering. When fast neutrons are scattered, the recoiling nuclei acquire kinetic energy which is quickly transferred to the lattice and lost as heat and electromagnetic radiation. Because the cross-section for elastic scattering is of the order of 10^{-24}cm^2., and is much greater than the cross-sections for most competing reactions, the majority of the background scintillations arise from the stopping of recoiling nuclei. If NaI is used as the target-detector, scattering of 14MeV neutrons by Na^{23} nuclei gives a recoil spectrum with a maximum energy of 2.2MeV. While the scintillation response for Na^{23} ions is only $\sim$0.35 of that for protons of the same energy(Sh59), this response is still sufficiently great that elastic scattering by Na^{23} nuclei provides an intense rectangular spectrum out to $\sim$1MeV equivalent proton energy.

Interactions with Gamma Rays. Inelastic scattering and capture reactions, within the crystal and the surrounding materials, results in large numbers of gamma rays and electrons. These may interact with the scintillator causing scintillations of a size as great as that from protons having an energy of several MeV. These background events may be diminished in size, by decreasing the linear dimensions of the crystal, but escape corrections set a lower limit to the size of detector which can be usefully employed. When studying (n,p) interactions from 14MeV neutrons the maximum range of the protons produced sets the smallest linear dimensions of crystals at $\approx$0.1".

Charged Particle Backgrounds. Reactions in the walls of the chamber surrounding the crystal must be minimized by covering the crystal with materials having small cross-sections for charged particle emission. High Z materials are undesirable as they are more efficient gamma ray converters; probably the most suitable material is C^{12} which has a large negative Q-value for (np) reactions. The glass of the photomultiplier is a strong source of charged particles and one problem of design of a satisfactory experiment is the necessity of arranging the detection system so that particles from the photomultiplier cannot enter the scintillation crystal.

Section (5.3.): Centre of Mass Effect.

The absence of discrete groups in the energy spectra from the scintillation detector can be understood if consideration is given to the effects from centre-of-mass motion:

The total energy released in an (n,p) transition between two definite states will be a constant, independent of the angle at which the reaction is observed:

$$E_T = E_p(\theta) + E_R(\theta')$$

where $E_p(\theta)$ is the energy of the proton observed at the angle θ.

$E_R(\theta')$ is the energy of the recoiling nucleus at the conjugate angle θ'.

Because of centre-of-mass motion, both $E_p(\theta)$ and $E_R(\theta')$ are functions of the angle of emission, being greatest in the forward direction and least in the backward.

The scintillation response, $S(\theta)$, to an event of this type may be written:

$$S(\theta) = k.E_p(\theta) + k' E_R(\theta')$$

where k and k' are the scintillation response of the crystal to protons and Ne^{23} ions. For Ne^{23} ions, the recoiling nucleus from $Na^{23}(n,p)$, $k \neq k'$ and because of this, each discrete group is broadened significantly.

The magnitude of this effect is sufficiently great that a group of protons, having 15MeV in the centre-of-mass system, is broadened by the order of 1MeV when detected with an inorganic scintillator having 4π geometry. Thus, a spectrum composed of a number of sharp groups would show little structure unless the separations are greater than 1MeV.

Section (5.4.): Conclusions and Suggestions for Future Experiments.

While the technique appears to have a number of attractive features, it also suffers from some disadvantages:

(i) When 14MeV neutrons are used the background counting rates are intense. However, it is possible that the technique may be valuable for obtaining data at lower energies.

(ii) Several elements are present in most inorganic scintillators, making the interpretation of any spectra obtained ambiguous.

(iii) It is doubtful if proton and deuteron events can be distinguished. This remark may need revision, however, in the light of suggestions by Story et al.(St58a) for particle identification.

(iv) Angular distributions cannot be measured.

(v) Centre-of-mass effects would be expected to broaden the width of discrete energy groups.

Possible Technique for Eliminating Backgrounds and Centre-of-Mass Effects.

Figure 32 is a schematic of a counting arrangement which would eliminate centre-of-mass effects and the background of charged particles from the materials surrounding the scintillator. Two inorganic crystals, each of thickness somewhat less than the range of the particles to be counted, are viewed by separate photomultipliers. One of the crystals is placed within a cone of neutrons where the

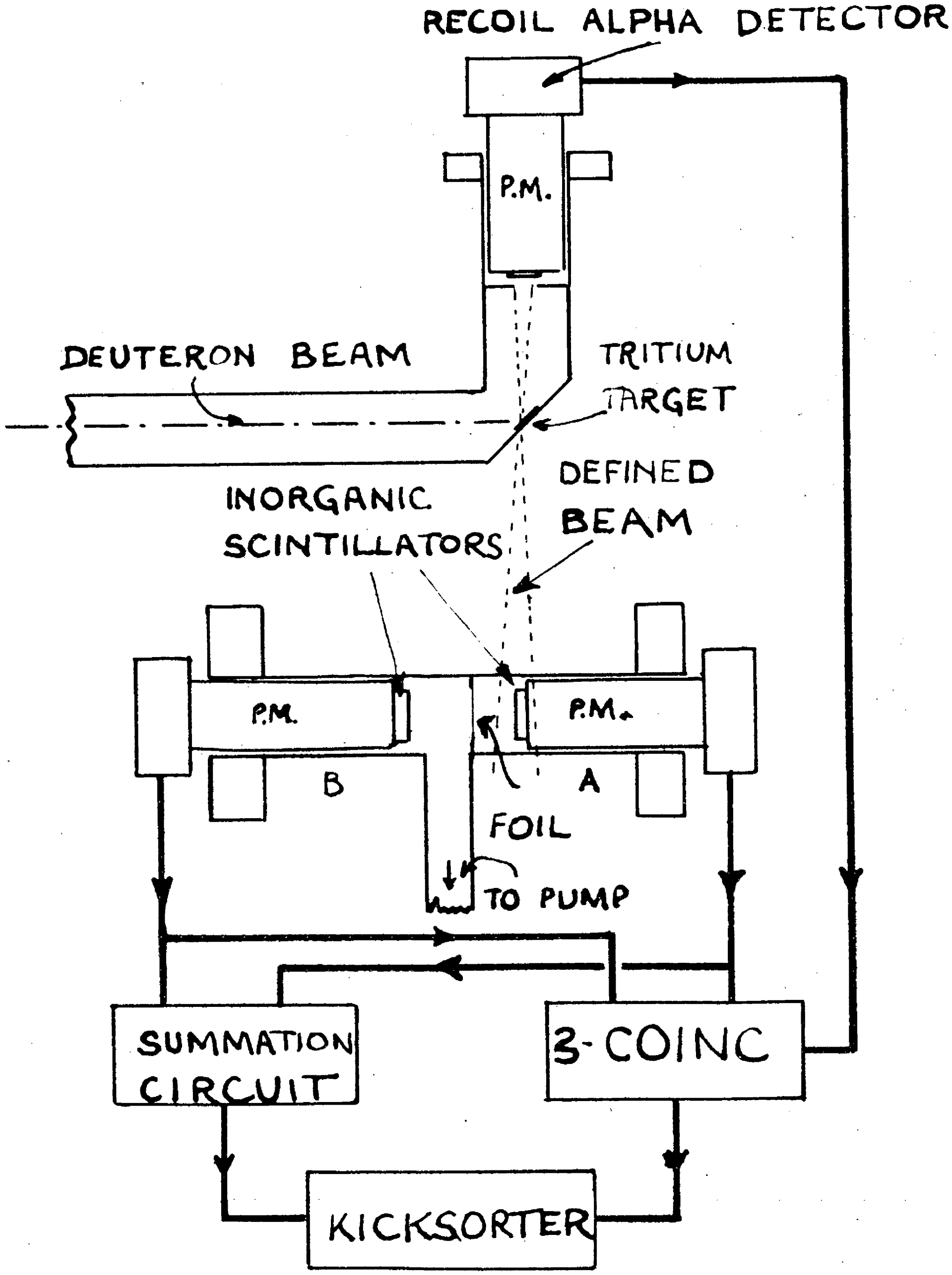

FIGURE 32: SCHEMATIC DIAGRAM OF PROPOSED COINCIDENCE ARRANGEMENT FOR ELIMINATING CENTRE-OF-MASS EFFECTS.

times of emission of each are known by detecting the associated alpha particles from the $T(d,n)He^4$ reaction. The other crystal is kept from this defined beam at all times. The outputs from the two photomultipliers A and B are fed to a summation circuit whose output is only recorded by an analyzer when a high speed triple coincidence is registered between the scintillation counters and the recoil alpha particle detector. Under these conditions, neutron induced reactions could only be recorded when the interaction takes place within the scintillator A and travels in the correct direction to be stopped within the scintillator B. As thick targets could be employed good counting rates could be anticipated. Angular distributions could be measured if the counter B remained out of the defined beam.

CHAPTER VI

A SEARCH FOR LEVELS OF Li^7 BETWEEN 9.0MeV AND 9.55MeV EXCITATION

Section (6.1.): Introduction.

The success of the intermediate coupling shell model in predicting the properties of nuclei with unfilled 1p-shell configurations (El 57) has been the cause of great interest in the experimental details of nuclei in the He^4 to O^{16} region. Important gaps remain, however, which make a test of the theory difficult. A case in point is the nucleus Li^7 where a number of levels, suggested by the results from photodisintegration experiments, remain to be confirmed by other reactions. The experiment reported here sought to confirm the presence of the level thought to be at 9.3MeV and to find its charater by examining the structure of the yield curve for interference effects.

One feature of the $Li^6(n,H^3)He^4$ reaction which has puzzled some workers is that, with the exception of the broad p-wave resonance at 255keV, no structure is apparent in the cross-section curve over the whole of the measured energy range (see Figure 33), (Fr54; We54; Hu55; Ri56; Ke58; Bo58). The lack of structure in this curve is surprising, as several levels of Li^7 are thought to be present in the corresponding range of excitation (Aj59).

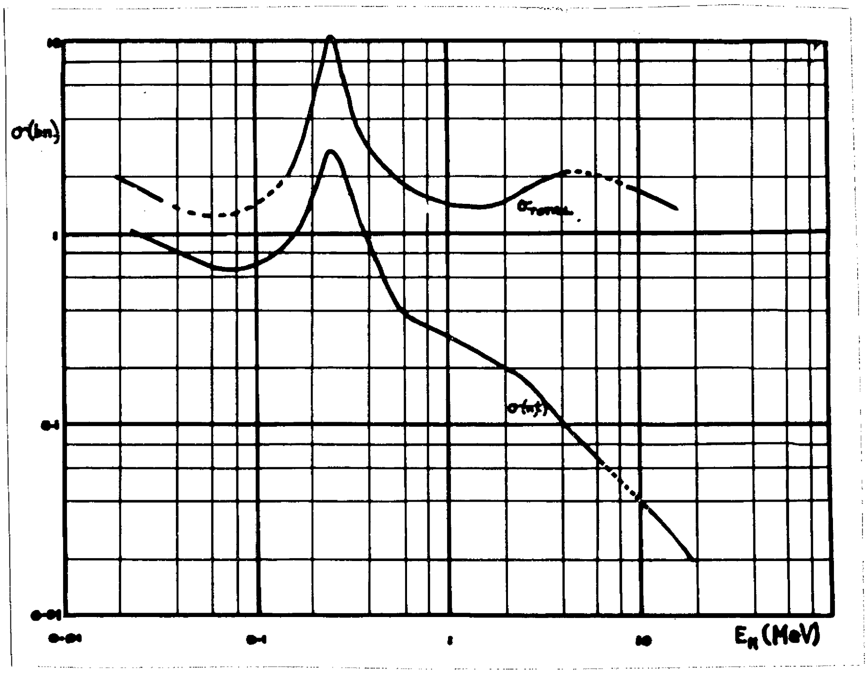

FIGURE 33: σ_T AND $\sigma(n,t)$ CROSS-SECTIONS FOR $Li^6(n,t)He^4$ FROM 20keV TO 18MeV.

Dabrowski and Sawicki (Da55; Sa55a,b) have suggested that the bulk of the reaction $Li^6(n,H^3)He^4$ goes by a direct process which does not involve the compound system Li^{7*} at all. Sawicki's calculations, which include coulomb corrections, are in reasonable agreement with measured cross-section and angular distribution data (Da53; Fr54; We54) and it seems likely that part of the reaction, at least, does require such an explanation. However, while the direct transition matrix elements may be large, it is still difficult to understand the apparent absence of resonance structure in the yield curve.

Section (6.2.): Evidence for a level of Li^7 at 9.3MeV Excitation.

The existence of a level Li^7 in the neighbourhood of 9.3MeV was first demonstrated by Titterton and Brinkley (Ti53a) who used nuclear emulsions to measure the differential cross-section of the reaction $Li^7(\gamma,H^3)He^4$. The cross-section was found to have a peak at 9.3MeV with an experimental half-width of several hundred keV. By comparing these results with cross-section measurements carried out by Titterton (Ti53), using 6.13, 14.8 and 17.6MeV gamma rays, an approximate integrated cross-section of 0.2×10^{-3}MeV.barns was associated with the reaction going through this level.

Other workers (St53; St54; Er54; Mi55a), using similar techniques to Titterton, have also found resonance absorption of gamma rays between 9.0MeV and 9.5MeV. Goldemberg and Katz (Go54) have measured an integral spectrum for the reaction $Li^7(\gamma,n)Li^6$; their results show a prominent break in the yield curve at 9.6MeV which they ascribe to a level in Li^7 with an integrated cross-section of approximately 0.2×10^{-3}MeV.barns. Further evidence for the existence of the level has been suggested by the inelastic scattering data of Allan (Al54) who used 14MeV neutrons on Li^7 and by Silver (Si57) who scattered 31.8MeV protons from Li^7. Recently, Titterton (personal communication) has remeasured the differential cross-section using synchrotron bremsstrahlung of maximum energy 12MeV. His preliminary results confirm the existence of resonant absorption of gamma rays around 9.3MeV. Because of the low energy of the incident radiation, the possibility is eliminated that the level which is present is populated by gamma ray cascades from Li^{7*} levels at higher excitation. In this work it was assumed that the 9.3MeV level, excited by the $Li^7(\gamma,t)He^4$ experiments, is the same level as that found at 9.6MeV by Goldemberg and Katz.

Section (6.3.): Experimental Details.

In these experiments the cross-section for $Li^6(n,H^3)He^4$ was measured with good energy resolution over the neutron energy range 2.0 - 2.65MeV. This energy range corresponds to an excitation of the compound Li^{7*} system from 9.0MeV to 9.55MeV where a level is thought to be present (Ti53a). By inserting the neutron and triton partial widths, which have been established for this level by gamma absorption experiments (Ti53; Go54), into the Breit-Wigner formula, it would appear that, to an order of magnitude, the resonance cross-section of this level by neutron absorption in Li^6 should be several hundred millibarns.

The experimental arrangement is shown in Figure 34 and consisted of a $Li^6I(Eu)$ crystal as target and detector for $Li^6(n,H^3)He^4$ reactions. This crystal was rotated about the neutron source to obtain energy variation. The technique was sufficiently sensitive that a 20mb change in cross-section of width 40keV should have been readily detected.

The scintillator was mounted on a thin glass plate, after being polished within a dry box to the dimensions 0.252" x 0.534" x 0.090". The $Li^6I(Eu)$ had a measured density of $3.93g/cm^3$ and was protected from moisture by a thin layer of vaseline and aluminium foil. The crystal was mounted 14.7 ± 0.2cms from the neutron source. Figure 35 shows a scintillation spectrum from the detector using an incident neutron energy of 2.6MeV. The low energy peak was caused by the flux of thermal and epithermal neutrons present in the target area arising from scattering of the primary neutrons, and from contamination and deuterium build-up on the defining stops of the accelerator tube. The half-width of the thermal peak was about 8% for a freshly mounted crystal and provided a useful calibration line for checking the gains and resolution of the circuitry.

The high energy peak arose from $Li^6(n,t)He^4$ initiated by fast neutrons. The peak had full-width at half-height

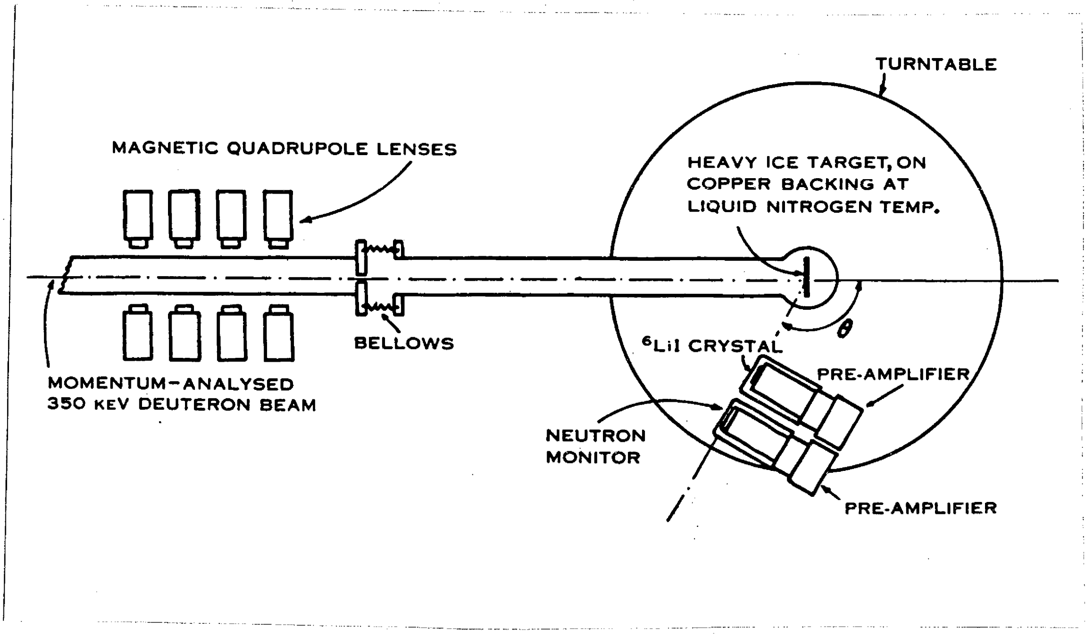

FIGURE 34: SCHEMATIC DIAGRAM OF EXPERIMENTAL ARRANGEMENT.

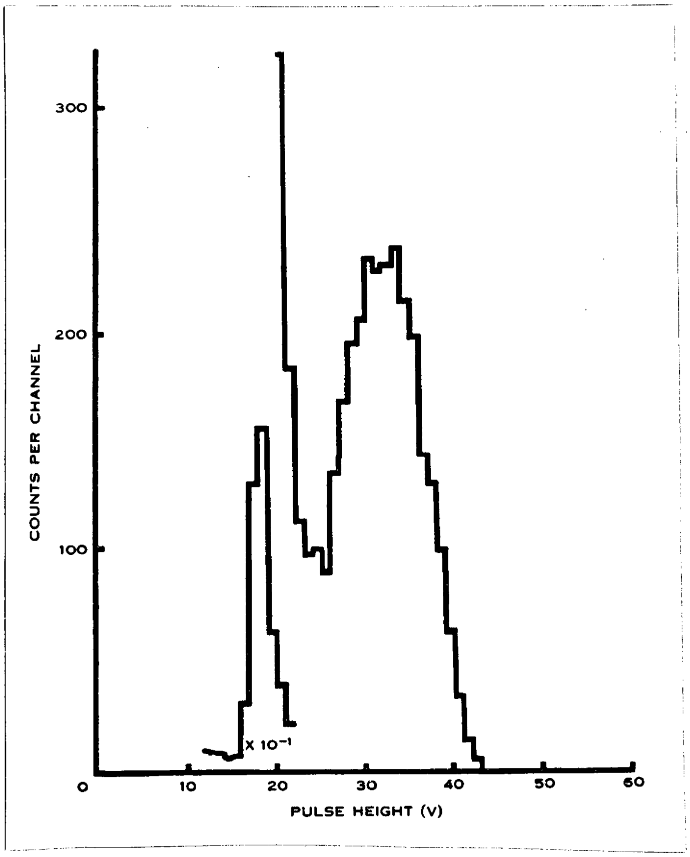

FIGURE 35: PULSE-HEIGHT DISTRIBUTION FROM Li^6I DETECTOR.

considerably greater than the resolution of the equipment. Several authors (Mu58; Op58; Ke58) have suggested that this large width is due to the difference in scintillation response of Li^6I for tritons and alpha particles; this is effective because, for a given neutron energy, the centre of mass motion of the system gives the emitted triton and alpha particles a range of energies in the laboratory system. The shape of the peak also depends upon the angular distribution for the reaction. Spectra taken at various neutron energies, showed little variation in the shape of the high energy peak indicating that the angular distribution for the reaction remained constant over the energies studied. Cross-section measurements were made by setting a bias at a known point in the high energy peak and recording all events producing a pulse greater than this level. The bias level was set sufficiently high that no pulses from the thermal peak were counted. Simultaneously, pulse height spectra were recorded to permit correction for the events which were missed because of the high setting of the discriminator bias.

Neutron Source. The production of monoenergetic neutrons from the $d(d,n)He^3$ reaction was made difficult because of the large background of neutrons coming from collisions of the deuteron beam with the defining apertures and with the walls of the magnet vacuum chamber. While the flux of these unwanted neutrons was minimized by shielding and by locating the defining apertures well away from the neutron source, it was still necessary to use comparatively thick targets so that the yield was well above background. Background measurements were made by counting $Li^6(n,H^3)He^4$ events, without a heavy-water target, for the same time-integrated beam current as was used in the experiments.

Unfortunately, thick targets reduce the range of the angle θ (and neutron energy) which is available for a given energy resolution. Figure 36 shows the energy resolution of the neutrons obtained from a 100keV thick target for a deuteron beam energy of 350keV as a function of the emitted neutron energy and the angle θ as calculated from the tables of Fowler and Brolley (Fo55).

Section (6.6.): Results.

Figure 37 shows the results of these cross-section measurements. The horizontal bars indicate the energy spread inherent in this type of neutron source; the vertical bars are the estimated errors in the measurements. The main sources of error at each point when determining the shape of the cross-section curve are the background subtractions, 3%; uncertainties in the geometry, 5%; counting errors, 4%. The absolute determination of the cross-section is also dependent upon geometry of the recoil-counter telescope and its location with respect to the heavy-ice target; this introduces a further uncertainty of 7%; the total error ±10%.

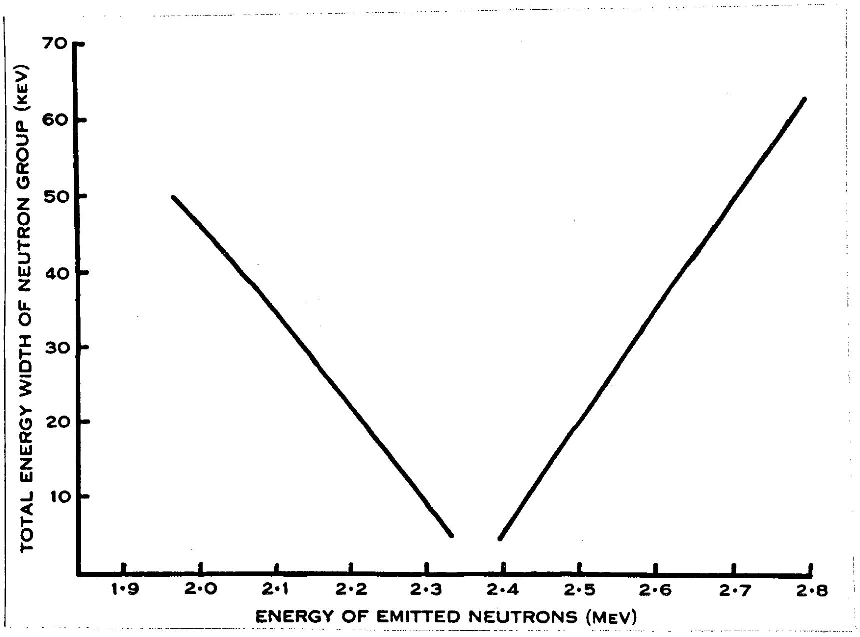

FIGURE 36: ENERGY RESOLUTION OF NEUTRONS OBTAINED FROM A 100keV-THICK TARGET OF HEAVY ICE USING AN INCIDENT DEUTERON ENERGY OF 350keV.

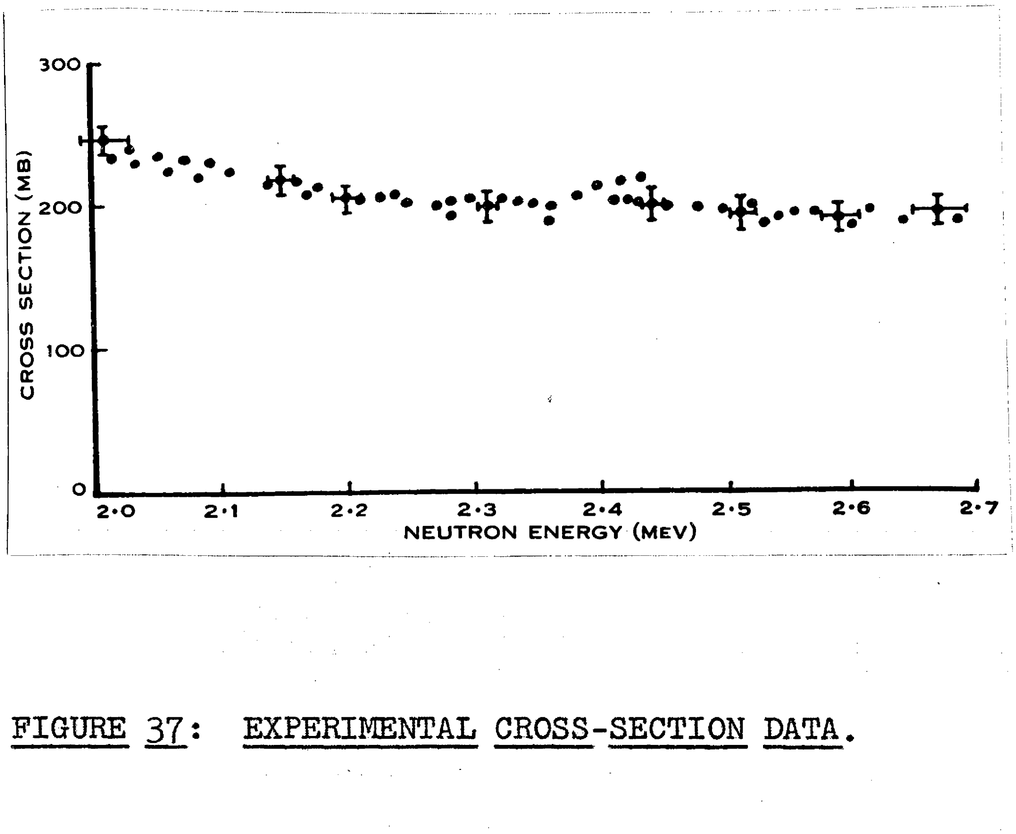

FIGURE 37: EXPERIMENTAL CROSS-SECTION DATA.

Over the energy range of 2.0MeV to 2.7MeV the cross-section data shows no significant indication of resonance structure but falls smoothly with increasing neutron energy. This would seem to indicate that, either the level (or levels) found by gamma ray experiments are not present in the energy range covered by these experiments, or alternatively, that the triton partial width is very small (10keV or less).

According to the simple shell model (E157), the ground state of the nucleus Li^6 has a configuration of $(1s)^4(1p)^2$ and has a spin and parity of 1^+. Thus, a neutron entering the Li^6 configuration to form the same Li^{7*} systems as are formed by the dipole absorption of gamma rays, would enter as s or d partial waves with the Li^6 nucleus providing the rest of the configuration. For neutron energies used in these experiments and assuming a radius for Li^6 of 2.9×10^{-13}cm. the transparency of the centrifugal barrier for d-wave neutrons is only 10% of that for s-wave neutrons. This low transparency will have the effect of reducing the partial widths for d-wave neutrons.

If the level of Li^7 at 9.3MeV has a spin and parity of $5/2$, both neutron and triton partial waves in the reaction channels will be d-waves. The low transparency of the centrifugal barrier to these particles could give the narrow partial widths necessary to account for the experimental results and the apparent lack of compound nucleus formation.

As there is uncertainty that the energy range has been adequately covered, further experimentation appears to be justified using a neutron source capable of covering a wider range of energies.

BIBLIOGRAPHY

BIBLIOGRAPHY

Aj 59 Ajzenberg-Selove, F. and Lauritsen, T.
Nuclear Physics 11, 1, (1959).

Al 54 Allan, D.L.
Nature 174, 267, (1954).

Al 55 Allan, D.L.
Proc. Phys. Soc. (London) A68, 925, (1955).

Al 57 Allan, D.L.
Proc. Phys. Soc. (London) A70, 195, (1957).

Al 58 Allan, D.L.
Nuclear Phys. 6, 464, (1958).

Al 59 Allan, D.L.
Nuclear Phys. 10, 348, (1959).

Ar 60 Armstrong, A.H. and Rosen, L.
Nuclear Phys. 19, 40, (1960).

As 55 Aschenbrenner, F.A.
Phys. Rev. 98, 657, (1955).

As 59 Ashby, V.J. and Catron, H.C.
U.S.A.E.C. Report UCRL - 5419 (1959).

Au 53 Austern, N., Butler, S.T., and McManus, H.
Phys. Rev. 92, 350, (1953).

Au 60 Austern, N.
Fast Neutron Physics. (Interscience, New York; to be published).

Ba 52 Barschall, H.H.
Rev. Mod. Phys. 24, 120, (1952).

Ba 52a Barschall, H.H., Rosen, L., Taschek, R.F. and Williams, J.H.
Rev. Mod. Phys. 24, 1, (1952).

Ba 54 Barschall, H.H. and Walt, M.
Phys. Rev. 93, 1063, (1954).

Ba 56 Badoni, C; Colli, L and Facchini, U.
Nuovo Cimento 4, 1618, (1956).

Ba 57 Bame, S.J., Haddard, E., Perry, J.E. and Smith, R.K.
Rev. Sci. Instr. 28, 997, (1957).

Be 37 Bethe, H.
Rev. Mod. Phys. 9, 69, (1937).

Be 59 Benveniste, J., Mitchell, A.C., Schrader, C.D. and Zenger, J.H.
U.S.A.E.C. Report UCRL - 5619 (1959).

Bl 52 Blatt, J.M. and Weisskopf, V.F.
Theoretical Nuclear Physics (John Wiley and Sons, New York, 1952).

Bl 52a Bleuer, E. and Goldsmith, G.J.
Experimental Nucleonics. (Rinehart, New York, 1952).

Bo 29 Bothe, W.
Z. Physik. 59, 1, (1929).

Bo 58 Bonner, T.
Tabulated Neutron Cross-sections UCRL - 5226 (Compiler: Howerton, R.J.).

Br 57 Brown, G., Morrison, G.C., Muirhead, H. and Morton, W.T.
Phil. Mag. 2, 785, (1957).

Br 57a Brown, G. and Muirhead, H.
Phil. Mag. 2, 473, (1957).

Br 58 Briscoe, W.L.
Rev. Sci. Instr. 29, 401, (1958).

Bu 51 Butler, S.T.
Proc. Royal Soc. A208, 559, (1951).

Bu 57a Butler, S.T.
Nuclear Stripping Reactions (John Wiley & Sons, Inc., New York, 1957).

Bu 57b Butler, S.T.
Phys. Rev. 106, 272, (1957).

Bu 58 Butler, S.T., Austern, N. and Pearson, C.
Phys. Rev. 112, 1227, (1958).

Ca 57 Carlson, R.R.
Phys. Rev. 107, 1094, (1957).

Ca 59 Carver, J.H. and Turchinetz, W.
Proc. Phys. Soc. (Lond.) 73, 585, (1959).

Ch 49 Chance, B., Hughes, V., MacNichol, E.F., Sayre, D. and Williams, F.C.
Waveforms (McGraw Hill (1949).

Ch 57 Christy, R.F.
Proc. Univ. Pittsburgh Conf. on Nuclear Structure, 421ff (1957).

Co 54 Cohen, B.L., Newman, R.H., Charpie, R.A. and Handley, T.H.
Phys. Rev. 94, 620, (1954).

Co 55 Cohen, B.L., Newman, R.H. and Handley, T.H.
Phys. Rev. 99, 723, (1955).

Co 56 Cohen, A.V. and White, P.H.
Nuclear Physics 1, 73, (1956).

Co 56a Colli, L. and Facchini, U.
Nuovo Cimento 4, 671, (1956).

Co 57a Cohen, B.L.
Conference on Nuclear Structure. (University of Pittsburgh, 1957).

Co 57b Cohen, B.L.
Phys. Rev. 105, 1549, (1957).

Co 57c Colli, L. and Facchini, U.
Nuovo Cimento. 5, 309, (1957).

Co 58a Colli, L., Facchini, U., Ioni, I., Mercazzan, G., Sona, A. and Pignanelli, M.
Nuovo Cimento 7, 400, (1958).

Co 58b Colli, L., Pignanelli, M., Rytz, A. and Zurmuhle, R.
Nuovo Cimento 9, 280, (1958).

Co 59 Colli, L., Facchini, U., Ioni, I., Marcazzan, G., and Sona, A.M.
Nuovo Cimento 13, 730, (1959).

Co 59a Colli, L., Cvelbar, F., Micheletti, S., and Pignanelli,M.
Nuova Cimento 13, 858, (1959).

Co 59b Colli, L., Cvelbar, F., Micheletti, S., and Pignanelli, M.
Nuovo Cimento 14, 81, (1959).

Co 59c Colli, L., Cvelbar, F., Micheletti, S. and Pignanelli, M.
Nuovo Cimento 14, 1120, (1959).

Da 53 Darlington, L.E., Haugsnes, J., Mann, H.M. and Roberts, J.H.
Phys. Rev. 90, 1049, (1953).

Da 55 Dabrowski, J. and Sawicki, J.
Acta Physica Polonica 14, 323, (1955).

De 58 De Benedetti, S. and Findley, R.W.
Handbuch der Physik 45, 222, (1958).

Di 53 Dickenson, W.C. and Dodder, D.C.
Rev. Sci. Instr. 24, 428, (1953).

Do 59 Douglas, A.C. and MacDonald, N.
Nuclear Phys. 13, 382, (1959).

Do 60 Dostrovsky, I., Fraenkel, Z. and Winsberg, L.
Phys. Rev. 118, 781, (1960).

Ei 54 Eisberg, R. M.
Phys. Rev. 94, 739, (1954).

El 57 Elliott, J.P. and Lane, A.M.
Handbuch der Physik 39, 241, (1957).

En 53 English, W.N. and Hanna, G.C.
Can. J. Phys. 31, 768, (1953).

En 57 Endt, P.M. and Braams, C.M.
Rev. Mod. Phys. 29, 683, (1957).

Er 54 Erdos, P., Stoll, P., Wachter, M. and Wataghin, V.
Nuovo Cimento 12, 639, (1954).

Eu 58 Eubank, H.P., Peck, R.A., Hassler, F.L.
Nuclear Phys. 9, 273, (1958).

Fa 56 Fairstein, E.
Rev. Sci. Instr. 27, 475, (1956).

Fa 60 Facchini, U., Ioni, I. and Menichella, E.
Nuova Cimento 16, 1109, (1960).

Fe 54 Feshbach, H., Porter, C.E. and Weisskopf, V.F.
Phys. Rev. 96, 448, (1954).

Fi 52 Fischer, J. and Marshall, J.
Rev. Sci. Instr. 23, 417, (1952).

Fo 56 Fowler, J.L. and Brolley, J.E.
Rev. Mod. Phys. 28, 103, (1956).

Fr 54 Fry, G.M.
Phys. Rev. 93, 1086, (1954).

Fr 55 Friedman, F.L. and Weisskopf, V.F.
Niels Bohr and the Development of Physics.
(Editor: Pauli, W. Pergamon Press Ltd, London, 1955).

Fu 58 Fulmer, C.B. and Cohen, B.L.
Phys. Rev. 112, 1672, (1958).

Ga 50 Garwin, R.L.
Rev. Sci. Instr. 21, 569, (1950).

Ga 53 Garwin, R.L.
Rev. Sci. Instr. 24, 618, (1953).

Gl 59 Glendinning, N.K.
Phys. Rev. 114, 1297, (1959).

Go 46 Good, W.M., Peaslee, D. and Deutsch, M.
Phys. Rev. 69, 313, (1946).

Go 54 Goldemberg, J. and Katz, L.
Phys. Rev. 95, 471, (1954).

Gr 53 Graves, E.R. and Rosen, L.
Phys. Rev. 89, 343, (1953).

Gr 58 Green, R.E. and Bell, R.E.
Nuclear Instruments 3, 127, (1958).

Gu 54 Gugelot, P.C.
Phys. Rev. 93, 425, (1954).

Gu 56 Gugelot, P.C. and Rickey, M.
Phys. Rev. 101, 1613, (1956).

Ha 49 Hanson, A.O., Taschek, R.F. and Williams, J.H.
Rev. Mod. Phys. 21, 635, (1949).

Ha 57 Haling, R.K., Peck, R.A. and Eubank, H.P.
Phys. Rev. 106, 971, (1957).

Ha 57a Hayakawa, S. and Yoshida, S.
Prog. Theor. Phys. (Kyoto) 14, 1, (1957).

Hi 47 Hirzel, O. and Waffler, H.
Helv. Phys. Acta 20, 373, (1947).

Hu 53 Huby, R.
Prog. Nuclear Phys. 3, 177, (1953).

Hu 55 Hughes, D.J. and Harvey, J.A.
U.S.A.E.C. Report BNL - 325 (1955).

Ig 54 Igo, G. and Eisberg, R.M.
Rev. Sci. Instr. 25, 450, (1954).

Ig 57 Igo, G.
Phys.Rev. 106, 256, (1957).

Ja 60 Jack, W. and Ward, A.
Proc. Phys. Soc. 75, 833, (1960).

Jo 56 Johnson, C.H. and Trail, C.C.
Rev. Sci. Instr. 27, 468, (1956).

Ke 58 Kern, B.D. and Kreger, W.E.
Phys. Rev. 112, 926, (1958).

Ki 57 Kikuchi, K.
Prog. Theor. Phys. (Kyoto) 17, 643, (1957).

Ki 57a Kinsey, B.B.
Handbuch der Physik. 40/1, 202, (1957).

Ko 56 Konijn, J., van Nooijen, B., Mostert, P. and Endt, P. M.
Physica 22, 887, (1956).

Ko 58 Konijn, J., Hagedoorn, H.L. and van Nooijen, B.
Physica 24, 129, (1958).

Ku 60 Kumabe, I. and Fink, R.W.
Nuclear Physics 15, 316, (1960).

La 54 Lang, J.M.B. and Le Couteur, K.J.
Proc. Phys. Soc. A67, 586, (1954).

Le 54 Lewis, I.A.D. and Wells, F.H.
Millimicrosecond pulse techniques (McGraw Hill, 1954).

Le 59 Le Couteur, K.J. and Lang, D.W.
Nuclear Phys. 13, 32, (1959).

Le 59a Le Couteur, K.J.
Nuclear Reactions I (Editors: Endt, P.M. and Demeur, M. North Holland, 1959).

Li 37 Livingston, M.S. and Bethe, H.A.
Rev. Mod. Phys. 1, 263, (1937).

Lu 59 Lubitz, C.R.
Numerical Table of Butler-Born Approximation Stripping Cross-Sections. U.S.A.E.C. Report: AECU - 3990 (1959).

Ma 55 Mayer, M.G. and Jensen, J.H.D.
Elementary Theory of Nuclear Shell Structure. (John Wiley & Sons, New York - 1955).

Ma 57 Mann, A.K., Ophel, T.R. and Wright, I.F.
Bull. Am. Phys. Soc. 2, 181A, (1957).

Ma 58 March, P.V. and Morton, W.T.
Phil. Mag. 3, 1256, (1958).

Ma 58a March, P.V. and Morton, W.T.
Phil. Mag. 3, 143, (1958).

Ma 58b March, P.V. and Morton, W.T.
Phil. Mag. 3, 577, (1958).

Ma 58c Marcazzan, G., Sona, A.M., Pignanelli, M.
Nuovo Cimento 10, 155, (1958).

Ma 60 MacFarlane, M.H. and French, J.B.
Rev. Mod Phys. 32, 567, (1960).

Mc 58 McCartney, W.
Electronics 31, 78, (1958).

Me 54 Metropolis, N.
Symposium on Monte Carlo Methods. (Editor: Mayer, H.A. John Wiley, 1954).

Mi 55 Miller, J.A., Soltes, A.S. and Scott, R.E.
Electronics 28, 160, (Feb. 1955).

Mi 57 Miller, J.M. and Houck, F.S.
Bull. Am. Phys. Soc. 4, 60, (1957).

Mu 58 Murray, R.B.
Nuclear Instruments. 2, 237, (1958).

Ne 58 Nemeth, J.
Nuclear Phys. 6, 686, (1958).

Ok 58 Okhuysen, P.L., Bennett, E.W., Ashe, J.B. and Millett, W.E.
Rev. Sci. Instr. 29, 983, (1958).

O'N 54 O'Neill, G.K.
Phys. Rev. 95, 1235, (1954).

Op 58 Ophel, T.R.
Nuclear Instr. 3, 45, (1958).

Op 58a Ophel, T.R. and Wright, I.F.
Proc. Phys. Soc. 71, 389, (1958).

Ov 59 Overseth, O.E. and Peck, R.A. Jr.
Phys. Rev. 115, 993, (1959).

Pa 53 Paul, E.B. and Clarke, R.L.
Can. J. Phys. 31, 267, (1953).

Pe 55 Peaslee, D.C.
Ann. Rev. of Nuclear Science. 5, 99, (1955).

Pe 57 Peck, R.A. Jr.
Phys. Rev. 106, 965, (1957).

Pe 58 Peck, R.A. and Eubank, H.P.
U.S.A.E.C. Report NYO - 7862.

Pe 59 Peck, R.A., Eubank, H.P. and Howard, R.M.
Nuovo Cimento 14, 397, (1959).

Pe 59a Peck, R.A., Eubank, H.P. and Low, J.
Rev. Sci. Instr. 30, 703, (1959).

Pe 60 Perry, J.E.
Fast Neutron Physics I (Editors: Marion, J.B. and Fowler, J.L. Interscience - 1960).

Ri 54 Ribe, F.L. and Seagrave, J.D.
Phys. Rev. 94, 934, (1954).

Ri 56 Ribe, F.L.
Phys. Rev. 103, 741, (1956).

Ri 57 Ribe, F.L.
Phys. Rev. 106, 767, (1957).

Ro 49 Rossi, B. and Staub, H.H.
<u>Ionization Chambers and Counters.</u>
(McGraw-Hill, New York. 1949).

Ro 52 Rossi, B.B.
<u>High Energy Particles</u>. (Prentice-Hall, New York, 1952).

Ro 55a Rosen, L. and Stewart, L.
<u>Phys. Rev</u>. <u>99</u>, 1052, (1955).

Ro 56 Rosen, L. and Armstrong, A.H.
<u>Bull. Am. Phys. Soc</u>. <u>1</u>, 224, (1956).

Ro 57 Rosen, L. and Stewart, L.
<u>Phys. Rev</u>. <u>107</u>, 824, (1957).

Sa 55a Sawiki, J.
<u>Nuovo Cimento</u> <u>1</u>, 957, (1955).

Sa 55b Sawiki, J.
<u>Nuovo Cimento</u> (10) <u>2</u>, 1322, (1955).

Sc 54 Scott, J.M.C.
<u>Phil. Mag</u>. <u>45</u>, 441, (1954).

Se 55 Seagrave, J.D.
<u>Phys. Rev</u>. <u>97</u>, 757, (1955).

Sh 53 Shapiro, M.M.
<u>Phys. Rev</u>. <u>90</u>, 171, (1953).

Sh 57 Sherr, R.
<u>Proc. Univ. Pittsburgh Conf. on Nuclear Structure. (1957)</u>.

Sh 59 Shipley, E.N., Owen, G.E. and Madansky, L.
<u>Rev. Sci. Instr</u>. <u>30</u>, 604, (1959).

Si 57 Silver, R.
<u>U.S.A.E.C. Report</u> <u>UCRL</u> - 3887 (1957).

So 58 Souch, A.E. and Sweetman, D.R.
<u>Rev. Sci. Instr</u>. <u>29</u>, 794, (1958).

St 53 Stoll, P. and Wachter, M.
<u>Nuovo Cimento</u> <u>10</u>, 347, (1953).

St 54 Stoll, P.
<u>Helv. Physica Acta</u>. <u>27</u>, 395, (1954).

St 58 Stokes, R.H., Boyer, K. and Northrop, J.A.
Rev. Sci. Instr. 29, 61, (1958).

St 58a Storey, R.S., Jack, W. and Ward, A.
Proc. Phys. Soc. 73, 523, (1958).

St 58b Strominger, D., Hollander, J.M. and Seaborg, G.T.
Rev. Mod. Phys. 30, 585, (1958).

St 60 Storey, R.S., Jack, W. and Ward, A.
Proc. Phys. Soc. 75, 526, (1960).

Ti 53 Titterton, E.W. and Brinkley, T.A.
Proc. Phys. Soc. A66, 579, (1953).

Ti 53a Titterton, E.W. and Brinkley, T.A.
Proc. Phys. Soc. A66, 194, (1953).

To 55 Topping, J.
Errors of Observation and their Treatment.
(Monograph; Institute of Physics, London, 1955).

To 57 Tobocman, W.
Phys. Rev. 108, 74, (1957).

Ve 57 Verbinski, V.V., Hurlimann, T., Stephens, W.E. and Winhold, E.J.
Phys. Rev. 108, 779, (1957).

Wa 50 Waffler, H.
Helv. Phys. Acta 20, 373, (1950).

Wa 50a Waffler, H.
Helv. Phys. Acta 23, 239, (1950).

Wa 55 Wapstra, A.H.
Physica 21, 367, 385, (1955).

We 37 Weisskopf, V.F.
Phys. Rev. 52, 295, (1937).

We 54 Weddell, J.B. and Roberts, J.H.
Phys. Rev. 95, 117, (1954).

We 57 Weisskopf, V.F.
Rev. Mod. Phys. 29, 174, (1957).

Wo 51 Wolfenstein, L.
Phys. Rev. 82, 690, (1951).

A P P E N D I X

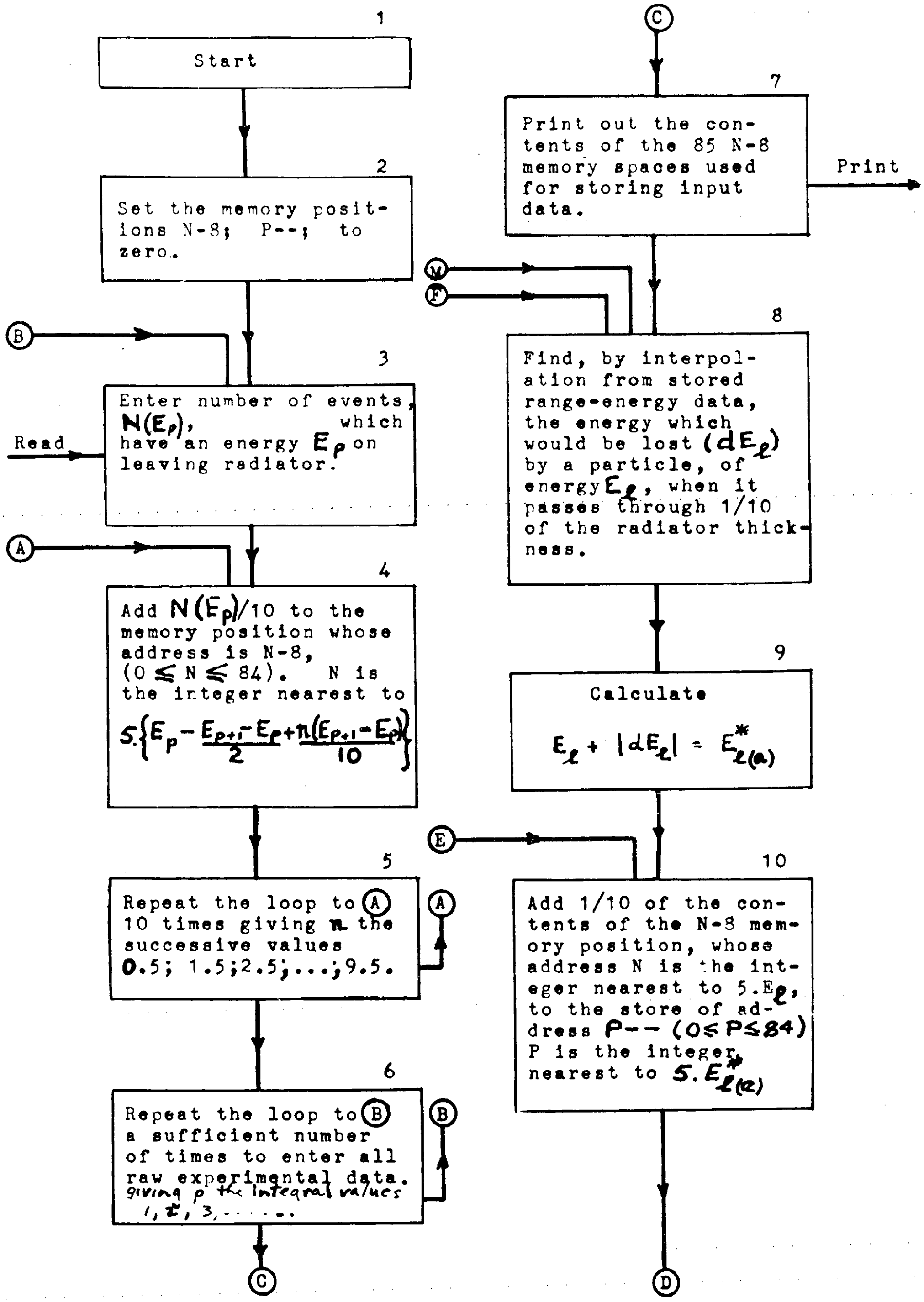

Figure 38 : Flow Chart of Data Reduction Proceedure.

(1)

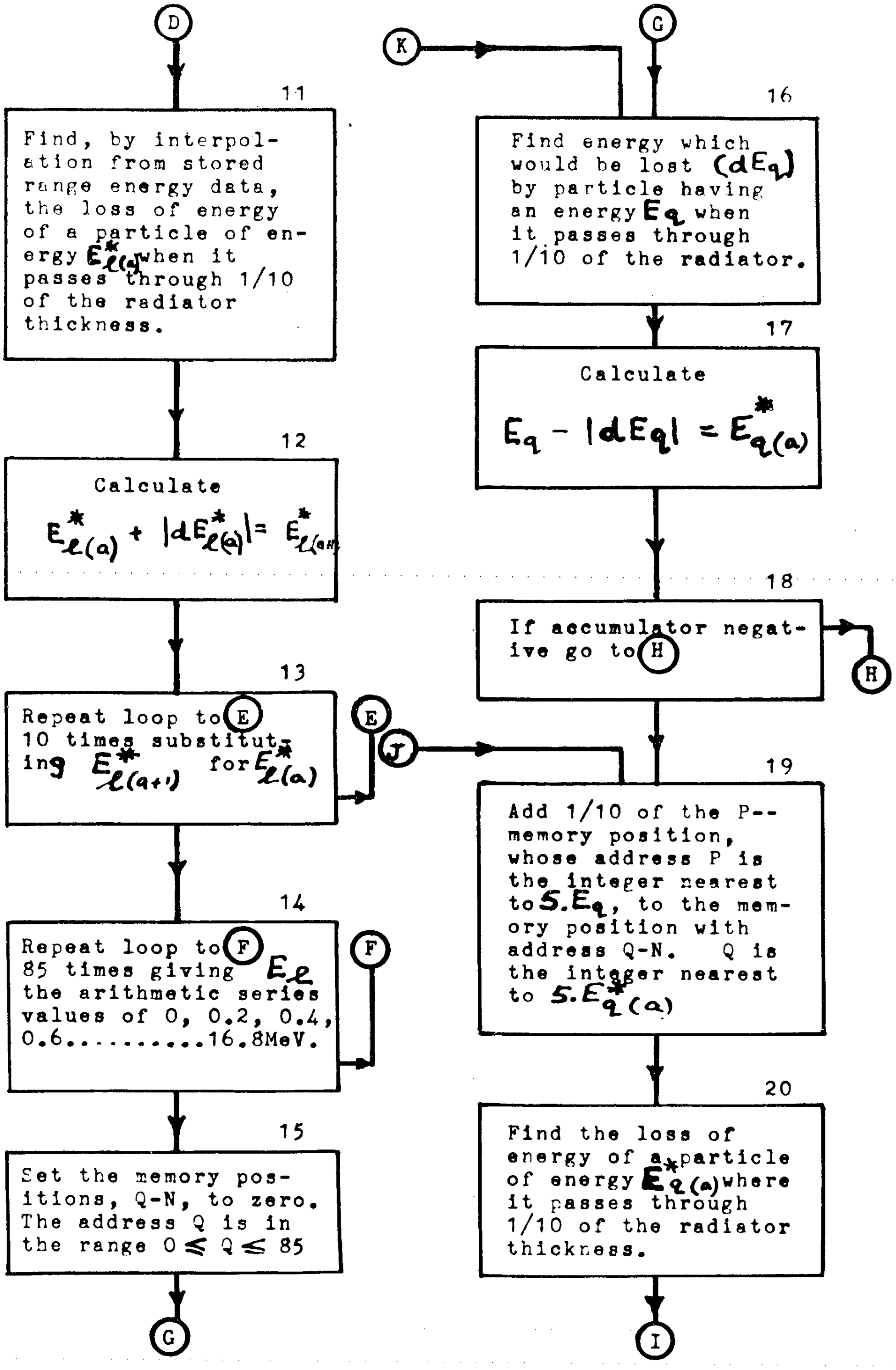

Figure 38 (cont.).
(2)

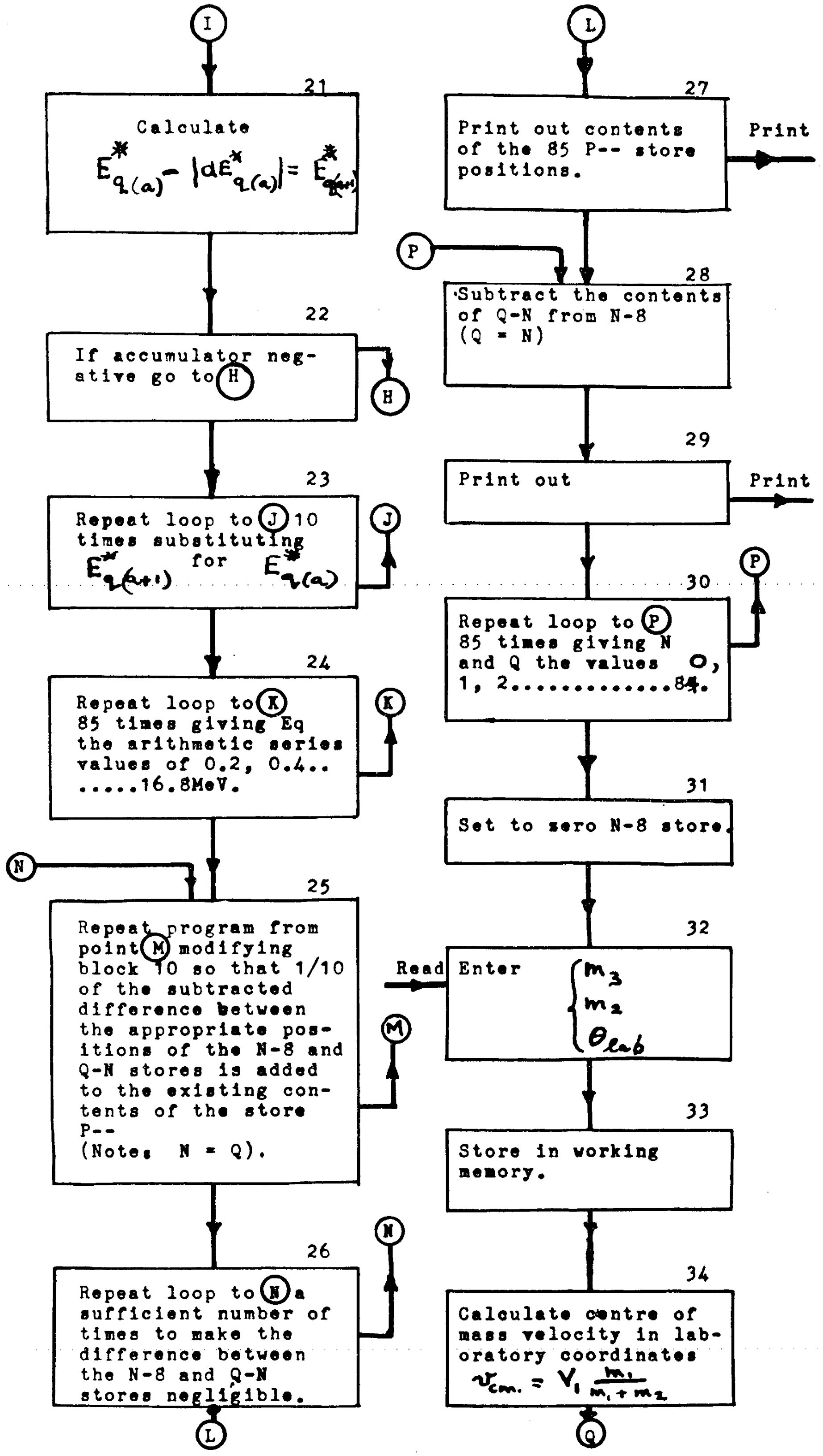

Figure 38 (cont.).
(3)

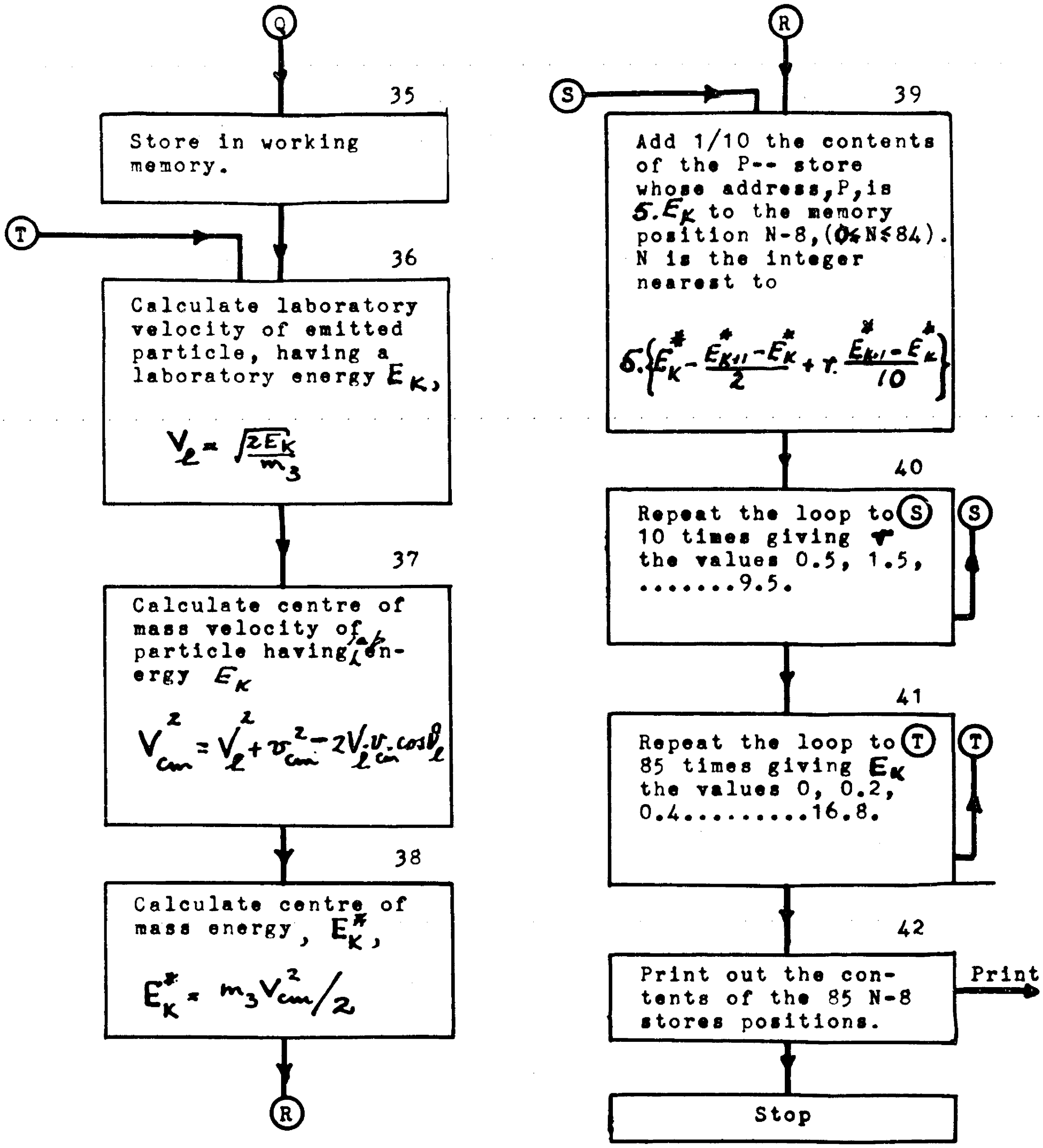

Figure 38 (cont.).